

SCALABLE HUMAN INTESTINE MODEL WITH PERFUSABLE VASCULATURE

SCALABLE HUMAN INTESTINE MODEL WITH ACCESSIBLE LUMEN AND
PERFUSABLE BRANCHED VASCULATURE

BY: KRISTEN L. HAYWARD, B.SC.

A Thesis Submitted to the School of Graduate Studies in Partial Fulfillment of the
Requirements for the Degree Master of Applied Science

McMaster University © Copyright by Kristen L. Hayward, July 2021

McMaster University MASTER OF APPLIED SCIENCE (2021) Hamilton, Ontario

(Chemical Engineering)

TITLE: Scalable Human Intestine Model with Accessible Lumen and Perfusable
Branched Vasculature

AUTHOR: Kristen L. Hayward, Hons. B.Sc. (York University)

SUPERVISOR: Boyang Zhang, Ph.D.

NUMBER OF PAGES: xv, 154

Some sentences in this work have been reproduced with permission from Hayward, K. L., Kouthouridis, S. & Zhang, B. Organ-on-a-Chip Systems for Modeling Pathological Tissue Morphogenesis Associated with Fibrosis and Cancer. *ACS Biomaterials Science & Engineering*, doi:10.1021/acsbomaterials.0c01089 (2020). Copyright 2020 American Chemical Society.

Lay Abstract

Two-dimensional cell culture and animal models inadequately represent human drug metabolism and diseases like inflammatory bowel disease and colorectal cancer. The objective of this work is to develop a more physiologically relevant human intestine model. Using fabrication techniques pioneered by the semiconductor industry, a custom organ-on-a-chip platform in the format of a 384-well plate was developed. This platform is compatible with standard laboratory equipment and practices and can accommodate up to 128 human intestine models comprised of the intestinal epithelium and associated network of blood vessels. In this platform, the cells of the intestinal epithelium and vasculature are supported by a network of natural proteins. This allows processes like vessel growth to be modelled in this platform. Vessel growth plays a key role in the progression of inflammatory bowel disease and cancer, and this model could help scientists better understand these diseases.

Abstract

Two-dimensional cell culture and animal models inadequately represent human pharmacokinetics and diseases like inflammatory bowel disease and colorectal cancer. This means missed diagnostic and therapeutic opportunities, high drug attrition rates, and a portfolio of approved drugs that underdeliver the desired benefits to patient outcomes. This encourages the development of a more physiologically relevant intestine model. The objective of this work was to develop a 384-well plate organ-on-a-chip platform, IFlowPlate™, that can accommodate up to 128 human intestine models with accessible lumens and perfusable branched vasculature in an ECM environment. Fibrin-Matrigel® was used as a structurally supportive and biologically instructive substrate that enabled: (1) prolonged cell culture (at least 15 days) with routine refreshment of aprotinin-supplemented medium, (2) formation of a confluent Caco-2 monolayer with barrier function, and (3) de novo assembly of a vascular network with barrier function. A fluorescent dextran permeability assay was used for in situ real-time measurements of epithelial barrier function in a high-throughput manner. Mixed co-culture of endothelial cells and fibroblasts in fibrin-Matrigel® resulted in the formation of an interconnected network of patent vessels that retained an albumin surrogate tracer within the luminal space indicating endothelial barrier function. To improve the success rate of anastomoses between living vessels and fluidic channels, the modification of inherently hydrophobic PDMS and polystyrene culture surfaces with ECM protein was explored. To address the limitations of a cancer cell line-derived intestine model, the replacement of Caco-2 cells with biopsied-derived colon organoid cells was investigated. Different gel formulations were assessed for their ability to induce colon organoid fragments to form monolayers. Finally, the incorporation of multiscale intestinal topography and luminal flow was considered through a modified approach to plate fabrication, whereby moulded alginate is embedded in ECM and sacrificed to generate a scaffold. Work to make the moulded alginate more robust is presented.

Acknowledgements

I would like to thank my supervisor, Dr. Boyang Zhang, for introducing me to organ-on-a-chip technology and giving me an opportunity to engage in challenging and innovative work. I greatly value the breadth of knowledge and skills I have cultivated by working at the intersection of engineering, biomaterials science, and cell biology. I would also like to thank my examining committee members, Dr. Li Xi and Dr. Sandeep Raha, for the time and effort they extended in this role.

Thank you to all the past and present members of the Zhang Lab that I had the pleasure of working with. I appreciate that sharing was an important pillar of our workplace culture. We shared more than just a Google calendar. We shared knowledge, resources, the joy of each other's successes, laughs, but thankfully never coronavirus.

I would like to express my gratitude for the financial support I received during my graduate studies in the form of the Queen Elizabeth II Graduate Scholarship in Science and Technology and the Clifton W. Sherman Scholarship.

Many thanks to the patients who consent to the biobanking of collected tissue for research. Your contribution is invaluable for advancing scientific understanding of health and disease.

To my extraordinary parents, Judy and Terry, this accomplishment is as much yours as it is mine. Thank you for all your sacrifices, love, and support that made this possible.

Table of Contents

Lay Abstract	iii
Abstract	iv
Acknowledgements	v
List of Figures	x
List of Tables	xiii
List of Abbreviations	xiv
Declaration of Academic Achievement	xv
1. Introduction	1
2. Literature Review	3
2.1 Intestine Physiology	3
2.2 In Vitro Models	4
2.2.1 2D Cell Line Cultures	4
2.2.2 Organoids	6
2.2.3 Microstructured Scaffolds	6
2.2.4 Organ-on-a-chip	8
3. Materials and Methods	12
3.1 IFlowPlate™ Fabrication	12
3.1.1 Photolithography for SU-8 Master Template Fabrication	13
3.1.2 Soft Lithography for PDMS Mould 1 Fabrication	14
3.1.3 Replica Moulding for Fabrication of Epoxy and PDMS Moulds	14
3.1.4 Silanization	19

3.1.5 Injection Moulding to Pattern Styrene Plate Bottom	21
3.1.6 IFlowPlate™ Assembly and Disinfection	24
3.2 SynoPlate™ Fabrication	26
3.3 SynoPlate™ Cell Culture	33
3.4 IFlowPlate™ Cell Culture	35
3.4.1 Cells and Culture Conditions	36
<i>Endothelial Cells</i>	<i>36</i>
<i>Fibroblasts.....</i>	<i>37</i>
<i>Caco-2 Cells</i>	<i>38</i>
<i>Cell Passage Number</i>	<i>38</i>
<i>Culture Conditions for Cell Lines</i>	<i>39</i>
3.4.2 Hydrogels	39
<i>Fibrin</i>	<i>42</i>
<i>Matrigel®</i>	<i>44</i>
<i>Fibrin-Matrigel®</i>	<i>46</i>
<i>Collagen</i>	<i>47</i>
<i>Gelatin</i>	<i>51</i>
3.4.3 Cell Culture in IFlowPlate™	52
<i>Selection of Microfluidic Systems</i>	<i>52</i>
<i>Temporary Sealing of Microfluidic Channels with Gelatin</i>	<i>53</i>
<i>Cell Harvest and Encapsulation</i>	<i>53</i>
<i>Replacement of Gelatin with Culture Medium</i>	<i>55</i>

<i>Endothelialization of Microfluidic Channels with GFP-HUVECs</i>	58
<i>Seeding Caco-2 Cells on Gel Surface</i>	58
<i>Gravity-Driven Flow</i>	58
3.5 Characterization of Epithelial Barrier	59
3.5.1 Formation of Caco-2 Confluent Monolayer on Fibrin-Matrigel®	59
3.5.2 Immunofluorescence Staining	59
3.5.3 Paracellular Permeability to Fluorescent-Dextrans	61
3.5.4 Transepithelial Electrical Resistance (TEER)	70
3.6 Characterization of Self-Assembled Vessels	71
3.6.1 Paracellular Permeability of Vessels to 70 kDa TRITC-dextran	72
3.6.2 Image Acquisition	72
3.7 Coating IFlowPlate™ Microfluidic Channels with ECM Protein	73
3.8 Colon Organoid-Derived Monolayer Experiment	76
3.8.1 Source of Colon Organoids	76
3.8.2 Seeding Colon Organoid Fragments on Collagen Gel Surface	76
3.8.3 Colon Organoid Culture Conditions	77
Chapter 4: Results and Discussion	78
4.1 IFlowPlate™ Avascular Intestine Model	78
4.1.1 Modelling Intestine Epithelium with Caco-2 Cell Line	78
<i>Caco-2 Cells Polarize and Form a Functional Barrier</i>	78
<i>Caco-2 Cells Form Confluent Monolayers on Fibrin-Matrigel®</i>	81
<i>Caco-2 Cells Express E-cadherin</i>	85

4.1.2 Barrier Function	86
<i>Paracellular Permeability to Fluorescent-Dextrans</i>	<i>86</i>
<i>Transepithelial Electrical Resistance (TEER)</i>	<i>92</i>
4.2 IFlowPlate™ Vascular Intestine Model	96
4.2.1 Self-Assembled Vascular Networks	98
4.2.2 Anastomoses of Self-Assembled Vessels with Fluidic Channels	104
<i>Sealing Gel</i>	<i>104</i>
<i>Bidirectional Anastomoses</i>	<i>108</i>
<i>Coating IFlowPlate™ Microfluidic Channels with ECM Protein</i>	<i>114</i>
4.3 Enhancing Physiological Relevance of IFlowPlate™ Intestine Model	121
4.3.1 IFlowPlate™ Primary Intestine Model	121
4.3.2 SynoPlate™ Intestine Model	129
Chapter 5: Conclusion	135
5.1 Summary	135
5.2 Prospective Application of IFlowPlate™ Intestine Model	141

List of Figures

Figure No.	Figure Title	Page
Figure 1	Anatomy of the small and large intestine	10
Figure 2	Timeline figure showing important milestones in the history of in vitro intestine model development	11
Figure 3	Schematic showing Part A and B of IFlowPlate™ fabrication	17
Figure 4	Schematic showing Part C of IFlowPlate™ fabrication	18
Figure 5	Schematic showing the possible arrangements of Pluronic® tri-block co-polymers on a hydrophobic PDMS substrate	22
Figure 6	Exploded diagram showing one of the 40 microfluidic systems of the intestine SynoPlate™	27
Figure 7	Schematic showing Part A of SynoPlate™ fabrication	31
Figure 8	Structure and swelling behaviour of calcium-alginate gel	32
Figure 9	Schematic showing Part B of SynoPlate™ fabrication	33
Figure 10	Exploded diagram showing one of the 128 microfluidic systems of IFlowPlate™	36
Figure 11	Cross-linkable natural polymers can reversibly form hydrogels in response to physical, chemical, and enzymatic stimuli	42
Figure 12	1 mg/mL collagen prepared by neutralization of acid-solubilized concentrated rat-tail collagen type I	49
Figure 13	Schematic showing stepwise procedure for establishing a vascular tissue model in an IFlowPlate™ microfluidic system	57

Figure 14	Schematic overview of the permeability assay procedure for assessing barrier function in IFlowPlate™ intestine model systems	63
Figure 15	Two-fold serial dilution of 0.5 mg/mL FITC- and TRITC-dextran solution	67
Figure 16	Day 7 standard curves of fluorescence intensity as a function of the amount of FITC- and TRITC-dextran	68
Figure 17	Day 15 standard curves of fluorescence intensity as a function of the amount of FITC- and TRITC-dextran	69
Figure 18	Exploded diagram showing the procedure for measuring the transepithelial electrical resistance of a Caco-2 monolayer in IFlowPlate™ using the EVOM2	71
Figure 19	PDMS has high surface hydrophobicity and requires surface modification treatment to increase hydrophilicity and facilitate cell adhesion	74
Figure 20	Caco-2 cells cultured on non-porous polystyrene substrates spontaneously form domes (<i>arrows</i>) indicating polarization and barrier function	79
Figure 21	Caco-2 cells form hallmark cobblestone epithelium on fibrin-Matrigel® and in mixed media that supports vasculature growth	84
Figure 22	Caco-2 cells stained for junction marker E-cadherin to assess barrier integrity	85
Figure 23	Microscopy images showing the permeability of a representative subconfluent (~80 % confluent) Caco-2 monolayer to high and low molecular weight fluorescent dextrans	89
Figure 24	Microscopy images showing the permeability of a representative postconfluent (+8 days from confluence) Caco-2 monolayer to high and low molecular weight fluorescent dextrans	90
Figure 25	Quantification of amount of eluted fluorescent dextran as an indicator of the barrier function of Caco-2 monolayers in IFlowPlate™	91
Figure 26	In-house fabricated IFlowPlate™ microfluidic systems exhibit inconsistent geometries	94

Figure 27	Fibrin gel-encapsulated GFP-HUVECs self-assemble into a vascular network by Day 6 of culture in IFlowPlate™	101
Figure 28	70 kDa TRITC-dextran is transported and retained in lumens indicating the formation of patent vessels with a functional endothelial barrier	103
Figure 29	Fibrin pre-gel cast in the middle well leaks into fluidic channels of IFlowPlate™ microfluidic systems and compromises perfusion of vascular networks	106
Figure 30	Schematic showing that anastomoses between living vessels embedded in gel and fluidic channels of IFlowPlate™ microfluidic systems can be induced bidirectionally	110
Figure 31	Encapsulated GFP-HUVECs migrate from the gel into fluidic channels and form a “leaky” anastomotic connection with only one of the fluidic channels	111
Figure 32	GFP-HUVECs loaded into fluidic channels of IFlowPlate™ microfluidic systems insufficiently endothelialize channels under perfusion culture conditions	112
Figure 33	GFP-HUVECs loaded into fluidic channels of IFlowPlate™ microfluidic systems insufficiently endothelialize channels under static culture conditions	113
Figure 34	IFlowPlate™ microfluidic systems were coated with ECM protein to modify inherently hydrophobic PDMS and polystyrene surfaces and enhance GFP-HUVEC adhesion	117
Figure 35	Migration of gel-encapsulated GFP-HUVECs from tissue chamber into ECM-coated lateral fluidic channels in response to a strong chemoattractant gradient	118
Figure 36	Patient-derived colon organoid fragments seeded on top of collagen hydrogels to assess substrate-dependent monolayer formation	124
Figure 37	Microscopy images of polystyrene patterned with alginate via injection moulding using a two-level or single-level PDMS template	134

List of Tables

Table No.	Table Title	Page
Table 1	Results of pilot study testing the measurement of electrical resistance of Caco-2 monolayers in IFlowPlate™ as a non-invasive method for assessing barrier function	93

List of Abbreviations

ECM	extracellular matrix
PEGDM	poly(ethylene glycol) dimethyl ether
PDMS	polydimethylsiloxane
UV	ultraviolet
HEPA	high-efficiency particulate air
dH ₂ O	distilled water
PEO	poly(ethylene oxide)
PPO	poly(propylene oxide)
CMC	critical micelle concentration
GFP-HUVECs	green-fluorescent protein-human umbilical vein endothelial cells
ECGM-2	endothelial cell growth medium 2
DMEM	Dulbecco's modified Eagle's medium
FBS	fetal bovine serum
G	α -L-galuronic acid
D-PBS	Dulbecco's phosphate buffered saline
BSA	bovine serum albumin
EHS	Engelbreth-Holm-Swarm
TEER	transepithelial electrical resistance
RGD	Arg-Gly-Asp
RCF	relative centrifugal force
FITC	fluorescein isothiocyanate
TRITC	tetramethylrhodamine isothiocyanate
PFA	paraformaldehyde
PI	propidium iodide
VEGF	vascular endothelial growth factor
MP	microplastic
PCBs	polychlorinated biphenyls

Declaration of Academic Achievement

I, Kristen Hayward, declare this thesis to be my own work, apart from the contributions outlined below.

Dr. Boyang Zhang conceptualized IFlowPlate™ and SynoPlate™ and drew their designs using AutoCAD.

Feng Zhang fabricated SU-8 master templates on silicon wafers in a clean room facility at the University of Toronto.

Feng Zhang and Mandeep Kaur Marway fabricated IFlowPlate™ epoxy moulds.

Shravanthi Rajasekar dissociated and seeded colon organoids.

Scientific drawings were created with BioRender.com

Chapter 1: Introduction

Angiogenesis is a hallmark of inflammatory bowel disorders¹ and cancer.² Angiogenesis plays a critical role in the proliferation and metastasis of colorectal cancer.² Colorectal cancer is among the top three most prevalent cancers worldwide and is the third leading cause of cancer-related deaths.² New vessels (1) supply the growing tumour with oxygen and nutrients to meet its increasing metabolic demands and (2) permit the dissemination of tumour cells to secondary sites; thus, contributing to metastasis. Not surprisingly, cancers with a poor prognosis are correlated with increasing production of angiogenic factors and increased density of tumour vasculature.³ For these reasons, antiangiogenic therapies represent an attractive approach to treating cancer. However, despite the widespread attention antiangiogenic therapies have received from the research community, they have not delivered the anticipated improvements to patient outcomes.⁴ Possible reasons for this are that antiangiogenic compounds can 1) promote metastasis through hypoxia-induced upregulation of paracrine factors that promote cancer cell motility and invasion,⁵ and/or 2) reinforce tumour circumvention of angiogenesis whereby tumours use alternative strategies for gaining access to blood supply, such as vasculogenic mimicry⁶ or vessel cooption.⁴

There is also growing interest in therapeutically targeting the tumour extracellular matrix (ECM) because it might represent less of a moving target than the genetically unstable cancer cells which frequently acquire new genetic alterations as they divide – a mechanism that can lead to drug resistance.⁷⁻⁹ While targeting the tumour ECM or the fibroblasts that produce/remodel it could represent an effective cancer therapy, current

understanding of how the ECM contributes to cancer morphogenesis is limited. Deciphering the complex bidirectional relationships between cells and the ECM encourages the reductionist approach of in vitro models.

Experimentally tractable human intestine models that can model angiogenesis and the ECM with stromal cells, have the potential to improve scientific understanding of complex intestinal diseases, and facilitate the development of more effective therapies. The most well-established intestine-on-a-chip systems (Section 2.3.4) are configured as two stacked planar channels which are made of PDMS and separated by a synthetic membrane. In the upper compartment, epithelial cells are cultured, and in the lower compartment, endothelial cells are cultured. Two notable limitations of these traditional organ-on-a-chip systems are: (1) they are low-throughput and poorly compatible with standard laboratory equipment and practices, and (2) they impose non-physiological constraints and thus are not suited for modelling tissue morphogenesis (e.g., angiogenesis) which occurs in the context of a three-dimensional ECM environment.

The objective of this work is to address the shortcomings of gut-on-a-chip systems through the development of a scalable vascularized intestine model in a custom 384-well microfluidic platform termed IFlowPlate™. This platform is (1) free of non-physiological constraints and incorporates an ECM-based hydrogel that supports tissue morphogenesis and incorporation of stromal cells, (2) compatible with standard laboratory equipment and practices, and (3) has the potential to deliver high-throughput experimental capabilities. To make judicious use of resources and to make it easier to diagnose and address problems, the development of an intestine model in IFlowPlate™ was pursued incrementally. This

work can be organized into three aims: (1) develop a Caco-2 epithelial barrier model, (2) develop a gel-embedded network of perfusable branched vasculature, and (3) enhance the physiological relevance of the model by a) incorporating primary intestine tissue, b) luminal flow, and c) multiscale intestine topography (i.e., tubular structure and crypts). Part b) and c) of the third aim requires reconfiguration of the IFlowPlate™ platform and a modified biofabrication approach. To reflect this departure, this platform is trademarked as SynoPlate™.

Chapter 2: Literature Review

2.1 Intestine Physiology

The lower gastrointestinal tract is comprised of the stomach, small intestine, and large intestine.¹⁰ The epithelial surfaces of the small and large intestine have distinct microstructures that support their specialized functions (**Figure 1**).¹⁰ Consistent with its role in nutrient absorption, the surface area of the small intestine is maximized by repeating units of luminal projections, villi, and invaginations, crypts.¹⁰ The epithelium of the large intestine possesses only crypts.¹⁰ This is consistent with its role in housing a highly dense and diverse community of microbes that ferment indigestible carbohydrates and produce absorbable metabolites essential for overall host health.¹⁰ A muscular layer surrounds the intestine and through a series of wave-like contractions, referred to as peristalsis, food/waste is simultaneously mixed and propelled unidirectionally along the gastrointestinal tract.¹⁰

The intestinal epithelium serves as a barrier between the luminal contents and the body.¹⁰ The lumen environment can be very harsh, and this requires the rapid turnover of epithelial cells.^{10,11} To support rapid tissue regeneration, stem cells are compartmentalized in sheltered niches at the base of crypts.^{10,11} The differentiated cells of the intestine originate from stem cells and migrate up the crypt to the villi (small intestine) or luminal surface (large intestine) where they can perform their special functions.¹⁰ Absorptive cells are the most abundant cell type in the intestine.¹⁰ They are covered in microvilli to maximize the absorptive surface area.¹⁰ Other cell types include mucus-secreting goblet cells, hormone-secreting enteroendocrine cells, and in the small intestine, specifically, microfold cells which present luminal antigens.¹⁰

2.2 In Vitro Models

In this section, important milestones in the history of in vitro intestine model development (**Figure 2**) will be discussed.

2.2.1 2D Cell Line Cultures

The failure to sustain differentiated normal primary intestinal epithelial cells ex vivo has led to the extensive use of cell lines established from gastrointestinal tumours.^{12,13} The Caco-2 cell line is the most well-established and widely used intestinal epithelial cell line for modelling the intestinal epithelium because it exhibits spontaneous differentiation and barrier and transport functions.¹³⁻¹⁶

In the body, intestinal epithelial cells are fed nutrients from their basolateral side surface which is in contact with the ECM facing the blood supply.¹⁷ When cultured on an

impermeable substrate (e.g., polystyrene or glass) (**Figure 2**), Caco-2 cells are fed from their apical luminal surface and this can induce abnormal phenotypes.¹⁷ Transwell culture systems represent a more physiological model, as they are based on a porous membrane insert that is inserted into wells of standard multi-well cell culture plate. In these systems, Caco-2 cells are cultured on top of the insert allowing both the apical and basolateral surfaces access to nutrients leading to improved morphological and functional differentiation (**Figure 2**).¹³ Moreover, these systems can be used to assess transport across the epithelial monolayer.

Oral drug administration is the most common and most preferred method of drug administration because it does not require trained medical personnel, is non-invasive, and has high patient compliance.^{18,19} The major site of metabolism of orally administered drugs is the intestine.^{20,21} Drug metabolism in the intestine is largely determined by the types and abundance of cytochrome P-450 enzymes which are different between mice and humans and thus undermine the efficacy of preclinical animal models to predict human pharmacokinetics.^{20,21} For this reason, Caco-2 transwell systems are routinely employed by the pharmaceutical industry to model the human small intestine.²⁰ However, the extrapolation of data from these models to predict drug metabolism and drug-drug interactions in humans is challenged by the low expression of cytochrome P-450 enzymes.²⁰

Other limitations of Caco-2 models include: (1) they do not not distinctly represent the small intestine or colon, rather they display characteristics of both,¹³ (2) they can form

multilayer regions that resemble polyp-like masses,²² and (3) having originated from a tumour, they cannot be used to study the transformation of precancerous cells.

2.2.2 Organoids

Organoid models rely on intestinal stem cells that reside in the crypts of biopsied intestinal tissue to generate a self-organizing miniaturized intestine that possesses all the differentiated cell types of the native epithelium.²³ Intestine stem cells are cultured in a 3D Matrigel[®] matrix.²³ This growth environment promotes the formation of polarized cysts with a central lumen (**Figure 2**).²⁴ The closed, cyst-like morphology characteristic of intestinal organoids complicates their use in studies of nutrient transport, drug absorption, and microbe-epithelium interactions that require direct access to the inside of the organoid which is analogous to the intestinal lumen.^{25,26} Moreover, the accumulation of secreted material and shed apoptosed cells inside of the organoid is non-physiological and necessitates their regular passaging to maintain them in culture.^{27,28} In the body, debris/waste that is shed into the intestinal lumen is continuously cleared by luminal flow. To overcome the limitations presented by the closed, spherical geometry of organoids, model systems that “open-up” 3D organoids into 2D monolayers with an accessible lumen have been developed.^{25-27,29}

2.3.3 Microstructured Scaffolds

Work in the field of mechanobiology supports the existence of a multiscale structural hierarchy from organ structure to intracellular structure (i.e., the cytoskeleton) that physically integrates mechanical forces with the nucleus, suggesting a mechanism by

which tissue geometry can regulate gene expression.³⁰ Tissue geometry can also exert its effects on cell phenotype and behaviour in a mechanical-independent manner by defining cell proximity and the local concentrations of secreted factors.³¹⁻³³ Reconstituting the 3D geometry of the native intestine has been shown to increase mucin production and improve metabolic function of cultured Caco-2 cells, compared to 2D models.³⁴

A significant limitation of 2D cell culture models and organoids is their lack of representation of native intestine 3D geometries. For example, a distinguishing feature of the small intestine is the presence of villus structures which are finger-like luminal projections that increase the absorptive surface area of the small intestine. Small intestine organoids inappropriately resemble colon organoids in that no villus structures are present.

Villous atrophy is a characteristic of many intestinal disorders, such as celiac disease, Crohn's disease,³⁵ and acute radiation syndrome,³⁶ and is diagnosed by visual inspection of tissue obtained from a biopsy. Villous atrophy results in malabsorption leading to nutrient deficiencies, weight loss, and diarrhea.³⁵ Modelling villous atrophy can facilitate the development of medical counter measures.³⁷

A typical approach to creating intestine models with villus and/or crypt structures, is the fabrication of a hydrogel mould upon which epithelial cells can be seeded. Laser ablation and soft lithography have been used to generate a PDMS template for moulding calcium-alginate into a secondary dissolvable template.³⁸ This calcium-alginate template was used to mould collagen gel into villi, before it was sacrificed to generate the final microstructured collagen scaffold which can be placed on a transwell insert (**Figure 2**).^{34,38} In contrast to the subtractive manufacturing approach just described, Creff et al. used a

high-resolution additive manufacturing approach to reproduce the complex villus-crypt geometries of the small intestine³⁹ Specifically, they employed 3D stereolithography printing whereby a UV laser is directed in a specific path across a photopolymerizable hydrogel to induce cross-linking of polymers into a hardened layer.³⁹

2.2.4 Organ-on-a-chip

Since scientists began culturing cells *ex vivo*, the focus has been on the chemical environment of cells. By manipulating the chemical composition of the cell culture medium, gene expression can be regulated to control cell survival, proliferation, and differentiation. Organ form and function emerge from the dynamic and complex interactions between cells and their surroundings. This urges the development of *in vitro* models that not only represent the chemical environment, but also the diversity and spatial organization of cell types, and the physical (e.g., ECM microstructure) and mechanical (e.g., flow and cyclic strain) environment. This has been accomplished by the convergence of biological principles with engineering to create organ-on-a-chip systems. The wide appeal garnered by organ-on-a-chip systems is largely for two reasons, (1) they can model human physiology/pathophysiology more closely than 2D cell culture and animal models and (2) they offer unprecedented control over the components of living systems that are represented and thus make it easier to disentangle cause and effect relationships.

The first and most well-established organ-on-a-chip model of the human intestine, Gut-on-a-Chip,⁴⁰ (**Figure 2**) is a PDMS-based device with two stacked perfusable planar channels for independent 2D culture of epithelium and endothelium. Epithelial cells are

cultured on top of an ECM-coated porous membrane that separates the upper and lower compartment.⁴⁰ Cyclic suction applied to lateral hollow vacuum chambers is used to mimic peristaltic motions of the gut.⁴⁰ It has been shown that when cultured in a mechanically active environment reminiscent of the living intestine, Caco-2 cells can be stimulated to undergo spontaneous morphogenesis into villi-like structures and differentiate into four different epithelial cell types of the small intestine – absorptive, enteroendocrine, Paneth and Goblet cells.⁴¹

To enhance the physiological relevance of the Gut-on-a-Chip cultured with Caco-2 cells, historically independent organoid and organ-on-a-chip approaches to tissue modelling were combined to create a new category of in vitro model – the organoid-on-a-chip. Compared to Caco-2 chip models, intestinal organoid-on-a-chip models have gene expression profiles that more closely resemble the native human intestine.^{20,27} For example, the Duodenum Intestine-Chip showed levels of CYP3A4 expression comparable to levels observed in the human adult duodenum and thus could be used to better predict human pharmacokinetics.²⁰ Moreover, intestinal organoid-on-a-chip models exhibit higher functional fidelity.²⁷ The Intestine-Chip (**Figure 2**) displayed a 10 times higher concentration of mucus which plays a critical role in tissue homeostasis.²⁷ It has also been shown that when cultured in the Intestine-Chip, organoid-derived duodenal cells display gene expression profiles that are more similar to the living human duodenum than duodenal organoids.²⁷ This suggests that recapitulation of the native cellular environment which includes endothelium and mechanical stimuli, plays an important role in modulating cellular gene expression.

Most recently, an intestine organoid-on-a-chip system that incorporates a microstructured ECM scaffold has been reported.²⁸ Laser ablation was used to generate crypt-like cavities in a natural collagen-Matrigel[®] hydrogel (**Figure 2**). Sox2 staining showed the physiological spatial segregation of stem cells to the base of crypts.²⁸

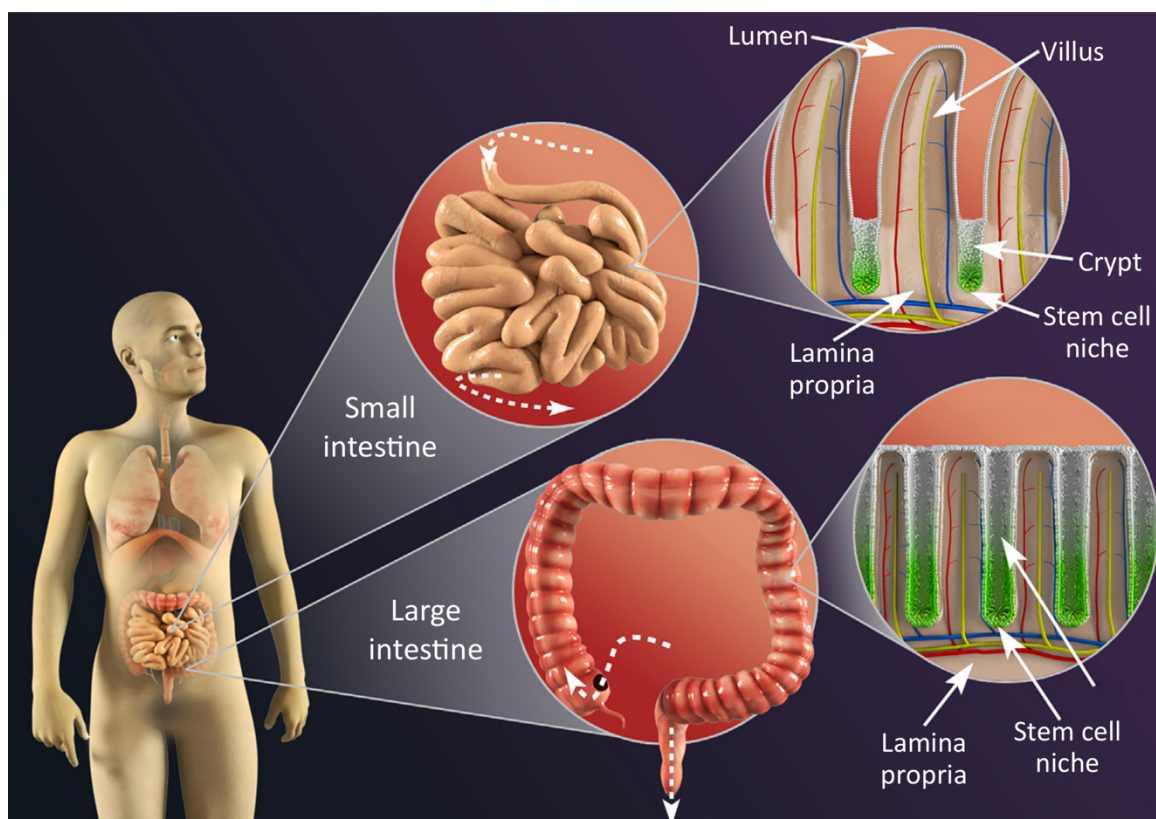


Figure 1. Anatomy of the small and large intestine. The epithelial surfaces of the small and large intestine have distinct microstructures that support their specialized functions. Stem cells (*green*) are enriched at the bases of crypts and differentiated cells (*white*) along the villi (small intestine) or luminal (large intestine) surface. The generic structure of the capillary bed within the intestinal mucosa is shown. Arterial (*red*) and venous (*blue*) circulation run parallel to each other. Lacteals are shown in *yellow*. Figure reproduced from Ref. 10.

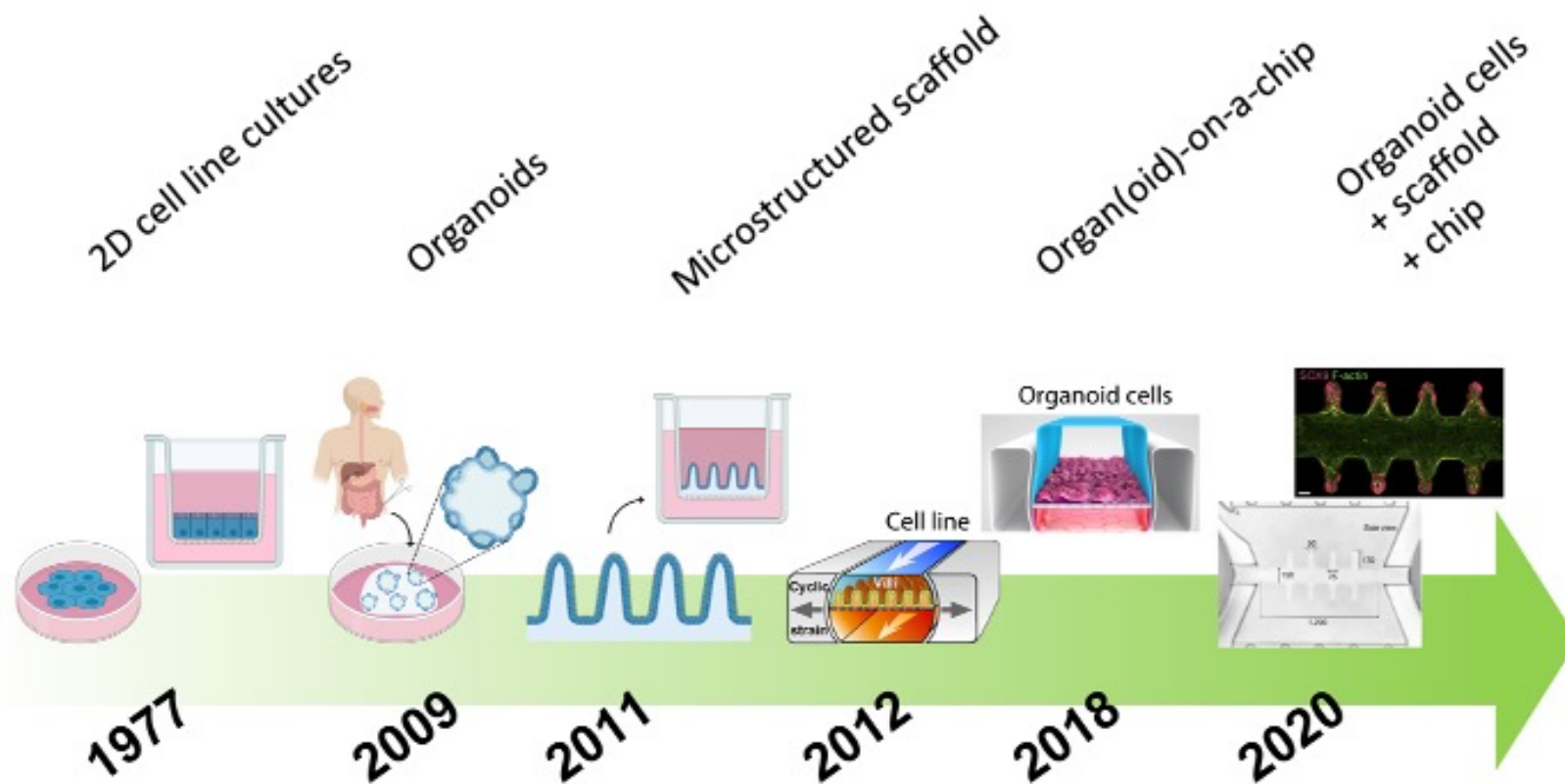


Figure 2. Timeline figure showing important milestones in the history of in vitro intestine model development. Organ-on-a-chip figures reproduced from Refs. 40 (Gut-on-a-Chip), 27 (Intestine-Chip, emulatebio.com), 28 (scaffold-guided homeostatic mini-intestine).

Chapter 3: Materials and Methods

3.1 IFlowPlate™ Fabrication

IFlowPlate™ is a custom 384-well plate with 128 independent microfluidic systems comprised of three-well units. The wells of each unit are connected by microfluidic channels allowing for the flow and exchange of fluid between wells. ECM pre-gel solution (with/without cells) is cast in the middle well and fluid flows from/into adjacent reservoir wells through the hydrogel. This is representative of interstitial flow in the body which is the flow of fluid around interstitial cells and through the ECM that surrounds tissues.⁴² Interstitial flow through ECM differs from open-channel flow through a conduit, such as a microfluidic channel or blood vessel, as fluid moves in all directions through the ECM and flow velocity is retarded by the high flow resistance of the ECM.⁴² “IFlowPlate™” is a portmanteau of the words “interstitial flow” and “plate.”

IFlowPlate™ is comprised of a standard black 384-well bottomless plate (Cat. # 82051-544, Greiner Bio-One) and a 11.6 cm x 7.5 cm x 0.081 cm (length x width x height) polystyrene sheet that serves as the plate bottom. The polystyrene sheet is patterned with a sacrificial polymer – poly(ethylene glycol) dimethyl ether (PEGDM, $M_n \sim 2,000$, Cat. # 445908, Sigma-Aldrich) using injection moulding. PEGDM is injected into a polydimethylsiloxane (PDMS) elastomer mould (SYLGARD™ 184 silicone elastomer clear, Cat. # 4019862, Dow) of an array of 128 channel-like grooves that bridge three adjacent wells. The PEGDM-patterned polystyrene sheet is glued to the bottomless plate and the PEGDM is subsequently dissolved with water to generate channels that connect three adjacent wells. This method represents a relatively inexpensive and technically facile

approach to integrating microfluidics with multiwell plates of different configurations (e.g., 6-well to 384-well plates) to deliver high-throughput experimental capabilities. The IFlowPlate™ fabrication method is described in detail in the sections below and a schematic illustrating the stepwise process is shown in **Figures 3** and **4**.

3.1.1 Photolithography for SU-8 Master Template Fabrication

The design for IFlowPlate™ was drawn using computer-aided software (AutoCAD, Autodesk). A photomask that met the specifications of the design was manufactured by an external supplier and used to fabricate the SU-8 master template on a silicon wafer (diameter: 150 mm, thickness: 0.65 mm, UniversityWafer, Inc., South Boston, MA) via conventional photolithography.

A thin film of light-sensitive epoxy-based material, SU-8 2050 negative photoresist (Cat. # Y1110720500L1GL, MicroChem, Westborough, MA) was spin-coated onto the silicon wafer and soft baked (**Figure 3A, step 1**). The patterned photomask was applied to the surface of the photoresist and the wafer was exposed to ultraviolet (UV) light (**Figure 3A, step 2**). Portions of the photoresist that were not masked were cross-linked by UV light and rendered insoluble by the liquid developer which the SU-8 was immersed in following a post-exposure hard bake step (**Figure 3A, step 3**). Fabrication of the SU-8 master template was done at the University of Toronto in a clean room equipped with a high-efficiency particulate air (HEPA) filter and UV filters. The SU-8 master template was placed inside a square bioassay dish (245 mm x 245 mm, Cat. # 29186-491, Corning) and secured using adhesive tape.

3.1.2 Soft Lithography for PDMS Mould 1 Fabrication

Unlike photolithography which relies on light exposure to transfer a pattern to a substrate, soft lithography relies on the physical deformation of a soft, elastomeric material (e.g., PDMS). To replicate the inverse of the SU-8 master features in PDMS, PDMS (SYLGARD™ 184) comprised of five parts by weight elastomer base and one part curing agent was poured on top of the SU-8 wafer in a bioassay dish. The PDMS was degassed under vacuum (-0.09 MPa gauge pressure, 30 minutes), cured at room temperature for 48 hours, and was cut and peeled from the SU-8 wafer (**Figure 3B, step 1**). This PDMS mould will hereafter be referred to as PDMS mould 1 to distinguish it from the PDMS moulds used as templates for injection moulding.

3.1.3 Replica Moulding for Fabrication of Epoxy and PDMS Moulds

PDMS mould 1 replicates the inverse features of the SU-8 master template and was used to create an epoxy mould that replicates the SU-8 master features in a process referred to as replica moulding. With the feature surface facing up, PDMS mould 1 was cut using a single edge blade. A 2 mm biopsy punch (Cat. # 21909-132, Integra York PA, Inc.) was used to punch a hole at the ends of each channel (**Figure 3B, step 2**). Punch waste was pushed through the holes using the fine tips of precision stainless steel tweezers and discarded. The holes in PDMS mould 1 generated posts in the epoxy mould which in turn generated holes in the cast and demoulded PDMS used as a template to pattern the polystyrene plate bottom. The holes in the PDMS template serve as ports for the injection of PEGDM and permit the escape of air during filling of microchannels with PEGDM.

The featureless surface of PDMS mould 1 was cleaned of debris using adhesive tape and activated using a BD-20A high frequency plasma generator (Cat. # 12011A, Electro-Technic Products, Chicago, IL) before being bonded to a cleaned and activated PDMS (SYLGARD™ 184) slab (**Figure 3B, step 3**). This PDMS slab was prepared by pouring 90 g of a mixture of 5:1 by weight PDMS elastomer base to curing agent into an empty square bioassay dish (245 mm x 245 mm, Cat. # 29186-491, Corning). After curing at room temperature, the PDMS was peeled from the dish and a single edge blade was used to cut a PDMS slab to the same length and width as PDMS mould 1. The two-layer PDMS mould 1 was treated with vaped trichloro (1H, 1H, 2H, 2H-perfluorooctyl) silane to deposit a “nonstick” film that would prevent irreversible bonding of the PDMS with epoxy (Section 3.1.5).

To fabricate the epoxy mould, a 15 cm x 9 cm x 5 cm (length x width x height) cardboard rectangular box was lined with a smooth aluminum foil insert. 18 g of PDMS (SYLGARD™ 184), prepared by mixing the elastomer base and curing agent in a ratio of 5:1 by weight, was poured into the box. The box was rotated to coat the bottom and half the height of the side walls with a thin film of PDMS. The liquid PDMS was partially cured at room temperature to achieve a semi-solid state with a viscosity and stickiness that resembles that of glue. Both faces (feature and featureless) of the silanized two-layer PDMS mould 1 were cleaned with adhesive tape to lift any debris. With the feature surface facing up, PDMS mould 1 was placed in the middle of the box on top of the glue-like PDMS. Following overnight incubation at room temperature, the glue-like PDMS was fully cured. 80 mL of equal parts by volume of epoxy resin and hardener (EasyCast® clear casting

epoxy, Cat. # 33016, Environmental Technology, Inc., Galesburg, MI) was vigorously mixed and cast on top of PDMS mould 1. After degassing under vacuum (- 0.09 MPa gauge pressure, 10 minutes), unpopped air bubbles that had risen to the surface of the resin were lifted off with a dry wooden craft stick and the epoxy was left to cure at room temperature. The epoxy mould was released from the aluminum foil and PDMS mould 1 was lifted from the epoxy mould using a double-ended microtapered stainless steel spatula and discarded (**Figure 3B, steps 4 – 5**). The epoxy mould was silanized with vapored trichloro (1H, 1H, 2H, 2H-perfluorooctyl) silane (See 3.1.5) and subsequently used to create PDMS moulds with holes and channel-like grooves to be used as templates for patterning the polystyrene plate bottom.

The PDMS mould for patterning the polystyrene IFlowPlate™ bottom was made by pouring PDMS (SYLGARD™ 184) comprised of thirty parts by weight elastomer base and one part curing agent into the IFlowPlate™ epoxy mould. The cast PDMS was degassed under vacuum (-0.09 MPa gauge pressure) for 1 hour to decrease the solubility of gas in the PDMS and remove air bubbles which could lead to defects in the cured mold. The PDMS mould was cured at 47 °C overnight and subsequently demoulded (**Figure 3B, steps 6 – 8**).

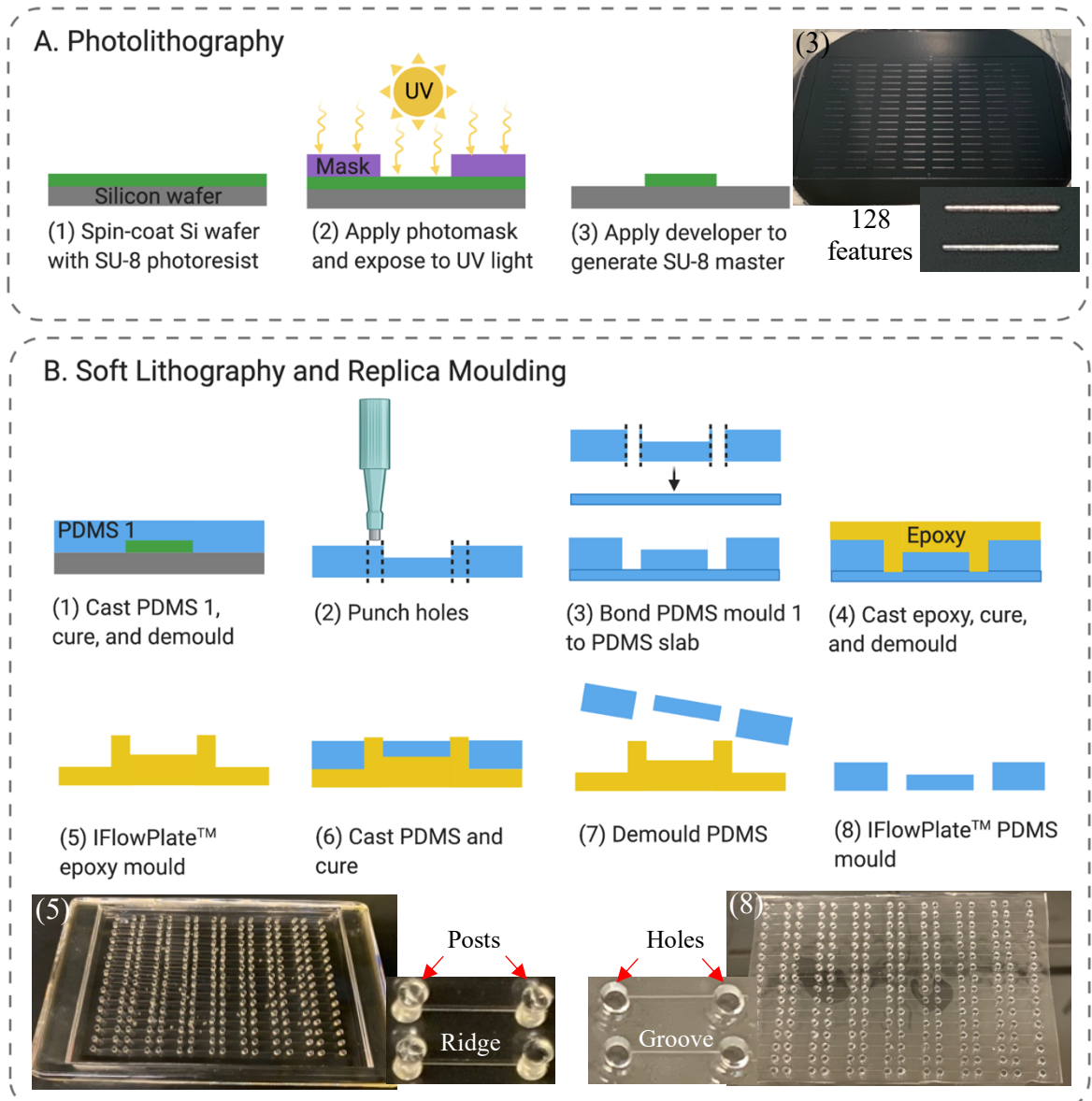


Figure 3. Schematic showing Part A and B of IFlowPlate™ fabrication. (A) Photolithography to generate SU-8 master template with 128 positive features on silicon wafer. (B) Soft lithography and replica moulding to generate PDMS moulds with negative features for patterning styrene sheets via injection moulding (See Part C, Fig. 4).

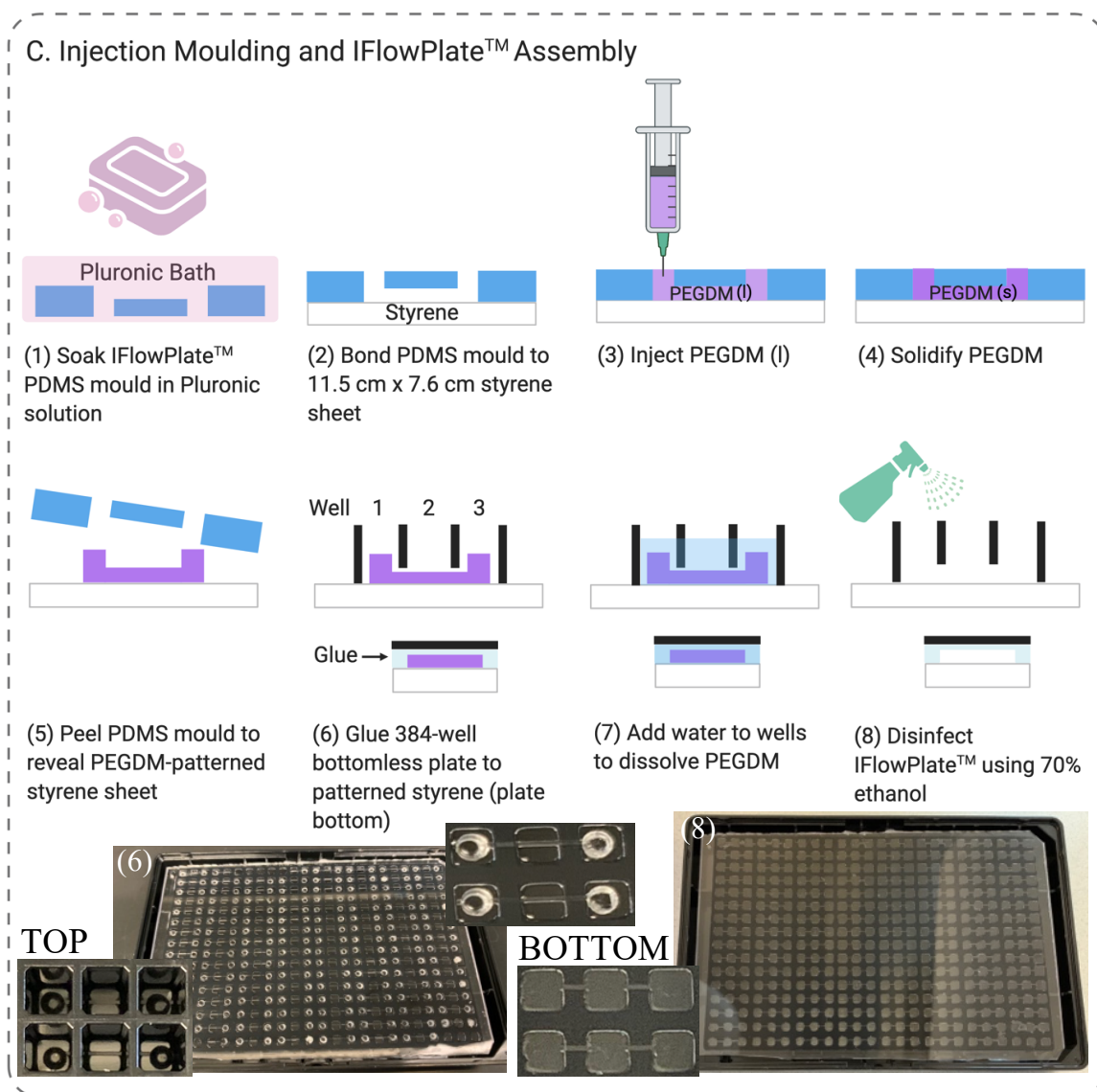


Figure 4. Schematic showing Part C of IFlowPlate™ fabrication (Figure 1 Cont'd). (C) Stepwise process to pattern a styrene sheet (plate bottom) with PEGDM via injection moulding and bond it to a 384-well bottomless plate to generate a custom 384-well microfluidic platform termed IFlowPlate™. IFlowPlate™ has 128 independent three-well microfluidic units. Channels between wells permit the flow and exchange of fluids.

3.1.4 Silanization

To prevent bonding of PDMS with epoxy, a “nonstick” film of vaporized trichloro (1H, 1H, 2H, 2H-perfluorooctyl) silane was deposited on (1) the two-layer PDMS mould used to make the epoxy mould (i.e., PDMS mould 1), and (2) the epoxy mould used to make PDMS moulds for patterning polystyrene plate bottoms. A square bioassay dish (245 mm x 245 mm, Cat. # 29186-491, Corning) with lid was used to create a closed chamber in which the liquid silane would vaporize at room temperature to generate a silane atmosphere. Due to the toxicity of trichloro (1H, 1H, 2H, 2H-perfluorooctyl) silane, silanization was performed inside a chemical fume hood. The procedures for silanizing two-layer PDMS moulds and epoxy moulds were nearly identical apart from how the moulds were secured to the square bioassay dish. PDMS moulds were secured to the dish using double-sided adhesive tape placed on the featureless surface of the two-layer mould. To secure epoxy moulds to the dish, masking tape was placed along the long and short edges of the mould. Two PDMS/epoxy moulds were secured to the dish one above the other in landscape orientation. The inside of the lid was covered with aluminum foil and 90 μ l of silane was deposited on the aluminum foil in equally spaced beads. Using a pipette tip, silane beads were streaked in a grid-like pattern for even exposure of mould surfaces to evaporated silane. To create the chamber, the dish was put inside the lid so that the moulds were suspended above the silane. Silanization time was 45 minutes and 1 hour for PDMS and epoxy moulds, respectively.

Using the procedure described, the vapor phase silane formed an opaque, white-coloured film on PDMS mould 1 indicating multi-layer deposition of silane molecules on

the PDMS surface. This proved to be problematic for downstream fabrication steps as the epoxy moulds generated from the silanized two-layer PDMS mould 1 also had an opaque, white-coloured film, as did the PDMS moulds generated from the epoxy moulds. These PDMS moulds were used as templates for patterning the polystyrene plate bottom via injection moulding and their precise alignment with a reference 384-well bottomless plate (See 3.1.6) relies on being able to see through a transparent mould to the reference plate. Moreover, polystyrene sheets patterned with PEGDM using opaque PDMS moulds showed substantial PEGDM leakage. It is speculated that the thick film of silane and/or mould of the surface roughness on the PDMS mould undermines bonding with the polystyrene sheet (See 3.1.6). Lastly, excess silane can fill in the negative features (e.g., holes) of a template mould and negatively change the dimensions of positive features (e.g., posts) of the replica mould.⁴³ This is particularly relevant for nanoscale features.

While silanes are known to chemically adsorb to material surfaces and form self-assembled monolayers, this process is usually highly variable.⁴³ Manipulating the volume of silane, duration of silanization, and ambient pressure by performing the reaction in a vacuum chamber/desiccator can help to improve the quality and consistency of silane deposition.⁴³ In addition to manipulating these parameters, a post-silanization processing step to remove silane can also help to achieve the desired result. Indeed, it was discovered serendipitously that adhesive tape works well to lift excess layers of silane molecules from PDMS mould 1 and restore its transparency. It is speculated that the ease with which the silane molecules could be removed is due to the disorganized multi-layer arrangement of silane molecules.⁴³ Therefore, following the removal of PDMS mould 1 from the silane

chamber, overlapping pieces of adhesive tape were placed on the feature face of the mould, smoothed over, and peeled off after 2 hours. This was repeated once more as lines of silane remained after the first tape application. These lines corresponded to the borders of tape pieces suggesting that the borders might be less adhesive than the interior of the tape.

3.1.5 Injection Moulding to Pattern Polystyrene Plate Bottom

Using a box cutter, a 0.081 cm optically transparent polystyrene sheet (Cat. # V16010, Jerry's Artarama) was cut to 11.5 cm x 7.6 cm to fit the dimensions of a black bottomless 384-well plate (Cat. # 82051-544, Greiner Bio-One). Using a single edge blade, the perimeter of the PDMS mould was trimmed to fit the dimensions of the polystyrene sheet and then bathed for 30 minutes in a 5% (w/v) solution of Pluronic[®] F-127 (Cat. # P2443, Sigma-Aldrich) in distilled water (dH₂O). With the mould submerged, features were tapped with fingertips to simultaneously purge inlet/outlet holes and microchannels of trapped air and fill them with amphiphilic Pluronic[®] F-127 solution (**Figure 4, step 1**). Pluronics[®] are tri-block co-polymers comprised of poly(ethylene oxide) (PEO) and poly(propylene oxide) (PPO).⁴⁴ These co-polymers self-assemble with the hydrophobic PPO block interfacing with the hydrophobic PDMS substrate and the hydrophilic PEO blocks interfacing with the water layer.^{44,45} This arrangement improves the hydrophilicity of the PDMS and deters other molecules from interfacing with the substrate via the large excluded volume and configurational entropic repulsion mechanisms.^{44,45} Previous studies have shown that the success of Pluronic[®] surface treatment is dependent on the solution concentration, and a concentration that does not exceed 5% - the critical micelle

concentration (CMC), is ideal to achieve a surface saturated with exposed PEO blocks (**Figure 5a**).⁴⁴ At concentrations below the CMC there is incomplete surface coverage (**Figure 5b**). At concentrations above the CMC, Pluronic[®] co-polymers can form bilayers with poorly exposed PEO blocks (**Figure 5c**), or micelle/aggregates (**Figure 5d**) that can be rinsed away. Modification of the PDMS mould surface chemistry using 5% Pluronic[®] F-127 solution was ideal for preventing irreversible bonding of the PDMS mould with the injected PEGDM or the polystyrene sheet.

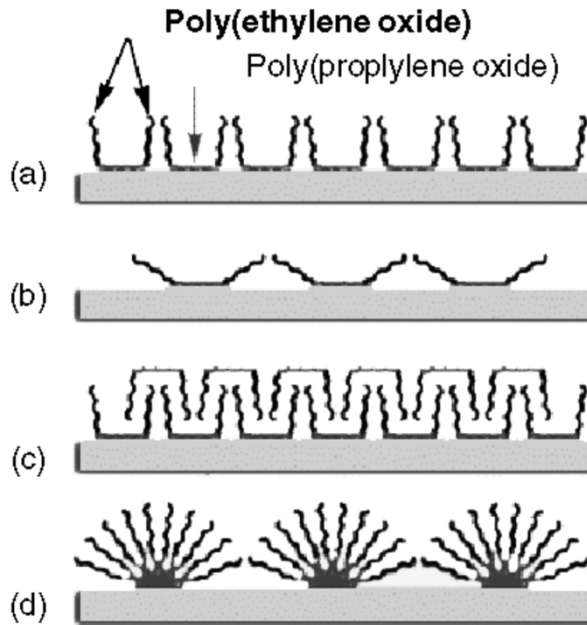


Figure 5. Schematic showing the possible arrangements of Pluronic[®] tri-block copolymers on a hydrophobic PDMS substrate. (a) high density monolayer, (b) low density monolayer, (c) bilayer, (d) micelle/aggregates. Figure is reproduced from Ref. 1.

The PDMS mould was rinsed with dH₂O and placed on top of low-linting absorbent tissue to dry. A 11.5 cm x 7.6 cm x 0.081 cm polystyrene sheet was plasma treated to functionalize the surface and enhance bonding of the PEGDM with the polystyrene sheet. Adhesive tape was used to lift debris off the feature surface of the dry PDMS mould before

it was superimposed onto the functionalized polystyrene sheet. For precise alignment of the mould features with wells, the polystyrene sheet was placed on a bottomless 384-well plate for reference of well positions. The PDMS mould was bonded with the polystyrene sheet (**Figure 4, step 2**). The device was lifted off the reference bottomless 384-well plate and exposed to vacuum (-0.04 MPa gauge pressure) for 15 minutes to remove air trapped between the PDMS mould and the polystyrene sheet.

The polystyrene sheet was patterned with poly (ethylene glycol) dimethyl ether (PEGDM, $M_n \sim 2,000$, Cat. # 445908-50G, Sigma-Aldrich) using injection moulding. The water solubility of PEGDM makes it attractive for use in applications requiring a sacrificial polymer, such as the fabrication of IFlowPlate™. Using a 10 mL syringe with a cropped 19 G needle, liquid PEGDM (melted at 65 °C) was injected into the inlet and outlet holes of the PDMS mould of an array of channel-like grooves that connect three adjacent wells (**Figure 4, step 3**). Because PEGDM quickly solidifies at room temperature, following injection, the device was placed in a 65 °C oven to return the PEGDM to a liquid state. With the PEGDM in a liquid state, the device was pulse centrifuged at 1000 RPM, and then incubated in a 65 °C vacuum oven at -0.05 MPa gauge pressure for 30 minutes. After incubation, the polystyrene sheet was pulse centrifuged at 1000 RPM and incubated at 65 °C for 30 minutes. This technique is a modification of a technique referred to as “vacuum filling” described in microfluidics literature.⁴⁶ When the polystyrene sheet is exposed to vacuum, displaced air in the channels will escape through the PEGDM liquid or the gas-permeable PDMS walls. Eventually, a pressure equilibrium will be reached and the pressure in the channels will be low. When the device is returned to atmospheric pressure,

there is higher pressure at the surface of the mould compared to inside the channels. This positive pressure differential pushes the PEGDM into the channels.

After channels were filled, excess PEGDM was removed from the inlet and outlet holes using a multichannel pipette attached to a vacuum aspirator. To minimize the risk of inadvertently aspirating PEGDM from the channel-like grooves, the pipette tips were oriented in the opposite direction of channels. To accelerate solidification of PEGDM, the polystyrene sheet was incubated at $-20\text{ }^{\circ}\text{C}$ for 10 minutes. The PDMS mould was peeled from the styrene sheet (**Figure 4, steps 4 – 5**) revealing the patterned $300\text{ }\mu\text{m} \times 150\text{ }\mu\text{m}$ PEGDM features. Localized debonding/incomplete bonding at the PDMS-polystyrene interface due to contaminants or air bubbles can result in PEGDM leakage. Patterned polystyrene sheets were inspected prior to assembly of IFlowPlate™. Leaked PEGDM on the back and edges of the polystyrene sheet was cleaned with a small, wetted polyfoam paint brush. For more delicate cleaning of leaked PEGDM around patterned features, a wetted pointed end tortillon (i.e., paper pencil used by artists for blending) was used.

3.1.6 IFlowPlate™ Assembly and Disinfection

To assemble IFlowPlate™, a black 384-well bottomless plate was bonded to the PEGDM-patterned polystyrene sheet using high-viscosity PDMS (SYLGARD™ 186 silicone elastomer clear, Cat. # 2137054, Dow) comprised of 10 parts by weight elastomer base and one part curing agent. PDMS is widely used in biomedical applications because it has many desirable properties including optical transparency, biocompatibility, and gas permeability.⁴⁷ It is because of these properties that PDMS was chosen to bond the

polystyrene plate bottom to the 384-well bottomless plate. The PDMS glue encases the PEGDM and when the PEGDM is dissolved, the PDMS will form the walls of the microfluidic channel, and thus be in direct contact with culture medium and cells.

5 g of high-viscosity PDMS (SYLGARD™ 186) was evenly spread in a thin layer across a glass slide (large glass microscope slide, Cat. # 260233, Ted Pella, Inc., Redding, CA) that was cut to the approximate size of the polystyrene sheet. For greater control over the amount of glue spread on the glass slide and thus transferred to the bottomless plate, two pieces of masking tape were layered on each long edge of the glass slide before spreading glue. The glass slide was placed on a plasma-treated 384-well bottomless plate to facilitate the transfer of the PDMS glue to the bottomless plate. The increased surface wettability of the plasma-treated bottomless plate improves the spread of the PDMS glue. The glass slide was lifted off of the bottomless plate and the PEGDM-patterned polystyrene sheet was aligned with the bottomless plate and then dropped into position. Gentle compression was used to bond the polystyrene sheet to the 384-well bottomless plate. A clean glass slide was placed on top of the polystyrene sheet and clamped to the assembled IFlowPlate™ using four extra-large paper clamps. After overnight curing of the PDMS glue at room temperature, the clamps and glass slide were removed (**Figure 4, step 6**). Glass slides with PDMS were cleaned with acetone and re-used.

To dissolve the PEGDM and reveal channels that connect units of three adjacent wells, dH₂O was added to the wells (**Figure 4, step 7**). The plate was pulse centrifuged at 40 G to simultaneously fill wells/channels with water and purge trapped air. The plate was placed on a rocker and incubated at 37 °C for 1 – 2 days before the PEGDM-dH₂O solution

was aspirated out. To disinfect IFlowPlate™ in preparation for cell culture, the plate was placed inside a square bioassay dish inside the biosafety cabinet. The bioassay dish, and IFlowPlate™ lid and wells were filled with 70% (v/v) ethanol. The bioassay dish was covered with the lid to minimize evaporative loss of ethanol and was left undisturbed for 1.5 to 2 hours (**Figure 4, step 8**).

Fabrication flaws that affect the performance of IFlowPlate™ microfluidic systems should be identified prior to cell culture. Each fabricated IFlowPlate™ was inspected for glue-related defects, such as too little or too much glue, that could result in leaking wells or obstructed channels, respectively. Firstly, the open connection between three-well units was confirmed by aspirating liquid from the middle well and observing a negative change in the liquid level in the connected inlet and outlet wells. Secondly, dried plates were inspected for incomplete seals around wells and channels. The alphanumeric codes of three-well units that met quality standards were recorded and these microfluidic systems were available for cell culture. To avoid edge of plate effects, microfluidic systems at the plate periphery were not selected for cell culture.

3.2 SynoPlate™ Fabrication

SynoPlate™ is a custom 384-well plate with 40 independent microfluidic systems. Each microfluidic system is a nine-well unit comprised of a triad of three-well units. Aside from having three times the number of interconnected three-well units, the most notable attribute of SynoPlate™ that distinguishes it from IFlowPlate™, is the integration of biologically inspired tissue-specific scaffolds. These scaffolds are tubular cavities that are

patterned in a fibrin-based hydrogel and serve as a compliant boundary that guides the assembly of cells into tissues that resemble their *in vivo* counterparts. Cell attachment to the ECM substrate supports open-channel flow through the cell-lined conduits. Each three-well unit is comprised of a dedicated inlet and outlet reservoir well connected via channels to a tissue scaffold in the centre well where the triad of three-well units converge. This configuration enables three compartmentalized, yet biologically interactive tissues with unique architectures, cell types, media requirements, and opportunities for independent sampling of effluent. The intestine SynoPlate™ has three independently addressable tissue scaffolds that guide the assembly of cells into a tubular intestine with crypt-like invaginations, and a branching vascular network above and below the intestine tube (Figure 6).

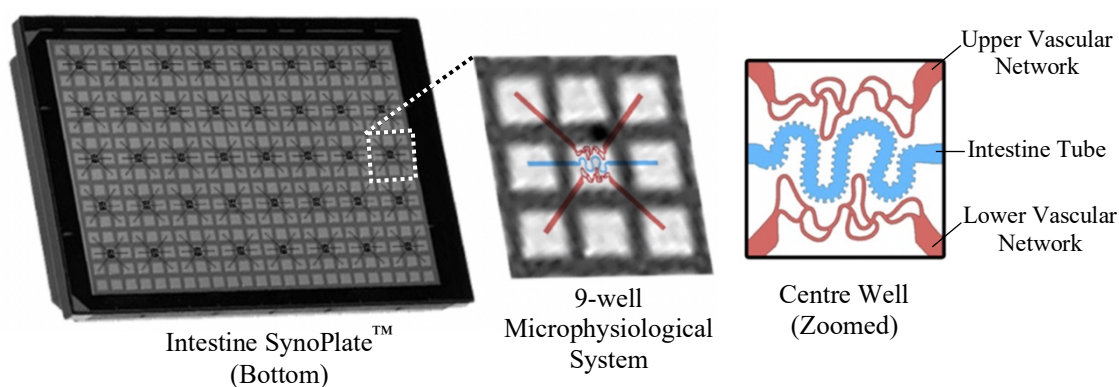


Figure 6. Exploded diagram showing one of the 40 microfluidic systems of the intestine SynoPlate™. Each microfluidic system is comprised of a triad of three-well units. Each three-well unit has a dedicated inlet and outlet reservoir well connected via channels to a tissue scaffold in a shared centre well. This configuration allows tissue scaffolds to be populated with different cell types (e.g., endothelial or intestinal epithelial cells) that can be nourished with different media. Tissues converge in the centre well (zoomed view) to form a microscale organ with intestinal tissue and supportive vasculature embedded in an extracellular matrix. Figure adapted from a grant proposal prepared and submitted by Boyang Zhang, Ph.D.

SynoPlate™ fabrication is like IFlowPlate™ fabrication with a few key differences that will be highlighted in the text and accompanying figures of this section. The 11.6 cm x 7.5 cm x 0.081 cm polystyrene sheet that serves as the bottom of SynoPlate™ was sequentially patterned with two different sacrificial materials. First, the polystyrene sheet was patterned with a 3% (w/v) solution of sodium alginate (Alginic acid sodium salt from brown algae, low viscosity, Cat. # A1112, Sigma-Aldrich) in dH₂O. Alginate is a polysaccharide derived from marine algae and is composed of 1,4-linked β-D-mannuronic acid (M) and α-L-guluronic acid (G) residues.^{48,49} Sodium alginate is dissolved in water to form a viscous solution that can be gelled at room temperature in the presence of divalent metal cations, such as Cu²⁺, Ba²⁺, and Ca²⁺.^{48,49} With the SynoPlate™ PDMS mould bonded with the polystyrene sheet, the device was submerged in a bath of 3% (w/v) sodium alginate solution (**Figure 7, step 2**). Features were filled with alginate using the vacuum filling approach described in Section 3.1.6, with all steps occurring at room temperature. To minimize spillage of alginate solution inside the centrifuge during pulse centrifugation, a custom lid was made for the one-well plate into which the alginate solution was poured. To prepare this lid, 41 g of PDMS (SYLGARD™ 184) comprised of forty parts by weight elastomer base and one part curing agent was poured into the one-well plate lid and cured at room temperature. Using three elastic bands, the custom PDMS lid was secured to the one-well plate filled with alginate. After a 40-minute incubation of the device in the alginate bath at atmospheric pressure, all features were filled (**Figure 7, step 2**). The alginate solution was discarded, and excess alginate was aspirated from inlet and outlet holes using a multichannel pipette attached to a vacuum aspirator.

The device was submerged in a bath of 5.5% (w/v) calcium chloride (Calcium chloride dihydrate, MW 147.01, Cat. # 223506, Sigma-Aldrich) and pulse centrifuged at 1000 RPM. Unpopped air bubbles at the surface of the inlet/outlet holes were eliminated by injecting calcium chloride solution into the inlet/outlet holes using a syringe and 19 G needle. In the presence of divalent calcium ions, alginate polymers are cross-linked, and a sol-gel transition occurs almost immediately (**Figure 7, step 3 – 4**). The gelation takes place via an ion-exchange mechanism in which monovalent sodium cations are exchanged for divalent cations that induce association between GG blocks of neighbouring polymer chains.^{48,49} The resulting structure of the calcium-alginate gel is popularly represented by the “egg-box model” (**Figure 8A**).⁴⁹ Among different divalent metal ions, such as copper and barium, the ability for alginate to bind calcium is comparatively weaker.⁴⁸ Calcium was chosen to induce gelation because it allows rehydration/swelling in the presence of a sodium ion-containing solution (e.g., fibrin pre-gel solution) to occur with ease – this is desirable for our application. After overnight incubation at room temperature, the calcium chloride solution was discarded, and the device was cleaned by briefly immersing it in a dH₂O bath to gently lift excess calcium-alginate gel from the PDMS and back surface of the device for removal. Excess water was absorbed with tissue before the device was placed inside the fume hood under a stream of compressed air to accelerate dehydration of the calcium-alginate gel. After 48 hours of drying, calcium-alginate features were microscopically examined (**Figure 7, step 5**). Dehydrated calcium-alginate features exhibited volumetric shrinkage which has been attributed to the formation of “egg-box multimers” resulting in more tightly packed polymers.⁵⁰ During air-drying, the increase in

calcium ion concentration induces the association of junction zones (i.e., where two alginate chains cross-link to form an “egg-box dimer”) and therefore, the formation of “egg-box multimers” (**Figure 8B**).^{49,50} Dehydrated calcium-alginate features patterned on the polystyrene sheet were encapsulated with PEGDM using injection moulding as described in Section 3.1.6. SynoPlate™ was assembled as described in Section 3.1.7.

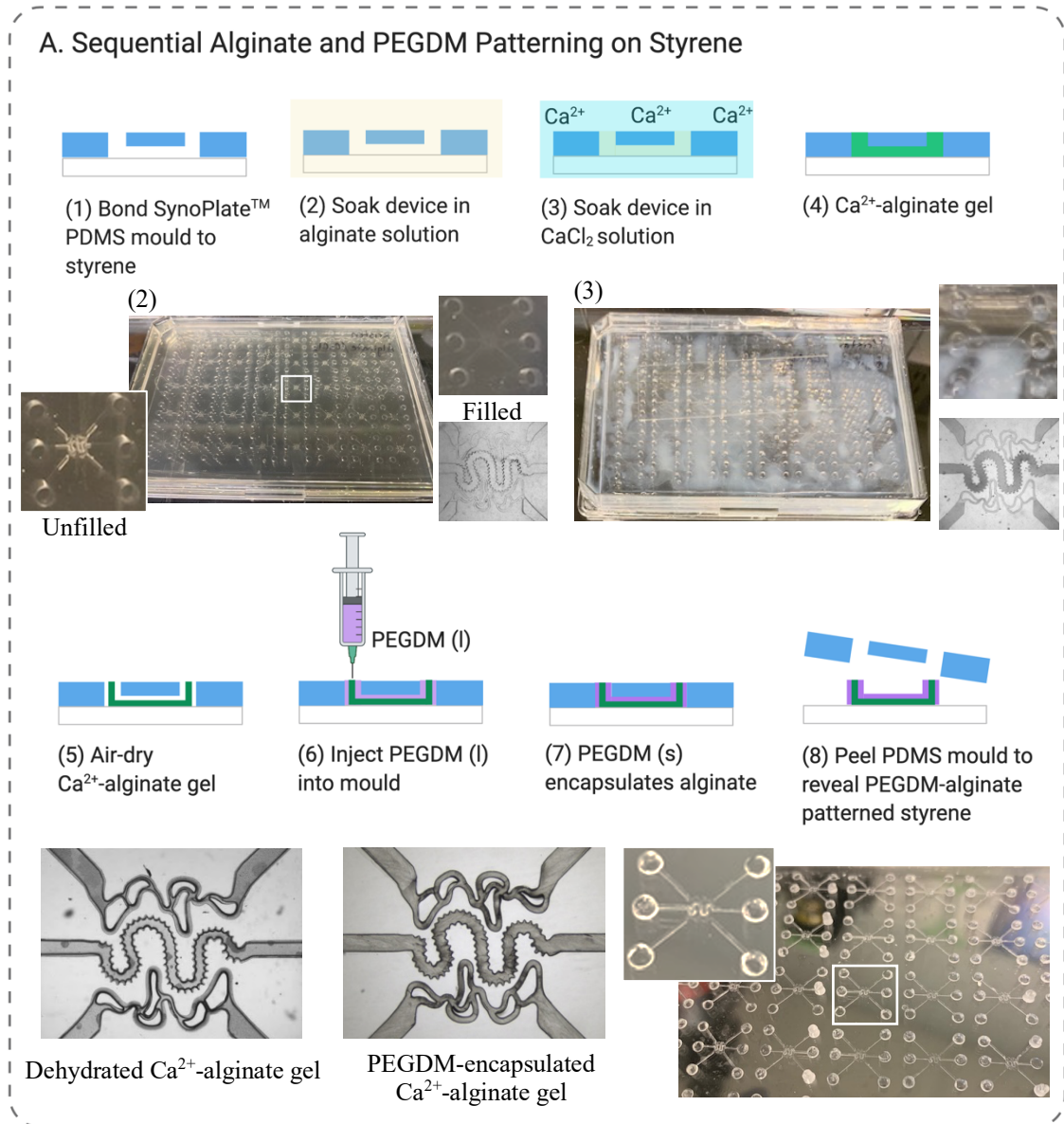


Figure 7. Schematic showing Part A of SynoPlate™ fabrication. Stepwise process to sequentially pattern a styrene sheet with alginate and PEGDM to generate a custom 384-well microfluidic platform termed SynoPlate™.

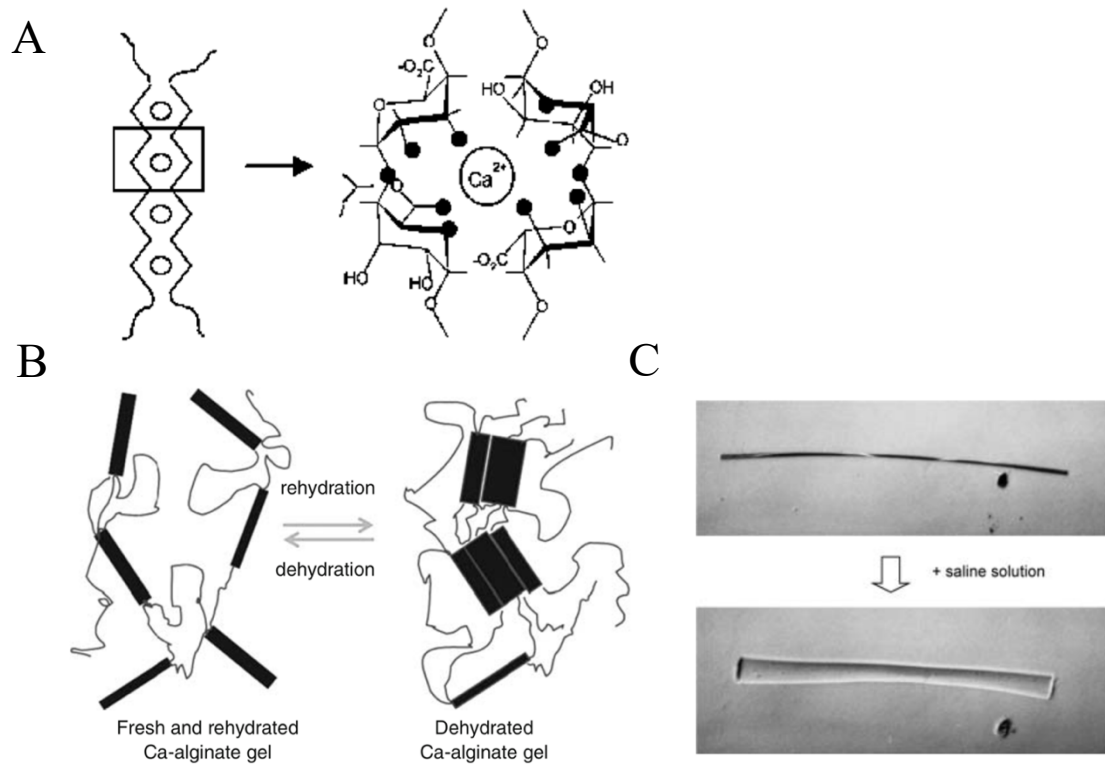


Figure 8. Structure and swelling behaviour of calcium-alginate gel. Schematic illustration of the (A) egg-box model for calcium-alginate gel and (B) association and disassociation of junction zones in calcium-alginate gel during dehydration and rehydration, respectively. (C) Photomicrograph of the swelling behaviour of a calcium-alginate fibre in saline solution, 200X. Figure (A) is reproduced from Ref. 49. Figure (B) is reproduced from Ref. 50. Figure (C) is reproduced from Ref. 48.

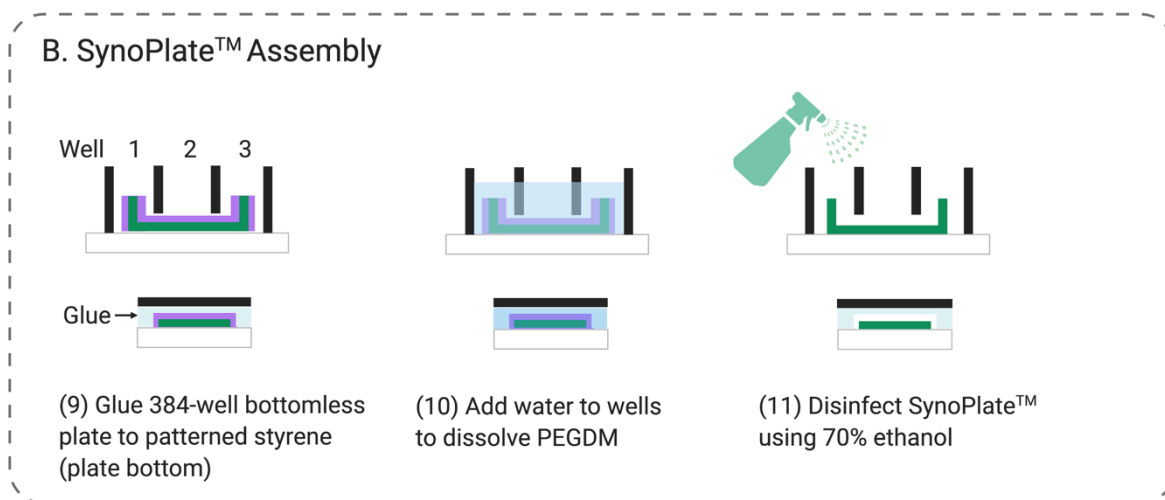


Figure 9. Schematic showing Part B of SynoPlate™ fabrication. To assemble SynoPlate™, alginate/PEGDM-patterned styrene sheet is bonded to a standard 384-well bottomless plate using high viscosity PDMS as glue. Water is added to the wells to dissolve PEGDM. Finally, SynoPlate™ is disinfected with 70% (v/v) ethanol in preparation for cell culture.

3.3 SynoPlate™ Cell Culture

SynoPlate™ was not used for any cell culture experiments; however, this paragraph will provide a brief description of how the plate is intended to be used as it gives context for work to minimize breakage of patterned calcium-alginate features (See Section 4.3.2). To prepare SynoPlate™ for cell culture, PEGDM is dissolved with dH₂O and the plate is disinfected with 70% (v/v) ethanol (**Figure 9, steps 10 – 11**). Acellular fibrin pre-gel solution is cast in the centre well and encapsulates the patterned calcium-alginate feature. Fibrin pre-gel solution is a source of sodium ions as its primary constituent, fibrinogen, is dissolved in 1 X Dulbecco's phosphate buffered saline (D-PBS, without calcium or magnesium, Cat. # 311-425-CL, WISENT Inc., Saint-Bruno, Quebec). In the presence of competing monovalent sodium ions which are non-crosslinking, the weak electrostatic egg-box dimer-dimer interactions are readily disrupted and the calcium-alginate gel is

rehydrated and swells (**Figure 8C**).⁵⁰ As a result, the calcium-alginate feature, initially patterned in two-dimensions, lifts from the polystyrene plate bottom and changes volume and shape in three dimensions inside of the fibrin gel.

The appeal of this approach, which combines 2D patterning with the stochasticity of swelling kinetics, is that it yields microtissues of highly reproducible shapes and sizes while introducing some anatomical variability. This parallels the robustness and plasticity that is characteristic of tissue morphogenesis during human development to generate organs of stereotypical, but not identical size and shape. As a high-throughput platform that could be applied to testing the safety and efficacy of drugs – a “clinical-trial-on-a-plate”, the inherent variability in SynoPlate™ microtissues is an attribute that is embraced as it simulates inter-individual anatomical variation. The importance of representing population-level variation is underscored by the drug approval process which involves large-scale randomized clinical trials to better estimate population-level treatment effects.

After gelation of the fibrin pre-gel solution, the re-hydrated calcium-alginate gel is degraded by perfusing D-PBS through the tissue networks. In the presence of a high concentration of salt ions, “egg-box dimers” are disrupted and the alginate polymers uncrosslink and dissolve in aqueous solution. After the system is flushed, a moulded cavity within the fibrin gel is revealed. These independently addressable tissue-specific cavities are populated with endothelial and intestinal epithelial cells to form a 3D microtissue with perfusable branched vasculature and an intestine tube. Overall, the (1) water insolubility of the cross-linked alginate which enables the calcium-alginate gel to remain intact during PEGDM dissolution in water and 70% (v/v) ethanol disinfection, (2)

dehydration/rehydration dynamics and (3) mild degradation conditions, make calcium-alginate gel an idealistic sacrificial material for the described application.

3.4 IFlowPlate™ Cell Culture

IFlowPlate™ is an array of 128 microfluidic systems each consisting of two reservoir wells connected via channels to a middle tissue well with a fibrin-based hydrogel⁵¹ (**Figure 10**). Hydrogel-encapsulated endothelial cells self-assemble into a vascular network. Anastomotic connections of vessels with microfluidic channels enables perfusion of the vascular network. The reservoir wells hold culture medium that is passively and bidirectionally circulated between the three wells using gravity-driven flow sustained by placing the plate on an interval rocker. Intestine cells are cultured as a monolayer on the surface of the hydrogel to give access to the luminal surface and emulate the anatomical organization of the intestine and associated microcirculation.

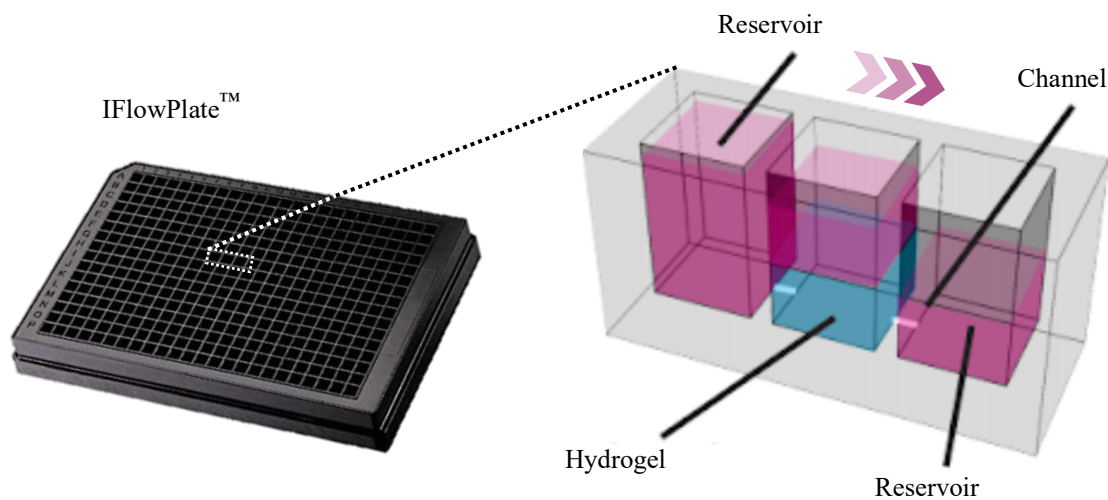


Figure 10. Exploded diagram showing one of the 128 microfluidic systems of IFlowPlate™. Each microfluidic system is comprised of three adjacent wells connected by channels. The middle well contains an ECM-based hydrogel. The height of the medium column in reservoir wells is manipulated to establish a hydrostatic pressure gradient that stimulates the passive flow of fluid down the gradient (i.e., from higher pressure to lower pressure). For indefinite perfusion, the plate is placed on an interval rocker platform that continuously re-establishes the medium height differential between reservoir wells. Figure adapted from Ref. 51.

3.4.1 Cells and Culture Conditions

Endothelial Cells

Green fluorescent protein-expressing human umbilical vein endothelial cells (GFP-HUVECs) were purchased from Angio-Proteomie (Cat. # cAP-0001GFP) and cultured in endothelial cell growth medium 2 (ECGM-2, Cat. # C-22111, PromoCell). HUVECs are the most widely studied and commonly used human endothelial cell type.⁵² Of note, more than half of the studies involving endothelial cell assembly in fibrin gel have used HUVECs.⁵² Given the interspecies differences in endothelial cell biology, the popularity of HUVECs can be explained by their human relevance and the ease with which they can be

acquired and cultured.⁵² Indeed, HUVECs are isolated from the veins of umbilical cords which are frequently discarded as biomedical waste, and they can be expanded to very large numbers in vitro. The stable expression of GFP by HUVECs enables real-time fluorescence imaging of live cells for continuous monitoring of vascular network formation and anastomoses with channels. For these reasons, GFP-HUVECs were exclusively used for the development of IFlowPlate™ vascular models.

Fibroblasts

Human normal lung fibroblasts (ATCC® Cat. # PCS-201-013™, American Type Culture Collection, Manassas, VA) were cultured in Dulbecco's modified Eagle's medium (DMEM, Cat. # 319-005-CL, WISENT Inc., Saint-Bruno, Quebec) supplemented with 10% (v/v) fetal bovine serum (FBS, Cat. # 098-150, WISENT Inc., Saint-Bruno, Quebec), 1% (v/v) 1M HEPES (Cat. # 330-050-EL, WISENT Inc., Saint-Bruno, Quebec) and 1% (v/v) Penicillin-Streptomycin (Pen-Strep, 450-200-EL, WISENT Inc., Saint-Bruno, Quebec). Human normal lung fibroblasts are commonly cocultured with endothelial cells to support the spontaneous formation of microvascular networks in vitro.⁵³⁻⁵⁵ Fibroblasts stimulate the formation of microvascular networks and sustain them through the release of paracrine factors (e.g., hepatocyte growth factor), deposition of ECM proteins,^{54,55} and pericyte-like behaviour, as demonstrated by their close physical association with endothelial tubes.^{53,56} For these reasons, IFlowPlate™ vascular models were established by coculturing human normal lung fibroblasts and GFP-HUVECs in a 3D fibrin-based matrix.

Caco-2 Cells

For modelling the intestine, the human intestinal colorectal adenocarcinoma cell line Caco-2 (C2BBE1, ATCC® Cat. # CRL-2102™, American Type Culture Collection, Manassas, VA) was used. The original Caco-2 cell line represents a heterogeneous population of cells of which only a subset assemble a brush border upon reaching confluence.⁵⁷ The presence of an apical brush-border membrane is a morphological indicator of a polarized and differentiated intestinal epithelial cell.⁵⁸ Caco-2 BBE1 cells were cloned from the parental Caco-2 cell line to create a homogeneous population of brush border expressing (BBE) cells.⁵⁷ Relative to their sister clone Caco-2 BBE2, BBE1 cells achieve confluency with less culture time and are more easily dissociated in the presence of trypsin during cell passaging.⁵⁷ For proof-of-concept studies in a nascent microfluidic platform, such as IFlowPlate™, the retention of some stem cell-like properties makes Caco-2 cells a valuable surrogate for primary intestinal tissue which is more difficult to acquire and resource intensive and costly to culture. Caco-2 BBE1 cells, hereafter referred to as Caco-2 cells, were cultured in DMEM (with glucose and L-glutamine) supplemented with 10% (v/v) FBS, 1% (v/v) 1M HEPES, and 1% (v/v) Pen-Strep. This formulation will hereafter be referred to as complete DMEM.

Cell Passage Number

In all experiments, cells between passage 2 and 4 were used, as passage number is associated with phenotypic and genotypic changes which could have experimentally

relevant consequences. For example, it has been reported that HUVECs older than passage 5 form tip cells and intracellular vacuoles less frequently and tubulogenesis is delayed.⁵⁹

A study of Caco-2 characteristics and passage number has shown that as passage number increases, growth rate, transepithelial electrical resistance (TEER) and sucrase activity also increase.²² Another study reported that early (P22) and late (P198) passage Caco-2 cells can differ as much as 50-fold in their glucose consumption rate and expression of sucrase-isomaltase.⁶⁰

Culture Conditions for Cell Lines

Cells were cultured in a humidified 37 °C, 5% CO₂ incubator. Cells were expanded in T75 flasks until approximately 80% confluent. For GFP-HUVEC expansion, T75 flasks were coated with 10 mL of 0.2% bovine skin, type B gelatin (Cat. # A9418, Sigma-Aldrich,) in D-PBS for 30 minutes at 37 °C.

For IFlowPlate™ bi- and tri-culture experiments involving GFP-HUVECs and fibroblasts, and GFP-HUVECs, fibroblasts, and Caco-2 cells, respectively, a 1:1 mixture by volume of ECGM-2 and complete DMEM was used for culture. For all experiments with fibrin gel, cell culture medium was supplemented with 1% (v/v) 2 mg/mL aprotinin (Aprotinin, Bovine Lung, Crystalline, Cat. # 616370, Sigma-Aldrich) in dH₂O to slow protease-mediated fibrin degradation.

3.4.2 Hydrogels

Hydrogels are three-dimensional networks of hydrophilic polymers that can hold large amounts of water.⁶¹ The cross-linkable nature of the polymers prevents their dissolution and maintains the three-dimensional structure of the hydrogel.⁶¹ The high water content and insolubility of the cross-linked polymers gives hydrogels physical characteristics similar to ECM of soft tissues making them well-suited for applications in research (e.g., 3D cell culture) and medicine (e.g., contact lenses, drug delivery systems, and scaffolds for tissue engineering).^{62,63}

Hydrogels can be broadly classified as natural, synthetic, or semi-synthetic according to the origin of polymer constituents.⁶³ Natural polymers derived from living tissue present high biofunctionality.⁶² Natural polymers (1) assemble into supramolecular architectures (e.g., fibres) that resemble the topography of native ECM, (2) contain cell-binding motifs that support cell adhesion, migration, and activation of intracellular signaling pathways, and (3) are recognized and metabolically processed by cells allowing for cell-mediated remodelling and release of sequestered bioactive molecules (e.g., growth factors).^{62,64} Therefore, natural hydrogels can provide a bioinstructive environment in which cells can proliferate, differentiate, and develop into tissues that more closely resemble the native tissue.⁶²

The structural and mechanical properties of natural hydrogels can be manipulated to elicit different cellular responses. For example, the microstructure (e.g., fibre thickness and density) of fibrin gels is determined by fibrinogen concentration and gelation time which is significantly affected by thrombin concentration.⁶⁵ Manipulation of these parameters can be used to modulate matrix (1) pore size, and thus transport of

macromolecules and nutrients for growth, survival, and cell-cell communication, and (2) stiffness.^{65,66} The effect of fibrin stiffness on cell behaviour has been widely investigated. Broguiere et al. showed that intestinal organoid expansion, defined as the frequency of cyst formation, was optimal in lower fibrinogen concentrations which corresponded to lower stiffness.⁶⁷ Duong et al. showed that based on proliferation and spreading morphology, fibroblasts favoured fibrin matrices of lower stiffness.⁶⁶

In this work, a diversity of cross-linkable natural polymers that can reversibly form gels in response to physical (e.g., temperature), chemical (e.g., ions, pH), or enzymatic stimuli (e.g., thrombin) were used (**Figure 11**). Importantly, while distinct triggers are used to initiate polymerization, the polymers have in common polymerization conditions mild enough to take place in the presence of cells without inducing cytotoxic effects. Section 3.2 introduced alginate which undergoes a reversible sol-gel transition in the presence of divalent metal ions (**Figure 11A**). Alginate hydrogel was used as a sacrificial material to mould fibrin gel into pre-defined geometries that when populated with cells guide the formation of 3D microtissues. This section will discuss the use of natural hydrogels, such as fibrin, Matrigel[®], and collagen, as mimetics of soft tissue ECM for cell culture. Particular attention will be paid to the preparation of a fibrin-Matrigel[®] composite gel to serve as a suitable scaffold for establishing a vascular intestine model in IFlowPlate[™]. The application of gelatin to temporarily seal IFlowPlate[™] microfluidic channels will also be discussed.

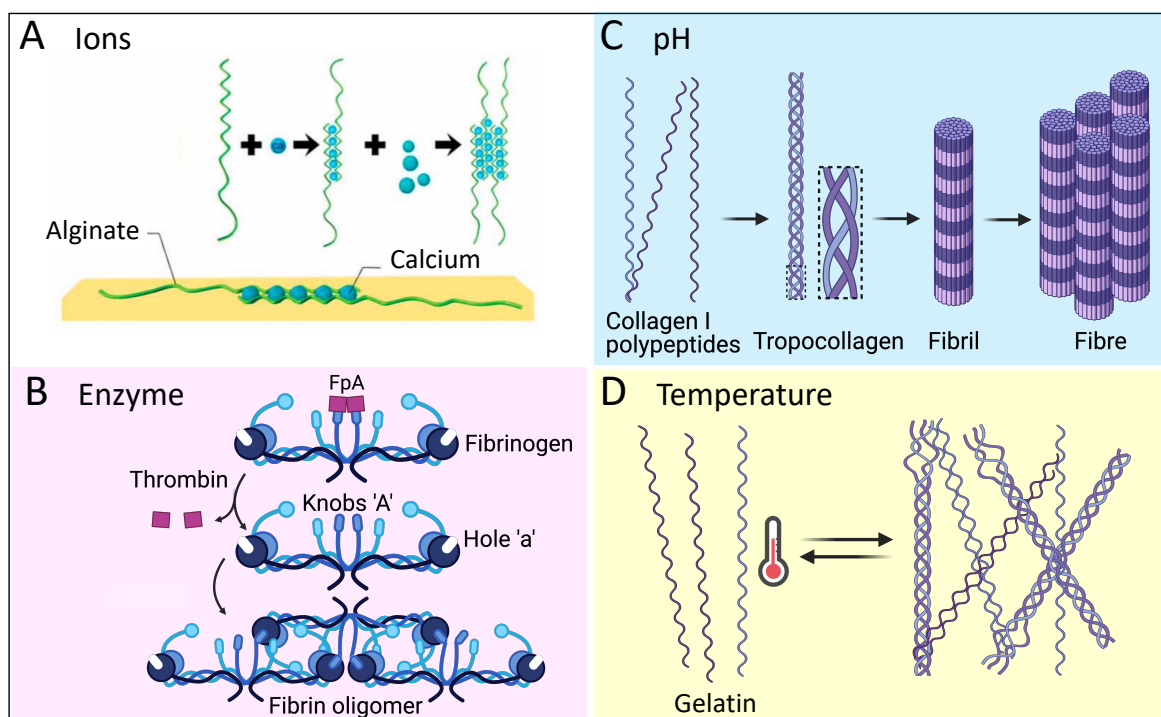


Figure 11. Cross-linkable natural polymers can reversibly form hydrogels in response to physical, chemical, and enzymatic stimuli. (A) Alginate cross-links in the presence of divalent calcium ions via an ion-exchange mechanism. Figure reproduced from Ref. 42. (B) Enzyme-activated polymerization of fibrin occurs when thrombin cleaves A fibrinopeptides (FpA) exposing knobs that interact with complementary holes on neighbouring fibrin monomers. (C) Hierarchical self-assembly of collagen I occurs at neutral pH. (D) Intermolecular crosslinks between aqueous gelatin (from bovine skin) form upon cooling (< 30 °C). Matrigel® (not shown) is also representative of a thermoresponsive natural hydrogel.

Fibrin

In vivo, fibrin plays a central role in haemostasis and wound healing making it well-suited for use in vitro as a scaffold for the development of microvasculature.^{52,68} Following vascular injury, provisional fibrin matrices are rapidly assembled from fibrinogen, an abundant protein of blood plasma.⁶⁸ Fibrin possesses cell-binding motifs that support the attachment of many cell types integral to the wound healing response, including platelets

that form clots to stop bleeding, immune cells that phagocytize dead/damaged tissue, fibroblasts that produce and deposit components of the basement membrane, and endothelial cells that rebuild the vasculature.^{52,68,69}

From a biological performance perspective, the natural capacity of fibrin to promote the development of blood vessels is a large part of its appeal for use in endothelial assembly models. However, in selecting a hydrogel for IFlowPlate™, fibrin also had to be considered from a practical application perspective. The suspension of GFP-HUVECs and fibroblasts in a liquid pre-cursor solution requires that the gelation process is cell friendly. As shown in **Figure 11B**, polymerization of fibrin is initiated by the cleavage of A fibrinopeptides (FpA) by thrombin.⁷⁰ The removal of A fibrinopeptides exposes knobs ‘A’ that are complementary to holes ‘a’. Knob-hole interactions give rise to fibrin oligomers which grow to become protofibrils that laterally aggregate to generate fibres.⁷⁰ The enzyme-activated polymerization of fibrin can occur at room temperature under physiological conditions making the process compatible with cells. Moreover, these conditions are compatible with the conditions required for gelation of Matrigel® which is a component of the fibrin-based gel used in IFlowPlate™, and gelatin which is loaded into fluidic channels, undergoes a sol-gel transition, and is used to prevent entry of the fibrin-based pre-gel solution. Another important feature of fibrin is the ability to slow its degradation by supplementing culture medium with aprotinin, a small molecule that is a competitive inhibitor for the active site of the protease plasmin.^{55,71,72} This preserves fibrin architecture for an extended period and allows for long-term cell culture.

Stock solutions of fibrinogen were prepared by dissolving fibrinogen from human plasma (Cat. # F3879, Sigma-Aldrich) in D-PBS to a concentration of 30 mg/mL or 10 mg/mL. Stock solutions of 10 U/mL thrombin from bovine plasma (Cat. # T4648, Sigma-Aldrich) were prepared by dissolving thrombin in 0.1% (wt/v) BSA. Stock solutions of 0.1% (wt/v) BSA (Cat. # A9418, Sigma-Aldrich) were prepared by dissolving BSA in D-PBS. Stock solutions of 2 mg/mL aprotinin (Bovine Lung, Crystalline, Cat. # 616370, Sigma-Aldrich) were prepared by dissolving aprotinin in dH₂O. Stock solutions were sterile filtered and stored at –20 °C as single use aliquots. Culture medium was supplemented with 1% (v/v) aprotinin to inhibit fibrinolysis.

Matrigel[®]

In the body, the basolateral surface of epithelial and endothelial cell monolayers is separated from connective tissue by the basement membrane.⁷³ The basement membrane is a 50 to 100 nm layer of specialized extracellular matrix that provides structural support to cells and can affect changes in cell behaviour via outside-in signalling.⁷³ The most abundant components of basement membrane are laminin, type IV collagen, nidogen and perlecan.^{73,74}

The mouse Engelbreth-Holm-Swarm (EHS) tumour produces large amounts of basement membrane components that can be extracted, solubilized, and assembled into a gel when warmed to 24 to 37 °C.^{73,74} The stability and structural integrity of basement membrane depends on the interaction of its major components. Collagen IV and laminin individually self-assemble into networks that are linked by nidogen and perlecan.⁷³ Sterile

EHS-derived basement membrane commercialized as “Matrigel[®]”, a portmanteau of the words “matrix” and “gel”, is commonly used as scaffold to support cell survival and differentiation *ex vivo*.^{73,74}

Pioneers in organoid development Sato et al. first reported that isolated intestinal stem cells, which are prone to anoikis outside of the normal tissue context, could be successfully cultured in Matrigel[®] to generate organoids that display the hallmarks of intestinal epithelium (i.e., crypt-villus compartmentalization, cell type composition, and self-renewal capacity).⁷⁵ Matrigel[®] is rich in laminin – a key component of intestinal crypt basement membrane.⁷⁵ Recent studies using soluble RGD (Arg-Gly-Asp) peptides as a competitive inhibitor suggest that integrin binding to RGD sites on matrix components, such as laminin, is necessary for organoid growth.⁷⁶ Fibrin also contains RGD domains; however, in fibrin alone, colony formation efficiencies were significantly lower compared to fibrin gels supplemented with Matrigel[®].⁷⁶ Doubling or tripling RGD concentration by coupling RGD ligands to the fibrin matrix had no effect on organoid growth suggesting that RGD concentration on fibrin was optimal.⁷⁶ It was hypothesized that Matrigel[®] possessed one or more components that provide the biological signals necessary for organoid growth.⁷⁶ Further experiments using purified preparations of the main components of Matrigel[®] identified laminin as the major biological signalling molecule that is required for organoid growth.⁷⁶

Matrigel[®] is a complex mixture of ill-defined chemical composition and high batch to batch variability. In-depth proteomic analysis of Matrigel[®] samples has revealed that Matrigel[®] is an assortment of identifiable and unidentifiable species with a range of

molecular weights.⁷⁷ In addition to the structurally important ECM proteins that constitute the bulk of Matrigel[®] (e.g., laminin and collagen IV), there are numerous other proteins including growth factors, transcription factors, binding proteins, and proteins with unknown roles in cell culture.⁷⁷ These proteins may play a supportive role in the survival and growth of certain cell types, such as stem cells, that are more sensitive to traditional culture conditions.⁴⁴ However, the ill-defined chemical composition and high batch to batch variability of Matrigel[®] could complicate the interpretation of experimental results and limit the application of Matrigel[®] cell cultures.⁷⁶⁻⁷⁸

Compared to standard Matrigel[®], growth factor-reduced Matrigel[®] is a more defined Matrigel[®] preparation that has been purified to a greater extent to reduce the abundance of growth factors (e.g., basic fibroblast growth factor, epidermal growth factor, insulin-like growth factor 1, transforming growth factor beta, etc.).⁷⁷ Single use aliquots of undiluted phenol red-free growth factor-reduced Matrigel[®] (9.06 mg/mL, lot 0055015, Cat. # CACB356231, Corning[®]) were stored at –20 °C and thawed on ice before use.

Fibrin-Matrigel[®]

Fibrin-Matrigel[®] composite gels were prepared by mixing 5 mg/mL fibrinogen (with or without cells) with 10% (v/v) phenol red-free growth-factor reduced Matrigel[®]. 10 mg/mL fibrinogen stock solution stored at –20 °C was warmed in a water bath and diluted with D-PBS to a final working concentration of 5 mg/mL. Matrigel[®] (9.06 mg/mL, lot 0055015) was thawed on ice and used undiluted. 10 U/mL thrombin stock solution stored

at $-20\text{ }^{\circ}\text{C}$ was thawed at room temperature and diluted with 0.1% (wt/v) BSA to a final working concentration of 1 U/mL.

125 μl of 5 mg/mL fibrinogen was dispensed into a microcentrifuge tube. To this, 12.5 μl of cold, undiluted Matrigel[®] was added. Matrigel[®] was kept cold to prevent premature gelation at warmer temperatures. 25 μl of 1 U/mL thrombin was added to the fibrinogen-Matrigel[®] solution to initiate polymerization. The final concentrations of fibrinogen and Matrigel[®] were 3.85 mg/mL and 7.7% (v/v), respectively.

Collagen

Human primary intestine monolayer models have been accomplished by culturing crypts/stem cells on collagen hydrogels.^{25,28} Collagen I is commonly used for cellular scaffolds because of its biocompatibility and availability which can be attributed to its abundance in natural ECM and relative ease of extraction with minimal contamination by other proteins.⁷⁹ **Figure 11C** shows a schematic illustration of the hierarchical assembly of a collagen fibre from collagen I polypeptide chains. Three collagen I polypeptide chains twist together to form a triple helix structure referred to as tropocollagen.^{79,80} Tropocollagen molecules assemble into a collagen fibril, and many collagen fibrils bundle together to form a collagen fibre.^{79,80} Finally, crosslinking of collagen fibres generates a matrix structure that in the presence of a water-based solvent will swell to produce a hydrogel.⁷⁹

Polymerization of acid-solubilized collagen polypeptides is initiated upon neutralization of the solution.⁷⁹ Collagen polymerization progresses in two phases: the nucleation phase during which collagen molecules assemble into fibrils, and the growth

phase during which crosslinking occurs.⁸¹ Reaction kinetics are temperature-dependent and can have a significant effect on hydrogel properties and cellular response.^{79,81,82} At higher temperatures, polymerization rate is accelerated resulting in a shorter nucleation phase and fibres with reduced diameter.^{79,81,82} Conversely, lower temperatures prolong the nucleation phase producing thicker fibres.^{81,82} Xie et al. found that compared to collagen gels polymerized at 4 °C, collagen gels polymerized at 37 °C form thinner, softer fibres that support increased spreading and proliferation of human mesenchymal stem cells.⁸² Collagen gels polymerized at 37 °C have been reported to support the formation of a self-renewing primary intestinal epithelial monolayer.^{25,28} In the interest of replicating these results for the development of a primary intestine model with an accessible lumen in IFlowPlate™, collagen gels were prepared and polymerized at 37 °C.

Collagen gels were prepared from acid-solubilized 10.80 mg/mL rat tail collagen type I (Cat. # CACB354249, Corning®). Neutralization solution was prepared with 10X Medium 199 (Cat. # M0650, Sigma-Aldrich), 1M HEPES (Cat. # 330-050-EL, WISENT Inc., Saint-Bruno, Quebec), 1 N NaOH, 0.075 g/mL NaHCO₃, and dH₂O. 1 N NaOH was prepared by diluting 10.0 N NaOH (Cat. # SX0607N-6, MilliporeSigma) with dH₂O. 0.075 g/mL NaHCO₃ was prepared by dissolving sodium bicarbonate powder (Cat. # S7651, Sigma-Aldrich) in dH₂O. Solutions were sterilized using a syringe filter with a pore size of 0.2 µm. Medium 199 contains phenol red used as a colour indicator of pH. Pale pink-orange colour indicates a near physiological pH. A pH test strip was also used to estimate the pH of the solution (**Figure 12**). A physiological pH of ~ 7.4 is ideal for gelation and

cell viability.²⁵ To confirm gelation, a sample of the neutralized collagen solution was inverted post-incubation at 37 °C for 30 minutes.



Figure 12. 1 mg/mL collagen prepared by neutralization of acid-solubilized concentrated rat-tail collagen type I. pH indicator dye phenol red turns pale pink-orange indicating a near physiological pH (~ 7.4). pH test strip results also estimate a pH between 7 and 8.

Three different collagen hydrogels were prepared: (1) 1 mg/mL collagen-only, (2) 4 mg/mL collagen with 25% (v/v) Matrigel[®], and (3) 1.6 mg/mL collagen with 10 mg/mL fibrin and 20% (v/v) Matrigel[®]. For each formulation, the volume of collagen stock solution required to prepare 0.5 mL of pre-gel solution was calculated based on the desired final concentration of collagen. The volume of 10X Medium 199 and 1M HEPES added comprised 10% and 1%, respectively, of the final volume of pre-gel solution. In this order, collagen, fibrinogen and/or Matrigel[®] (for composite hydrogels) were added to obtain the desired final concentrations. The volume of 1 N NaOH added was equal to 2.3% of the volume of collagen added. 0.075 g/mL NaHCO₃, a strong base, was added stepwise in small amounts to incrementally neutralize the solution and prevent overshooting the endpoint and producing a basic solution. Sterile dH₂O was added to make up the final volume of solution. For collagen-fibrin-Matrigel[®] composite gels, thrombin was the last component added to

prevent its precipitation at $\text{pH} \leq 5$ and premature initiation of fibrin gelation. All reagents (excluding fibrinogen and thrombin) were chilled to slow collagen gelation upon neutralization. Fibrinogen and thrombin were not chilled because fibrinogen is cold-insoluble and forms a precipitate, and the enzymatic activity of thrombin is optimal at near physiological temperature. After each addition, the mixture was homogenized by slow and careful pipetting up and down.

To prepare 0.5 mL of 1 mg/mL collagen-only pre-gel solution, 50 μl of 10X Medium 199 and 5 μl of 1 M HEPES buffer were added to a chilled microcentrifuge tube. Next, 46.30 μl of collagen stock solution was added to obtain a final concentration of 1 mg/mL. To this, 1.06 μl and 12.88 μl of NaOH and NaHCO_3 , respectively, were added.

To prepare 0.5 mL of collagen-Matrigel® pre-gel solution, 50 μl of 10X Medium 199 and 5 μl of 1 M HEPES buffer were added to a chilled microcentrifuge tube. Next, 185.19 μl of collagen stock solution was added to obtain a final concentration of 4 mg/mL. 125 μl of Matrigel® was added to obtain a 25% (v/v) final concentration. 4.26 μl and 8.88 μl of NaOH and NaHCO_3 , respectively, were added.

To prepare 0.5 mL of collagen-fibrin-Matrigel® pre-gel solution, 50 μl of 10X Medium 199 and 5 μl of 1 M HEPES buffer were added to a chilled microcentrifuge tube. Next, 74.07 μl of collagen stock solution was added to obtain a final concentration of 1.6 mg/mL. 166.66 μl of 30 mg/mL fibrinogen and 100 μl of Matrigel® were added to obtain final concentrations of 10 mg/mL and 20% (v/v), respectively. Next, 1.70 μl of NaOH and 8.88 μl of NaHCO_3 were added in this order. 77 μl of 1 U/mL thrombin was the final component added to the mix because it triggers rapid polymerization of fibrin.

Sterile dH₂O was added to make up the final volume of each collagen pre-gel solution. After thorough mixing by pipetting up and down, 15 µl of each neutralized collagen solution was cast per well in 6 wells of a standard 384-well plate. Following a 30-minute incubation at 37 °C, acellular gels were covered with ECGM-2-DMEM (1:1) supplemented with 1% (v/v) aprotinin to keep the gel hydrated, inhibit fibrinolysis, and resemble the conditions that would be used for gels with encapsulated GFP-HUVECs. The 384-well plate was returned to the 37 °C incubator and on Day 3, intestinal organoid fragments were seeded on the gel surface (Section 3.8). Acellular hydrogels were incubated at 37 °C and seeded on Day 3 because it was shown by Kaiser et al. that extended incubation (72 hours) at this temperature significantly increases hydrogel stiffness.⁸³ It has been speculated that additional cross-links or intermolecular interactions between polymers might develop over time to produce collagen-only⁸⁴ and blended collagen-fibrin⁸³ gels with increased stiffness.

Gelatin

Commercial gelatin is produced by denaturation of collagen obtained from mammalian (e.g., porcine or bovine skin) or nonmammalian (e.g., fish) sources.⁸⁵ The source of collagen influences the properties of gelatin, such as melting temperature.⁸⁵ The melting temperature of gelatin derived from warm-blooded mammals is significantly higher than gelatin derived from cold-water fish due to the higher hydroxyproline content.⁸⁵ For our application, gelatin derived from bovine skin was used because it is liquid at temperatures above 37 °C.⁸⁶ During the alkali denaturation process (referred to as type B),

the tertiary structure of tropocollagen is broken down to generate lower molecular weight species including single polymer chains.⁸⁷ Unlike collagen which is acid soluble, gelatin is water soluble.⁸⁸ 10% gelatin solution (from bovine skin, type B, Cat. # G9391, Sigma-Aldrich) was prepared by dissolving gelatin powder in dH₂O at room temperature. The solution was sterilized using an autoclave. Prior to casting the fibrin pre-gel solution in the middle well of an IFlowPlate™ microfluidic system, channels were loaded with 50 µl hot, liquid gelatin. The plate was refrigerated to accelerate gelation. Cooling of the gelatin solution increases the stability of non-specific interactions resulting in the formation of a triple helical structure and an infinite network connecting the chains/helices (**Figure 11D**).^{86,88,89} Gelled gelatin provided a physical barrier to the entry of the fibrin into connected fluidic channels. The sol-gel transition of gelatin is thermo-reversible since non-specific interactions among gelatin molecules can be easily broken by heating the gel (**Figure 11D**).⁸⁸ The unique thermo-reversible character of gelatin made it ideal for use as a temporary sealing gel in IFlowPlate™ because the gel undergoes a rapid gel-sol transition upon placing the plate in a 37 °C incubator. This allows the replacement of liquid gelatin by dilution with culture medium which precludes the challenge of filling dead-end microfluidic channels.

3.4.3 Cell Culture in IFlowPlate™

Selection of Microfluidic Systems

Based on the desired number of parallel experiments, experimental conditions, and technical replicates in the same device, n microfluidic systems of an ethanol disinfected IFlowPlate™ were selected for cell culture. These microfluidic systems were selected from a sub-set of IFlowPlate™ microfluidic systems in the plate interior that met quality standards (See 3.1.7).

Temporary Sealing of Microfluidic Channels with Gelatin

One day prior to seeding IFlowPlate™ microfluidic systems with cells, 50 μ l of hot 10% (wt/v) gelatin in dH₂O was dispensed into reservoir wells. The plate was placed flat in the incubator to allow the gelatin solution to fill channels (**Figure 13, step 1**). To accelerate the sol-gel transition, the plate was cooled in a refrigerator at 4 °C for 30 minutes (**Figure 13, step 2**). 50 μ l of D-PBS was added to the middle well and the plate was firmly tapped on the work surface in the biosafety cabinet to overcome surface tension and fill the well cavity. The plate was returned to the refrigerator overnight.

Cell Harvest and Encapsulation

On the day of seeding IFlowPlate™ microfluidic systems, ~80% confluent GFP-HUVECs and lung fibroblasts in T75 flasks were harvested. Culture medium was aspirated from the flasks and cells were rinsed with 5 mL of D-PBS. To dissociate adherent cells from the culture surface, 5 mL of 0.05% trypsin-EDTA (Cat. # 325-542-EL, WISENT Inc., Saint-Bruno, Quebec) was added to each flask and flasks were placed in the 37 °C incubator for ~2 minutes. Cells were observed under microscope to confirm $\geq 90\%$ cell detachment,

and 5 mL of warmed cell culture medium was added to flasks to inactivate trypsin. Cell suspensions were independently collected and transferred to centrifuge tubes. To obtain a homogenous single cell suspension necessary for an accurate cell count, cell suspensions were pipetted up and down using a 1000 μ L pipette with a narrow bore tip. A small sample of each cell suspension was loaded into one of the chambers of a hemocytometer and cells were counted. Cells were pelleted by centrifugation at 300 relative centrifugal force (RCF) for 5 minutes. GFP-HUVECs and fibroblasts were resuspended in 1% (v/v) ECGM-2-DMEM (1:1) to obtain a cell density of 1,625,000 cells/mL and 325,000 cells/mL, respectively. 1 mL of each cell suspension was added to a centrifuge tube. The mixture of GFP-HUVECs and fibroblasts was pelleted by centrifugation at 300 RCF for 5 minutes. The pellet was resuspended in 250 μ l of 5 mg/mL fibrinogen (prepared fresh from thawed stock solution as described in the previous section) and this mixture was divided evenly between two microcentrifuge tubes.

IFlowPlate™ was removed from the refrigerator and D-PBS was aspirated from the middle wells. Under the influence of gravity, cells in fibrinogen naturally settle towards the bottom of the tube and form a soft pellet. Using a 100 μ l pipette, cells were resuspended in fibrinogen by pipetting up and down. This was to ensure a homogenous mixture which is critical for achieving uniform cell density between wells and within the gel of a single well. To the cell and fibrinogen mixture, 12.5 μ l of cold, undiluted Matrigel® was added. 25 μ l of 1 U/mL thrombin (prepared fresh from thawed stock solution as described in the previous section) was added to the fibrinogen-Matrigel® solution to initiate fibrin

polymerization. Cells and liquid gel precursors were thoroughly mixed by pipetting up and down.

With each tube of pre-gel solution (162.5 μ l final volume), pre-gel can be cast in maximum of 10 wells at 15 μ l per well (**Figure 13, step 3**). Slow and careful pipetting was critical to avoid introducing air bubbles into the casting mix. The pipette plunger was depressed only to the first stop when pipetting up and down to mix cells with liquid gel precursors and dispensing this mix into wells. After each casting, IFlowPlate™ was firmly tapped on the work surface in the biosafety cabinet. This step was critical to overcome the surface tension of the fluid and ensure the well cavity was filled with gel.

The plate was left at room temperature for 30 minutes to allow gelation and encapsulation of cells. The concentration of GFP-HUVECs and fibroblasts in the gel was 5 million cells/mL and 1 million cells/mL, respectively. A HUVEC to fibroblast ratio of 5:1 was reported as optimal for the formation of capillary networks with open lumens in a fibrin gel.⁵³

Replacement of Gelatin with Culture Medium

IFlowPlate™ was incubated for 10 minutes at 37 °C to melt the gelatin used to seal microfluidic channels. Liquid gelatin was incompletely aspirated from inlet and outlet wells (**Figure 13, step 4**). Care was taken to avoid complete emptying of connected dead-end microfluidic channels of liquid as this could lead to trapped air at the liquid-gel interface. Trapped air at the liquid-gel interface can obstruct fluid flow and kill cells.⁹⁰ For this reason, melted gelatin was replaced by dilution with cell culture medium or D-PBS pre-warmed in

a 37 °C water bath (**Figure 13, step 5**). 70 µl of warmed cell culture medium or D-PBS was dispensed on top of gelatin and the plate was returned to the 37 °C incubator for 15 minutes. The dilute gelatin solution was aspirated, and fresh ECGM-2-DMEM (1:1) supplemented with 1% (v/v) aprotinin was added to reservoir wells and the middle tissue well. To minimize evaporative loss of culture medium, D-PBS was added to surrounding empty wells.

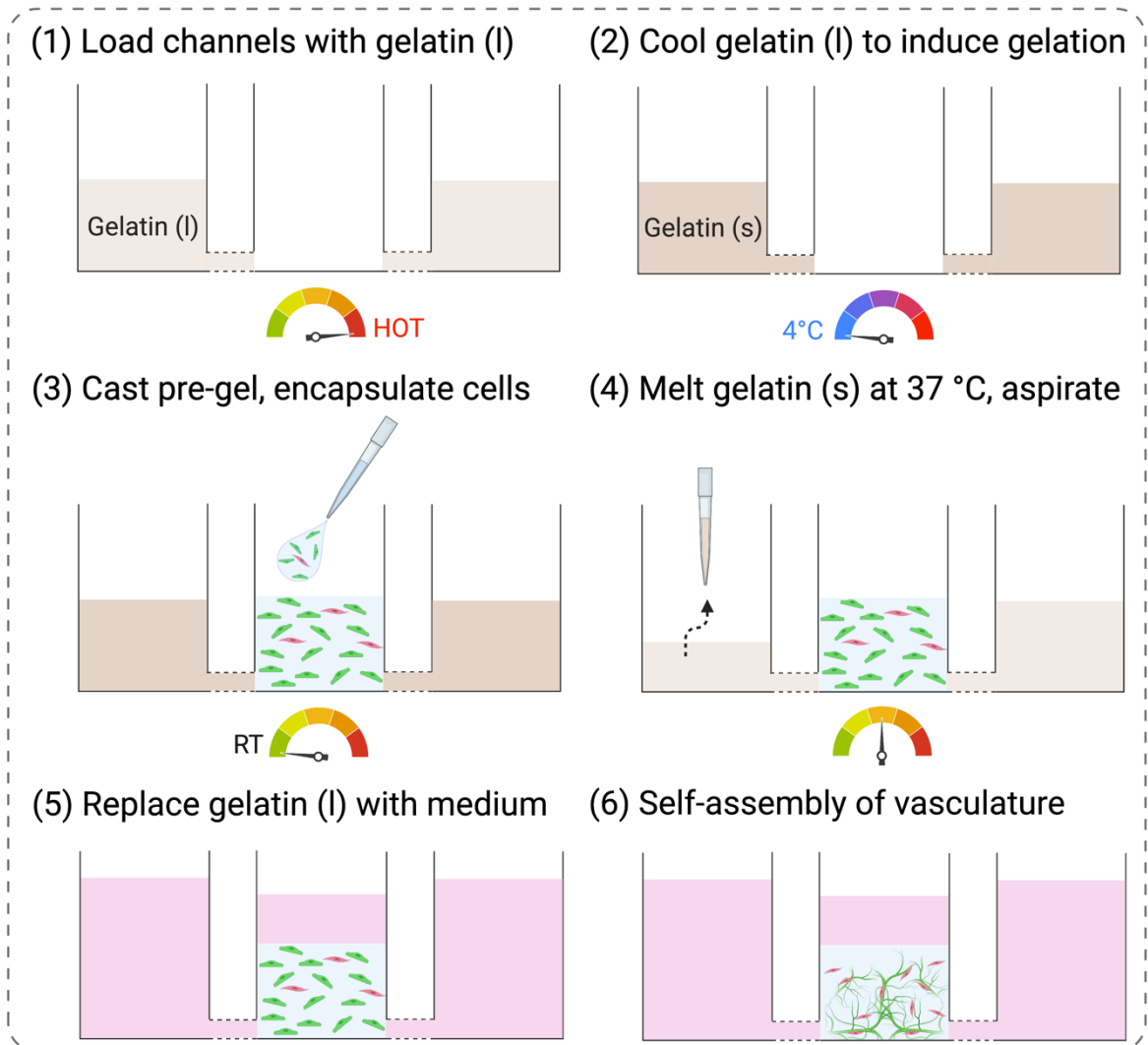


Figure 13. Schematic showing stepwise procedure for establishing a vascular tissue model in an IFlowPlate™ microfluidic system. Hot, liquid 10% (wt/v) bovine skin-derived gelatin is loaded into microfluidic channels (1) and undergoes a sol-gel transition upon cooling (2). Solid gelatin temporarily seals microfluidic channels and prevents entry of the cell-laden pre-gel solution cast in the middle well. At room temperature, fibrin-Matrigel® polymerizes and GFP-HUVECs (*green*) and fibroblasts (*red*) at a 5:1 ratio are encapsulated (3). Incubation of IFlowPlate™ at 37 °C melts gelatin, and gelatin is exchanged for cell culture medium by dilution replacement (4, 5). By Day 6 of cell culture, endothelial cells have self-assembled into a vascular network (6). For avascular tissue models, acellular pre-gel is cast instead of pre-gel with suspended GFP-HUVECs and fibroblasts.

Endothelialization of Microfluidic Channels with GFP-HUVECs

For the endothelialization of IFlowPlate™ microfluidic channels with GFP-HUVECs, cells were harvested and resuspended to a density of 600,000 cells/mL. 90 µl or 100 µl of cell suspension was added to inlet and outlet wells. The plate was incubated overnight at 37 °C under static conditions to allow for cell attachment before initiating perfusion culture.

Seeding Caco-2 Cells on Gel Surface

For intestine models in IFlowPlate™, Caco-2 cells were harvested at ~80% confluency using the same procedure for harvesting GFP-HUVECs and fibroblasts. For the avascular intestine model, Caco-2 cells were prepared at a density of 366,666 cells/mL and 60 µl (~22,000 cells) was added on top of acellular fibrin-Matrigel® constructs. For the vascular intestine model, Caco-2 cells were prepared at a density of 666,667 cells/mL and 75 µl (~50,000 cells) was added on top of fibrin-Matrigel® constructs with encapsulated GFP-HUVECs and fibroblasts.

Gravity-Driven Flow

Perfusion culture was initiated by placing IFlowPlate™ on an interval rocker in a 37 °C incubator. (Perfusion Rocker Mini, Mimetas, Leiden, The Netherlands) programmed to switch between a +15° and –15° angle of inclination every 15 minutes. Tilting the plate creates a difference in the height of the medium column in reservoir wells (**Figure 10**). This height differential establishes a hydrostatic pressure gradient that stimulates the

passive flow of fluid down the gradient from higher pressure to lower pressure. For indefinite perfusion, tilt was alternated at regular intervals to continuously establish a height differential.

3.5 Characterization of Epithelial Barrier

3.5.1 Formation of Caco-2 Confluent Monolayer on Fibrin-Matrigel[®]

To examine the substrate-dependent morphology of Caco-2 cells and verify the capacity of fibrin-Matrigel[®] to support the formation of confluent monolayers, cells were cultured on substrates representing a range of mechanical stiffness values. In order of decreasing stiffness, Caco-2 cells were cultured on polystyrene, fibrin-Matrigel[®], and Matrigel[®] in a standard tissue culture-treated 384-well plate (VWR[®] Standard Multiwell Cell Culture Plate, Cat. # 10814-226, VWR International). 15 μ l of pre-gel solution (prepared as described in Section 4.4.3) was cast in each well and polymerized at room temperature for 30 minutes. 60 μ l of 366,666 cells/mL of Caco-2 cell suspension was dispensed on top of each substrate (minimum of $n = 4$ per condition). D-PBS was added to surrounding empty wells to minimize evaporative loss of fluid. Cells were cultured in a humidified 37 °C, 5% CO₂ incubator. 4X montage-stitched images of the cell growth area were acquired using the Cytation[™] 5 Cell Imaging Multi-Mode Reader (BioTek[®] Instruments, Inc.).

3.5.2 Immunofluorescence

Immunofluorescence was performed to (1) assess epithelial barrier integrity and (2) visualize Caco-2 cells in tri-culture experiments with gel-encapsulated GFP-HUVECs and

fibroblasts. Caco-2 cells were cultured on the surface of fibrin-Matrigel[®] for 7 days and subsequently fixed with 4% paraformaldehyde (PFA) before being stained for E-cadherin and cell nuclei. 4% PFA was prepared by diluting 16% PFA aqueous solution, EM Grade (Cat. # 15710, Electron Microscopy Sciences) with D-PBS. Cell culture medium was removed, and three-well tissue units were washed three times with D-PBS. To fix cells, 50 μ l and 90 μ l of freshly prepared 4% PFA was added to the middle well and reservoir wells, respectively. Cells were fixed overnight on a rocker at 4 °C. The fixative was removed, and tissue units were washed three times with D-PBS. To permeabilize cell membranes and block non-specific antibody binding, 90 μ l of blocking buffer was added to the middle tissue well. Blocking buffer was prepared by diluting Triton[™] X-100 (Cat. # 9002-93-1, Sigma-Aldrich) and FBS in D-PBS to obtain a final concentration of 0.1% (v/v) and 10% (v/v), respectively. Cells were incubated in blocking buffer for 1 hour at room temperature and then washed three times with D-PBS before staining. Cells were incubated with 90 μ l of primary antibody against E-cadherin (mouse monoclonal, ab1416, Abcam), followed by 90 μ l of secondary antibody against mouse IgG conjugated to Alexa Fluor[®] 594 (goat polyclonal, ab150120, Abcam). Single use aliquots of undiluted primary and secondary antibodies were stored at –80 °C and diluted to 1:200 using staining buffer composed of 2% (v/v) FBS in D-PBS. Cells were incubated with primary and secondary antibodies for 2 hours at room temperature, and then washed three times with D-PBS. Cells were incubated with a mixture of secondary antibody and 1:1000 DAPI (Cat. # D9452, Sigma-Aldrich) for counterstaining cell nuclei. Cells were washed three times with D-PBS to remove unbound secondary antibody and DAPI. Cells were covered with fresh D-PBS and

then the plate was incubated overnight at 4 °C. For all incubation steps, the IFlowPlate™ was wrapped with parafilm to minimize evaporative loss of fluid and covered with aluminum foil to minimize exposure of fluorescent molecules to light which can cause photobleaching. Cells were imaged the next day, as antibody-antigen complexes can dissociate over time and result in low signal detection. Prior to imaging, cells were washed three times with D-PBS. To show the level of background fluorescence, due to non-specific binding of primary/secondary antibody, a negative “no Caco-2 cells” control lacking the antigen of interest (i.e., E-cadherin) was stained using the same procedure described above. Brightfield and fluorescence images were acquired with the Cytation™ 5 Cell Imaging Multi-Mode Reader (BioTek® Instruments, Inc.) using the Imager Manual Mode. GFP-HUVECs, Alexa Fluor® 594 (for detecting E-cadherin), and DAPI (for detecting cell nuclei) were visualized using the GFP (Ex. 469, Em. 525), PI (Ex. 531, Em. 525), and DAPI (Ex. 377, Em. 447) filters, respectively. Images were captured in 4X and stitched together to create a montage.

3.5.3 Paracellular Permeability to Fluorescent-Dextrans

Cell membrane-impermeable hydrophilic fluorescent-dextrans of high and low molecular weight were used to assess the barrier function of Caco-2 monolayers in IFlowPlate™. Fluorescein isothiocyanate-dextran with an average molecular weight of 70,000 Da, hereafter referred to as 70 kDa FITC-dextran, was purchased from Sigma-Aldrich in dry powder form (Cat. # 46945). Tetramethylrhodamine isothiocyanate-dextran with an average molecular weight of 4,400 Da, hereafter referred to as 4.4 kDa TRITC-dextran, was purchased from Sigma-Aldrich in dry powder form (Cat. # T1037). Stock

solutions were prepared by dissolving 70 kDa FITC-dextran and 4.4 kDa TRITC-dextran in D-PBS to a concentration of 1 mg/mL and 2 mg/mL, respectively. Single use aliquots were stored at $-20\text{ }^{\circ}\text{C}$ and used to prepare 0.5 mg/mL working solutions by dilution with 1% (v/v) aprotinin-supplemented complete DMEM. Working solutions were sterilized using a $0.2\text{ }\mu\text{m}$ syringe filter and stored at $4\text{ }^{\circ}\text{C}$. When working with fluorescent compounds in the biosafety cabinet, the light was turned off to minimize light exposure.

A 1:1 mixture by volume of 0.5 mg/mL 70 kDa FITC-dextran and 0.5 mg/mL 4.4 kDa TRITC-dextran was freshly prepared prior to initiation of paracellular permeability assays. To initiate the permeability assay, cell culture medium in the middle well (apical compartment) was replaced with $60\text{ }\mu\text{L}$ of 0.5 mg/mL FITC- and TRITC-dextran (**Figure 14**). An initial pilot study was performed using subconfluent (~ 50 to 60% confluent) cultures to, (1) confirm that high and low molecular weight fluorescent dextrans can diffuse through the pores of the fibrin gel meshwork and (2) determine an appropriate time point for detecting eluted fluorescent dextrans in reservoir wells. Fluorescence intensity was measured in wells of microfluidic systems after 1 hour, 4 hours, and > 24 hours. It was confirmed that 70 kDa FITC- and 4.4 kDa TRITC-dextran could pass through the fibrin gel and be received by reservoir wells; however, detection of fluorescent dextrans in reservoir wells was negligible at early time points, and a 22-hour time point was determined to be appropriate.

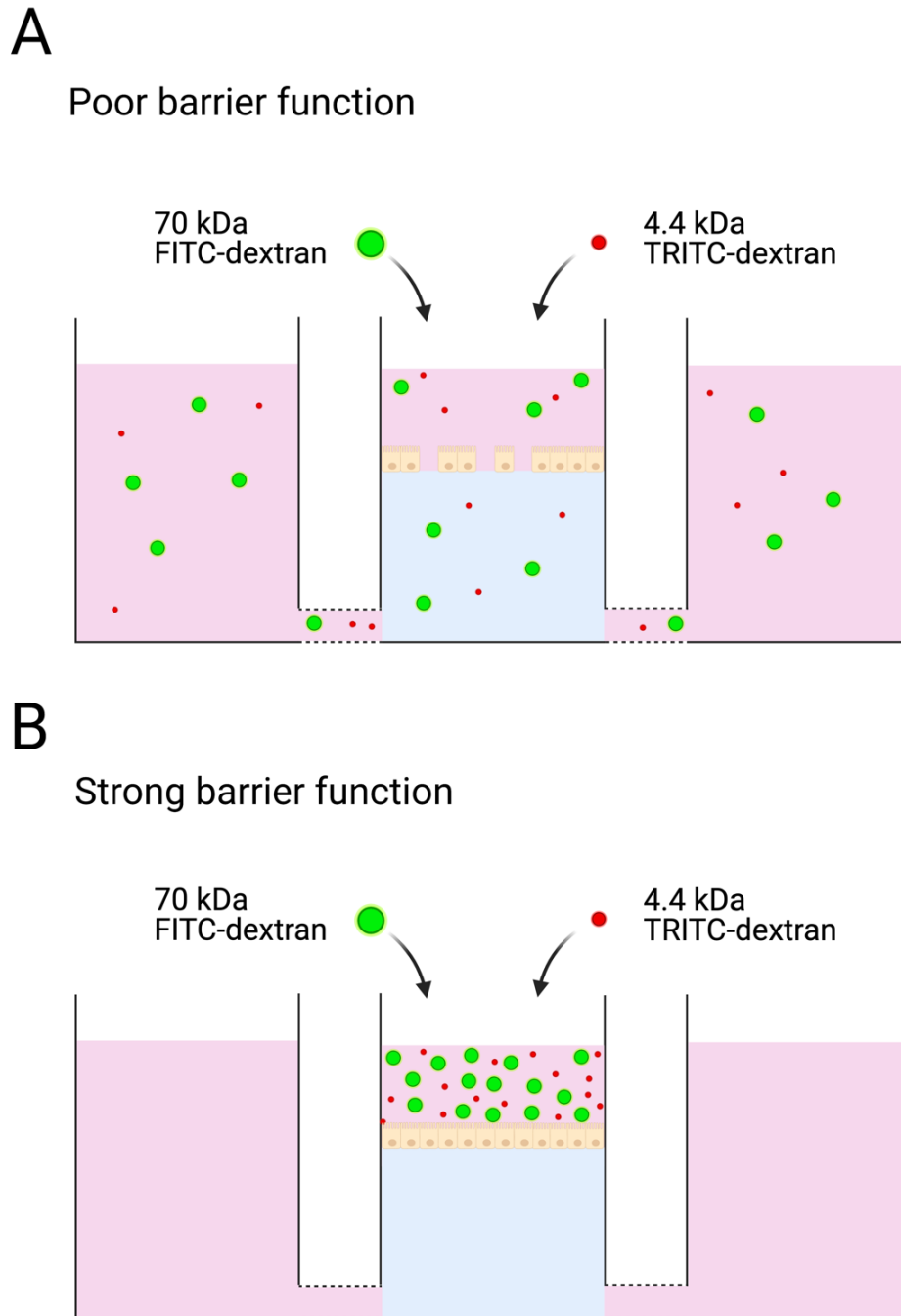


Figure 14. Schematic overview of the permeability assay procedure for assessing barrier function in IFlowPlate™ intestine model systems. A 0.5 mg/mL solution of 70 kDa FITC- and 4.4 kDa TRITC-dextran is added to the apical compartment. (A) Subconfluent monolayers exhibit poor barrier function. Fluorescent dextrans diffuse through the gel and are received by reservoir wells. (B) Postconfluent monolayers exhibit strong barrier function and retain fluorescent dextrans in the apical compartment.

Barrier function of Caco-2 monolayers was assessed using qualitative and quantitative methods. For visualization of barrier function, fluorescence images were acquired 0 hours and 22 hours after introducing fluorescent dextrans to the apical compartment of model systems. To quantify barrier function, fluorescence intensity was measured in reservoir wells. The amount of eluted fluorescent dextran was determined using standard curves. To construct standard curves that represent the relationship between measured fluorescence intensity and the quantity of fluorescent dextran in a sample, two-fold serial dilutions were prepared using 1% (v/v) aprotinin-supplemented complete DMEM as diluent. 100 μ l of 0.5 mg/mL FITC- and TRITC-dextran, 1:2 to 1:64 dilutions, and a medium-only “Blank” were dispensed in triplicate in empty wells of IFlowPlate™ (Figure 15). Standards were prepared fresh for each experiment and measured simultaneously with experimental wells. Tested monolayers were rendered unusable for further experiments, as chemical dyes have been purported to affect transport processes and/or barrier integrity.¹⁸

Using the Cytation™ 5 Cell Imaging Multi-Mode Reader (BioTek® Instruments, Inc.) fluorescence intensity was measured in reservoir wells of microfluidic systems immediately after fluorescent dextran was added to the apical compartment and 22 hours later. These time points were designated $t = 0$ and $t = 22$, respectively. Between fluorescence intensity readings, IFlowPlate™ was placed on the rocker in the 37 °C incubator. Excitation of FITC-dextran was performed at 485 nm and fluorescence was measured at 528 nm. Excitation of TRITC-dextran was performed at 545 nm and fluorescence was measured at 588 nm. Fluorescence intensity values were summed for

reservoir wells to obtain a single value that approximated fluorescence intensity in the basal compartment. Standard curves (**Figure 17 and Figure 18**) were used to convert arbitrary fluorescence intensity values to quantity of fluorescent dextran in micrograms. The amount of eluted fluorescent dextran was estimated by subtracting $t = 0$ values (background) from $t = 22$ values to obtain a value that excludes any contribution from fluorescent compounds in cell culture medium. Mean and standard deviation were calculated for cultures ($n = 3$) presumed to be of the same differentiation stage as defined by confluency (described below). A Student's t-test was performed to determine statistical significance. A p-value less than 0.05 was considered statistically significant.

Selection of IFlowPlate™ microfluidic systems to assess epithelial barrier function was guided by visual inspection of culture confluency. Caco-2 cell differentiation only starts once cells have reached confluency, as it is associated with cell cycle arrest and inhibited proliferation.^{13,91} The validity of (1) using the mean to summarize data from n different cultures and (2) comparing results from different experimental groups, depends on cultures being of the same differentiation stage. Caco-2 cells seeded in IFlowPlate™ at a density of $\sim 20,000$ cells/well reached confluency after different lengths of time in culture. It is speculated that non-planar gel surfaces, due to air bubbles in the gel and/or the meniscus effect, result in non-uniform distribution of cells on the gel surface and contribute to variability among cultures with respect to time to reach confluency, and thus differentiation stage. To better represent culture differentiation stage and improve the reproducibility of experimental results, culture age was defined by confluence, not days since seeding. That is, postconfluent cultures were defined as $+X$ days from confluence.¹³

The recommendation by Sambuy et al. to define culture age in this way, was motivated by the difficulty in comparing results published by different research groups since variations in culture-related factors (e.g., seeding density, medium formulation, substrate) can influence the evolution of Caco-2 cultures with respect to proliferation, cell cycle arrest, and differentiation.¹³

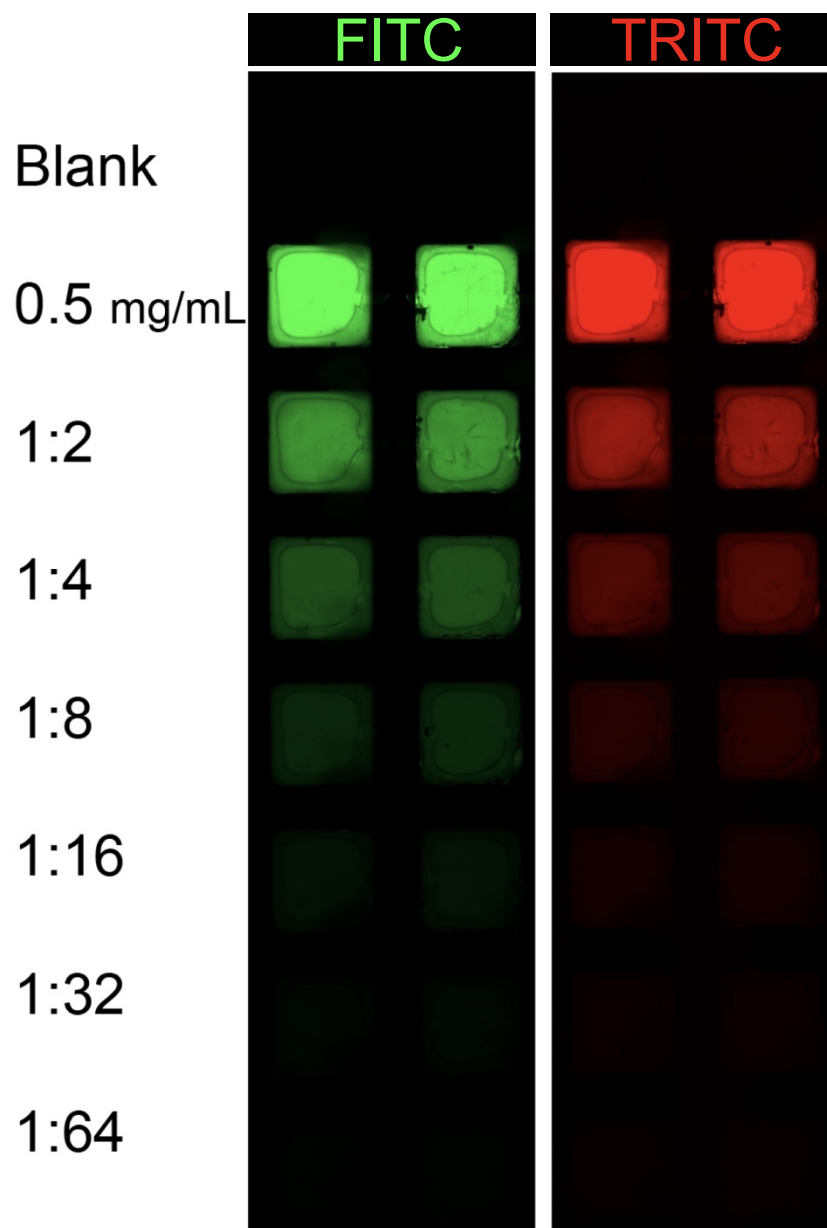


Figure 15. Two-fold serial dilution of 0.5 mg/mL FITC- and TRITC-dextran solution. Dilutions of 0.5 mg/mL 70 kDa FITC- and 4.4 kDa TRITC-dextran solution were prepared using complete DMEM as diluent. Each dilution was dispensed in triplicate in IFlowPlate™ microfluidic systems (2 of 3 wells shown). FITC (*left*) and TRITC (*right*) were visualized using the GFP (Ex. 469, Em. 525) and PI (Ex. 531, Em. 525) filters, respectively. Images are 1.25X, stitched montage.

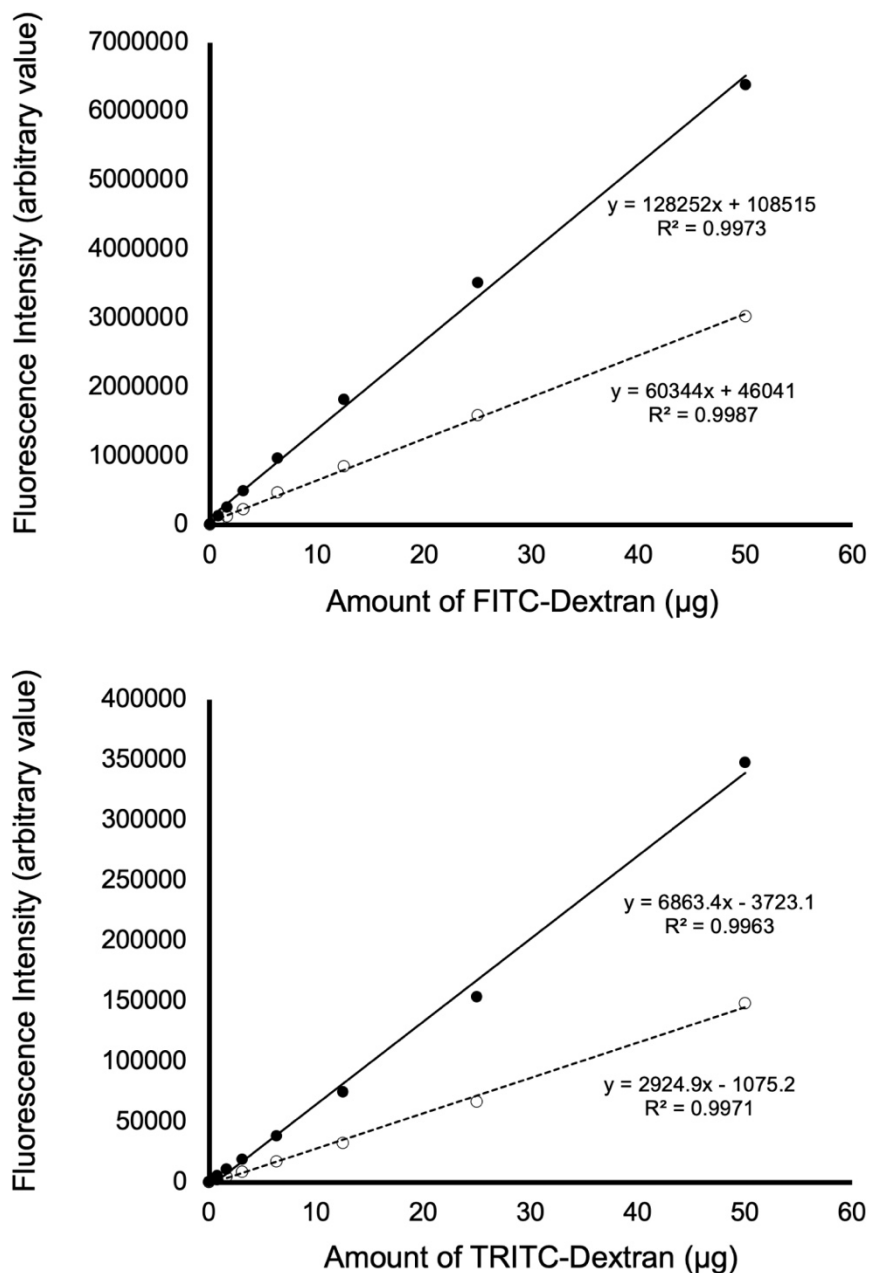


Figure 16. Experiment 1 standard curves of fluorescence intensity as a function of the amount of FITC- and TRITC-dextran. Two-fold serial dilutions of 0.5 mg/mL FITC- TRITC-dextran solution were prepared in triplicate, and fluorescence intensity of FITC (*upper graph*) and TRITC (*lower graph*) was measured using excitation/emission wavelengths of 485/528 and 545/588, respectively. Standards were measured at the same time as experimental samples. Closed circles and solid trendlines represent $t = 0$ measurements; open circles and dashed trendlines represent $t = 22$ measurements. Data points represent mean of $n = 3$.

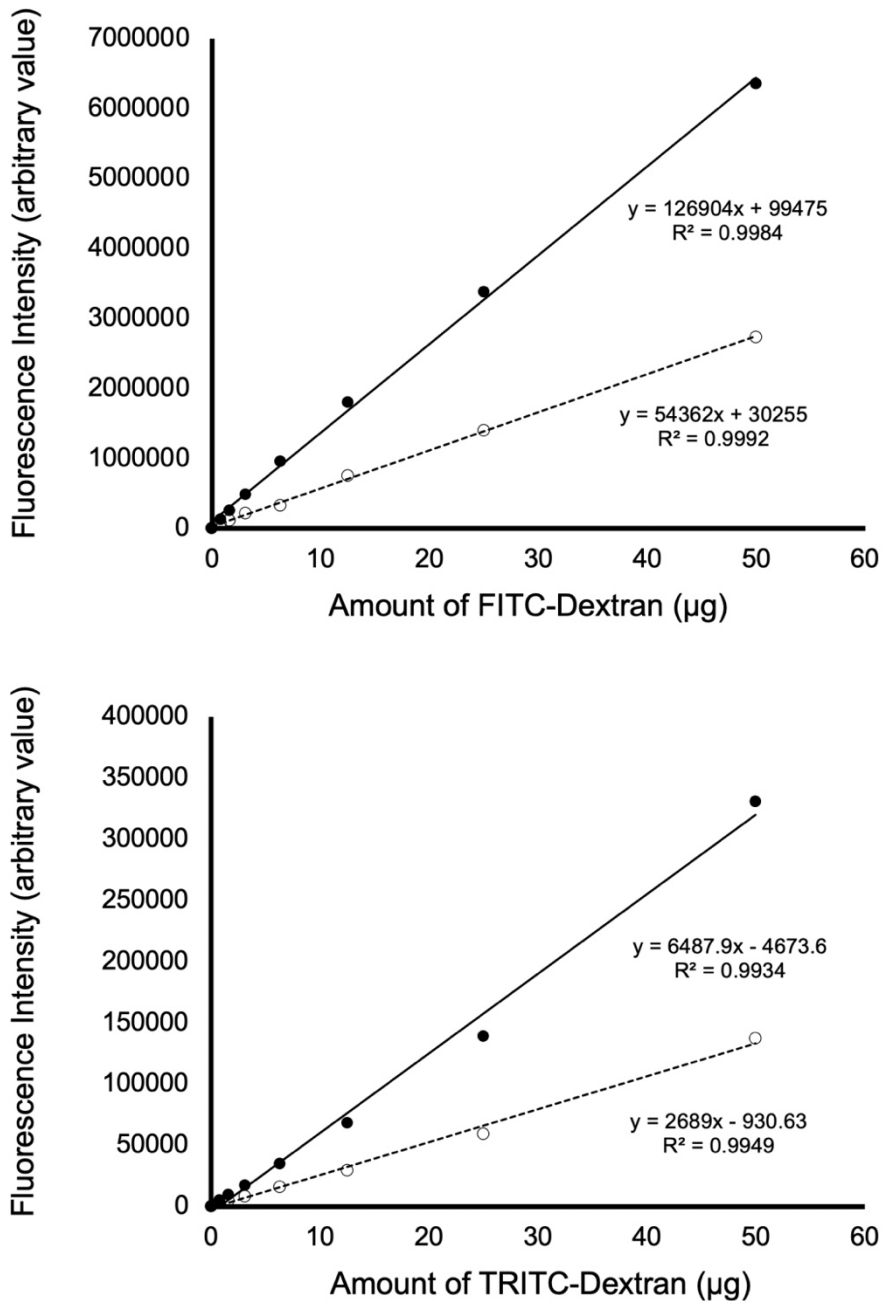


Figure 17. Experiment 2 standard curves of fluorescence intensity as a function of the amount of FITC- and TRITC-dextran. Two-fold serial dilutions of 0.5 mg/mL FITC- TRITC-dextran solution were prepared in triplicate, and fluorescence intensity of FITC (*upper graph*) and TRITC (*lower graph*) was measured using excitation/emission wavelengths of 485/528 and 545/588, respectively. Standards were measured at the same time as experimental samples. Closed circles and solid trendlines represent $t = 0$ measurements; open circles and dashed trendlines represent $t = 22$ measurements. Data points represent mean of $n = 3$.

3.5.4 Transepithelial Electrical Resistance (TEER)

The EVOM2 (Epithelial Voltohmeter 2nd generation, World Precision Instruments, Sarasota, FL) and STX100C96 electrodes (World Precision Instruments, Sarasota, FL.) were used to measure transepithelial electrical resistance (TEER) across Caco-2 monolayers cultured on fibrin-Matrigel[®] in IFlowPlate[™]. The low frequency AC supplied by the EVOM2 (12.5 Hz) predominantly flows through the path of least resistance which is through the spaces between cell bodies (i.e., paracellular pathway). Using the EVOM2, the establishment of cell-cell junctions and barrier function of cellular monolayers can be monitored.

Before making resistance measurements, the EVOM2 was calibrated using the 1000 Ω test resistor and the STX100C96 electrodes were disinfected by placing them in a well of 96-well plate that was filled with 70% (v/v) ethanol. Electrodes were soaked for < 30 minutes as longer soaking times in alcohol can weaken the protective coating on the electrode. Electrodes were preconditioned in a well filled with room temperature 1% (v/v) aprotinin-supplemented complete DMEM. The exchange of alcohol with saline based medium inside the electrode was indicated by a downward drifting resistance value. IFlowPlate[™] was equilibrated to room temperature to minimize the contribution of temperature differences to differences in TEER measurements.

STX100C96 electrodes were inserted in the middle well above the Caco-2 monolayer (or gel, in the case of blank resistance measurements) and the outlet well (**Figure 18**). Hands-free measurements were acquired by resting the STX100C96 on the wall shared by the middle and outlet wells. Four consecutive resistance measurements were

recorded per condition for three different conditions: (1) no cells, (2) subconfluent (~80% confluence), and (3) postconfluent (+6 days from confluence). To calculate TEER, the surface area of the growth area (in cm^2) would be multiplied by the net resistance. The net resistance is calculated by subtracting the blank resistance value (obtained from the acellular model) from the resistance value obtained from models with cells. An initial pilot study performed to test the feasibility of the TEER method in IFlowPlate™ did not yield meaningful data that could be used to calculate TEER. Therefore, the raw resistance values obtained are presented in this work (Table 1).

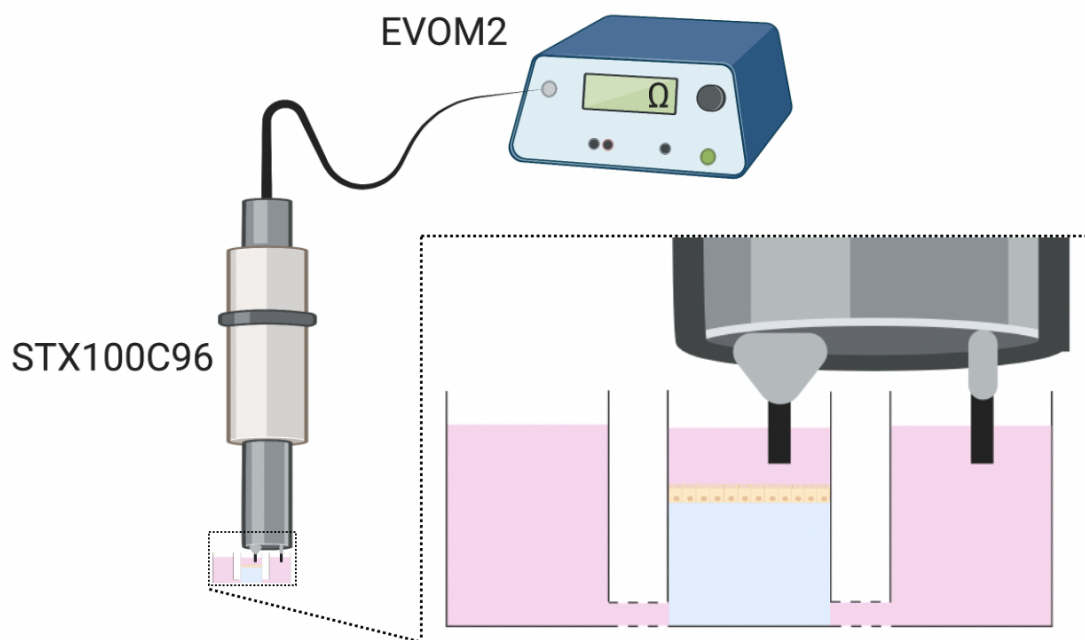


Figure 18. Exploded diagram showing the procedure for measuring the transepithelial electrical resistance of a Caco-2 monolayer in IFlowPlate™ using the EVOM2. STX100C96 electrodes were inserted in the middle well above the Caco-2 monolayer and outlet well of a three-well IFlowPlate™ microfluidic system.

3.6 Characterization of Self-Assembled Vessels

3.6.1 Paracellular Permeability of Vessels to 70 kDa TRITC-dextran

Tetramethylrhodamine isothiocyanate-dextran with an average molecular weight between 65,000 and 85,000 Da, hereafter referred to as 70 kDa TRITC-dextran, was purchased from Sigma-Aldrich in dry powder form (Cat. # T1162). Stock solution was prepared by dissolving 70 kDa TRITC-dextran in D-PBS to a concentration of 2 mg/mL. Single use aliquots were stored at $-20\text{ }^{\circ}\text{C}$ and used to prepare 0.5 mg/mL working solutions by dilution with D-PBS. Working solutions were sterilized using a $0.2\text{ }\mu\text{m}$ syringe filter. Selection of vascular networks to perfuse with 70 kDa TRITC-dextran was guided by visual inspection of networks for microvessel interconnectivity and presumed anastomosis with at least one of the fluidic channels.

Microfluidic systems were washed three times with D-PBS to remove cell culture medium. To establish a hydrostatic pressure gradient, $90\text{ }\mu\text{l}$ of 0.5 mg/mL 70 kDa TRITC-dextran was added to the inlet (or outlet) well, $60\text{ }\mu\text{l}$ of D-PBS was added to the middle well, and the outlet (or inlet) well was empty. 70 kDa TRITC-dextran was transported down the hydrostatic pressure gradient to perfuse the vascular network. Perfusion with 70 kDa TRITC-dextran was used to confirm: (1) the formation of an interconnected network of patent vessels, (2) anastomoses of vessels with fluidic channels, and (3) the formation of an endothelial barrier impermeable to macromolecules with molecular weights greater/equal to the molecular weight of albumin (70 kDa).

3.6.2 Image Acquisition

To visualize the perfusion and permeability of vessels, fluorescent images were acquired before introduction of 70 kDa TRITC-dextran into inlet (or outlet) wells and 5, 30, and 60 minutes after. All images were captured with the Cytation™ 5 Cell Imaging Multi-Mode Reader (BioTek® Instruments, Inc.) using the Imager Manual Mode. To visualize GFP-HUVECs and 70 kDa TRITC-dextran, the GFP (Ex. 469, Em. 525) and PI (Ex. 531, Em. 525) filters, respectively. To achieve high resolution images of vascular networks, images were captured in 4X and stitched together to create a montage of three-well tissue units. To terminate the assay, microfluidic systems were washed three times with D-PBS. Cell culture medium was refreshed, and IFlowPlate™ was returned to the rocker in the 37 °C incubator.

3.7 Coating IFlowPlate™ Microfluidic Channels with ECM Protein

Studies have shown that cell adhesion on native PDMS is significantly lower than on cell-culture grade microplates due to the high surface hydrophobicity associated with methyl groups (**Figure 19A**).^{92,93} Surface modification treatment to increase the hydrophilicity of PDMS is extensively used to enhance cell adhesion in PDMS-based microfluidic devices.⁹³ Common methods to increase the hydrophilicity of PDMS surfaces include: plasma treatment (**Figure 19B**) and coating the surface with synthetic and/or ECM protein (**Figure 19C**).^{92,93} Each treatment has its own advantages and disadvantages and treatments used in combination have been shown to be more effective than when used alone, particularly when cells are subjected to fluid shear stress.^{93,94} In addition to requiring specialized equipment not available in most laboratories, the effects of plasma treatment

are short-lived as the PDMS undergoes hydrophobic recovery within hours after treatment.^{92,93} PDMS surfaces coated with ECM protein better resemble the native cellular microenvironment and enhance cell adhesion by providing natural moieties for receptors on cell membranes to interact with.⁹³

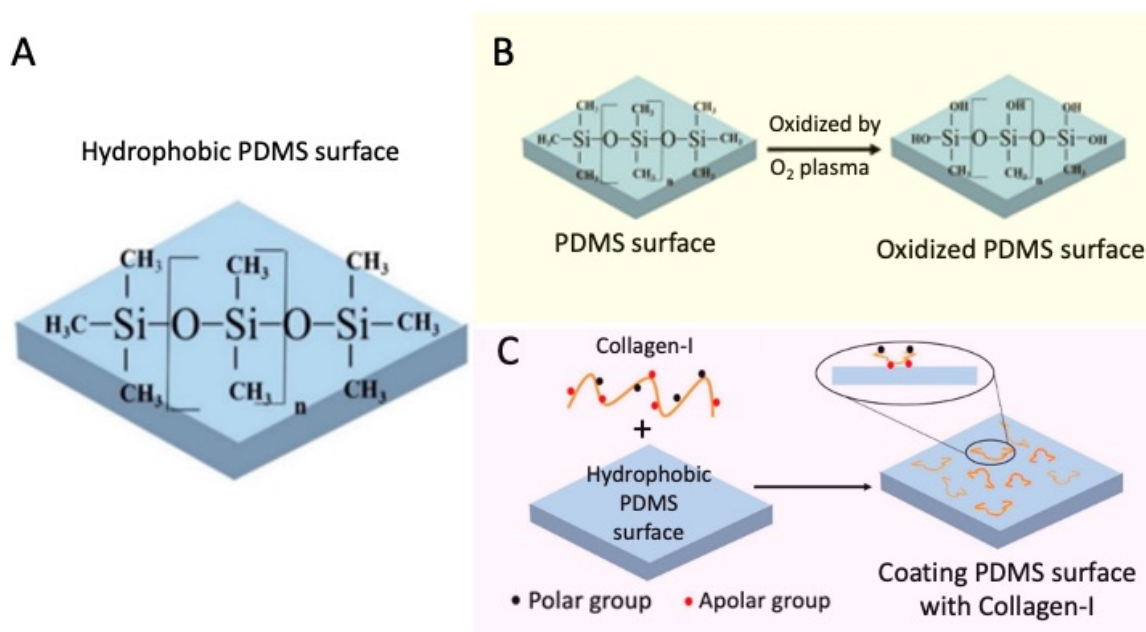


Figure 19. PDMS has high surface hydrophobicity and requires surface modification treatment to increase hydrophilicity and facilitate cell adhesion. (A) Native PDMS surface. (B) Modification of PDMS surface by oxygen plasma. Hydrophobic methyl ($-\text{CH}_3$) groups are replaced by hydrophilic silanol (SiOH) groups. (C) Modification of PDMS surface by coating with ECM protein. Collagen-I molecules self-assemble on the PDMS surface and provide a natural moiety for receptors on cell membranes to interact with. Figure adapted from Ref. 93.

IFlowPlate™ microfluidic channels are comprised of PDMS (3 out of 4 walls) and polystyrene. The inherent hydrophobicity of IFlowPlate™ channel surfaces is unfavourable for endothelial cell adhesion and compromises stable, leak-free anastomoses between living vessels in the tissue chamber and fluidic channels. To enhance endothelial cell adhesion, channels were coated with ECM protein. Three different ECM protein coatings,

fibrinogen, collagen-I, and Matrigel[®], were tested for their capacity to enhance GFP-HUVEC adhesion to IFlowPlate[™] culture surfaces. Fibrinogen mediates cell adhesion directly and indirectly via cell surface integrin receptors and the stimulation of fibronectin production, respectively.^{92,95} Among ECM proteins, collagen-I is the coating most commonly used for endothelial cell culture in PDMS-based microfluidic devices and increases the hydrophilicity of PDMS to the greatest extent.⁹³ Matrigel[®] is enriched with laminin which is a major component of vascular basement membranes and has been shown to promote endothelial cell migration and anastomosis when used as a coating inside of PDMS channels.⁹⁶

To prepare 250 µg/mL fibrinogen, 10 mg/mL fibrinogen (Cat. # F3879, Sigma-Aldrich) was diluted with D-PBS. To prepare 100 µg/mL collagen-I, 10.80 mg/mL of acid-solubilized rat tail collagen-I (Cat. # CACB354249, Corning[®]) was diluted in sterile filtered 0.02 N acetic acid. 0.02 N acetic acid was freshly prepared by diluting 99.7% pure acetic acid (Cat. # 695092, Sigma-Aldrich) in dH₂O. To prepare 3% (v/v) Matrigel[®], undiluted phenol red-free growth factor-reduced Matrigel[®] (9.06 mg/mL, lot 0055015, Cat. # CACB356231, Corning[®]) was diluted with culture medium.

The day after gel-encapsulation of GFP-HUVECs and fibroblasts in the middle well of microfluidic systems, culture medium was aspirated from reservoir wells. Reservoir wells were washed with D-PBS. To coat channels, 90 µl of ECM protein solution was added to reservoir wells. IFlowPlate[™] was incubated at 37 °C under static conditions for 2 hours to allow ECM protein adsorption. After incubation, ECM solution was aspirated from

reservoir wells. Reservoir wells were washed with D-PBS to remove excess ECM protein and neutralize the cell culture surfaces treated with collagen-acid solution.

100 μ l of GFP-HUVEC suspension at a concentration of 600,000 cells/mL was added to reservoir wells. IFlowPlate™ was incubated at 37 °C under static conditions to allow for cell attachment. Fluorescence images for each condition (n = 3) were acquired the next day to visualize the extent of GFP-HUVEC coverage.

3.8 Colon Organoid-Derived Monolayer Experiment

3.8.1 Source of Colon Organoids

Biopsied intestinal tissue contains functional adult stem cells that reside in the base of crypts. Organoids are derived from, and maintain, stem cells enabling seemingly indefinite propagation and the establishment of living biobanks. Living biobanks store cryopreserved organoids that upon revival can serve as a valuable source of untransformed cells for research. With approval from the Hamilton Integrated Research Ethics Board, the colon organoid model used in this study was obtained from the Princess Margaret Living Biobank in Toronto, Ontario, Canada. The colon organoid model was generated from a de-identified/coded endoscopic tissue biopsy of a macroscopically unaffected area of the colon in a 69-year-old female patient with colorectal adenocarcinoma. During the procedure, adjacent affected tissue was also biopsied and used to generate a patient-matched tumour organoid model (not used in this study).

3.8.2 Seeding Colon Organoid Fragments on Collagen Gel Surface

Acellular collagen pre-gel solutions were cast in a standard tissue culture-treated 384-well plate (VWR[®] Standard Multiwell Cell Culture Plate, Cat. # 10814-226, VWR International) on Day 0. On Day 3, colon organoid fragments were seeded on the top of gel. One vial of cryopreserved human intestinal colon organoids was removed from liquid nitrogen storage and rapidly thawed in a 37 °C water bath. Organoids were isolated from Matrigel[®] using Cell Recovery Solution (Cat. # CACB354253, Corning[®]) and dissociated enzymatically using 1 X TrypLE[™] Express Enzyme (Cat. # 12605010, Gibco[™]) as previously described.⁹⁷ Intestinal organoids were dissociated for 10 minutes to yield small multicellular fragments (longer enzymatic dissociation times yield single cells). It has been reported that the formation of confluent monolayers with barrier function is more efficient and reproducible (~90% versus ~40% success rate) when organoid fragments are seeded on top of an ECM-coated PDMS membrane versus single cells.²⁷ Although other studies report success using single cells,^{28,29} it is speculated this approach might require a substantial number of cells to compensate for intestinal stem cells lost during the isolation procedure. It has been reported that only about 6% of isolated intestinal stem cells generated organoids as the majority died shortly after plating in Matrigel[®] presumably due to stress incurred during the isolation procedure.⁴² Organoid fragments in suspension were equally distributed by volume among 9 wells with gel (n = 3 per condition).

3.8.3 Colon Organoid Culture Conditions

Organoids were cultured in Intesticult[™] Human Organoid Growth Medium (Cat. # 06010, STEMCELL Technologies) supplemented with 10 µM of the Rho kinase inhibitor

Y-27632 (Cat. # 72304, STEMCELL Technologies) and 1% (v/v) aprotinin. Intesticult™ Human Organoid Growth Medium is a product of a partnership between Dr. Hans Clevers and STEMCELL Technologies. Its formulation is based on work published by Clevers' group that identified stem cell niche factors (e.g., epidermal growth factor, Noggin, and R-spondin) that support long-term organoid culture.⁷⁵ Y-27632 is added to enhance recovery of cryopreserved intestinal organoids⁹⁸ and inhibit anoikis of intestinal stem cells during culture.⁷⁵ Cell culture medium was changed every other day.

Chapter 4: Results and Discussion

4.1 IFlowPlate™ Avascular Intestine Model

4.1.1 Modelling Intestine Epithelium with Caco-2 Cell Line

Caco-2 Cells Polarize and Form a Functional Barrier

The epithelial cells that line the lumen of the intestine are organized in a tightly packed monolayer of polarized cells.⁹⁹ This is critical for the barrier and vectorial transport functions that define normal intestinal epithelium.¹⁰⁰ The appeal of Caco-2 cells for in vitro modelling of the intestinal epithelium is explained by their capacity to (1) organize into a monolayer of polarized cells that establish a functional barrier, and (2) spontaneously differentiate into enterocytes characterized by an apical brush border and the expression of brush border-associated hydrolases.^{99,101} In standard culture of Caco-2 cells on plastic or glass substrates, the presence of fluid-filled hemicysts referred to as domes, is a widely reported indicator of cell polarization and barrier function.^{91,99,101} Consistent with the

literature, Caco-2 cells cultured in T75 flasks organized into monolayers and formed domes after reaching confluency (**Figure 20**).

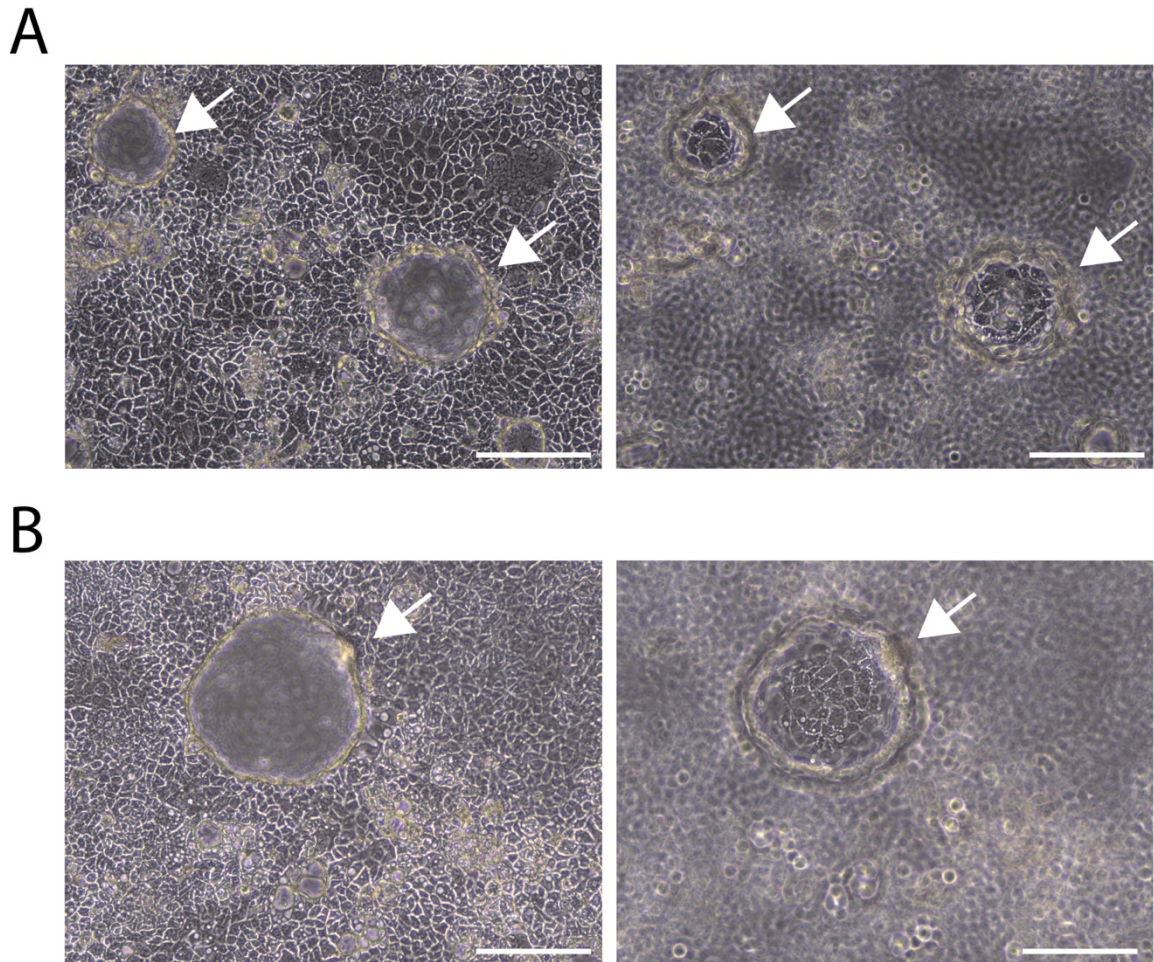


Figure 20. Caco-2 cells on non-porous polystyrene substrates spontaneously form domes (arrows) indicating polarization and barrier function. 10X microscopy images of (A) Day 6 and (B) Day 8 confluent Caco-2 monolayers cultured in T75 flasks. Left images, monolayer is in focus; right images, top of the dome is in focus. Scale bar, 1 mm.

Dome formation is a contact-dependent differentiation phenotype that is not unique to the Caco-2 cell line, but is also observed in other epithelial cell lines that form barriers and possess specialized transport functions, such as MDCK (Madin-Darby canine kidney)

and Clara (murine lung).^{102,103} Studies of dome-forming epithelial cells have identified several cellular prerequisites including (1) apical channels and basolateral pumps for vectorial transport of sodium, and (2) the presence of apical tight junctions that form a continuous paracellular barrier and prevent fluid back-leak.^{99,102-104} Treatment of epithelial cells with potent inducers of cellular differentiation (e.g., dimethyl sulfoxide),¹⁰² or coating plastic substrates with native ECM have been shown to enhance dome formation.¹⁰¹ Compared to cells cultured on uncoated plastic, the number and size of domes formed by cells on ECM-coated plastic is increased, and domes appear earlier in culture.¹⁰¹ Perturbation experiments suggest that integrin-mediated cell-ECM interactions reinforce cell-cell adhesion through increased E-cadherin tethering to the actin cytoskeleton.¹⁰¹ A proposed explanation for the delay in dome formation on uncoated plastic substrates is that the Caco-2 cells require time to deposit their own ECM.¹⁰¹

Although dome formation in confluent epithelial cell cultures has biological significance, it is a non-physiological phenomenon that is the result of fluid accumulation between the cell layer and a non-porous impermeable substrate.¹⁰¹⁻¹⁰³ This fluid accumulation is responsible for cell detachment and uplifting from the substrate.¹⁰³ Caco-2 transwell models which incorporate porous, permeable filter supports and allow access to both sides of monolayers, provide a more physiological and valuable model of the intestine epithelium and are extensively used today.¹³

IFlowPlate™ allows for epithelial cell culture on a natural ECM-based hydrogel that is porous and contains integrin binding sites. The porosity of the hydrogel obviates non-physiological dome formation, and integrin-mediated cell-ECM interactions support the

formation of a strong epithelial barrier.¹⁰¹ Having validated that Caco-2 cells form polarized monolayers with barrier function in a conventional culture environment (i.e., tissue culture-treated flask), the next step was to demonstrate the translatability of these results to IFlowPlate™. As a first step towards this goal, the capacity for fibrin-Matrigel® to support monolayer formation was tested.

Caco-2 Cells Form Confluent Monolayers on Fibrin-Matrigel®

Caco-2 cells are extensively cultured in two dimensions on solid supports and used as polarized epithelial monolayers in studies of transport and barrier function. Caco-2 cells have also been cultured in three dimensions within Matrigel® matrices to provide a more physiological environment for studies of 3D epithelial morphogenesis.^{105,106} In this context, Caco-2 cells spontaneously form polarized cysts with a central lumen.^{105,106} Intestinal organoids also show substrate-dependent changes in morphology and this has been exploited in recent years to convert 3D organoids to 2D monolayers with an accessible lumen.

In identifying culture conditions that support the formation of primary intestinal epithelial cell monolayers, the mechanical stiffness of the cell culture substrate has been identified as a key factor.^{25,26} Intestinal crypts cultured on top of a soft substrate, such as Matrigel® (Young's modulus ~50 Pa), fail to form a spreading 2D monolayer and instead form 3D organoids.²⁵ Alternatively, when plated on a stiff substrate, such as polystyrene (Young's modulus 3 – 3.5 GPa), crypts form a 2D monolayer.²⁵ To identify whether substrate stiffness or ECM contacts determined culture morphologies, Altay et al. produced

“soft” and “hard” Matrigel[®] substrates by coating polystyrene with thick and thin layers of Matrigel[®], respectively.²⁶ Whereas, a thick (~2 mm) layer of Matrigel[®] induced the formation of 3D organoids, crypts/stem cells formed 2D monolayers on a thin (~3 µm) layer of Matrigel[®] which has a stiffness that approaches that of the underlying polystyrene.²⁶

In pursuit of creating an IFlowPlate[™] intestine model that has a polarized epithelial monolayer with an accessible apical compartment, the first step was to validate that the formulated fibrin-Matrigel[®] gel possessed the right stiffness to support the formation of a Caco-2 cell monolayer. In a standard tissue culture-treated 384-well plate, Caco-2 cells were subcultured on three different substrates ranging in stiffness. Categorized as stiff and soft substrates, respectively, polystyrene and Matrigel[®] represent the extremes of the range and served as experimental controls for monolayer formation. As a composite of fibrin and Matrigel[®], fibrin-Matrigel[®] can be categorized as a substrate of intermediate stiffness. Day 0 images taken immediately after seeding Caco-2 cells show that surface area coverage by cells is high (**Figure 21A**). Matrigel[®] promoted the spontaneous organization of cells into 3D aggregates that resembled cysts resulting in decreased surface area coverage observed by Day 2 (**Figure 21A**). Cells cultured on comparatively stiffer fibrin-Matrigel[®] increased their surface area coverage through proliferative expansion resulting in a monolayer by Day 2 (**Figure 21A**). With increasing culture time, well-demarcated borders between tightly packed polygonal Caco-2 cells formed giving confluent monolayers the hallmark cobblestone appearance of intestinal epithelium (**Figure 21**). These results were consistent with those obtained on the polystyrene positive control (**Figure 21A and B**). It is noted that

Caco-2 cells reached confluency at a later time point on fibrin-Matrigel[®] compared to polystyrene. This could be due to the concave meniscus of the hydrogel resulting in non-uniform distribution of cells on the substrate surface.

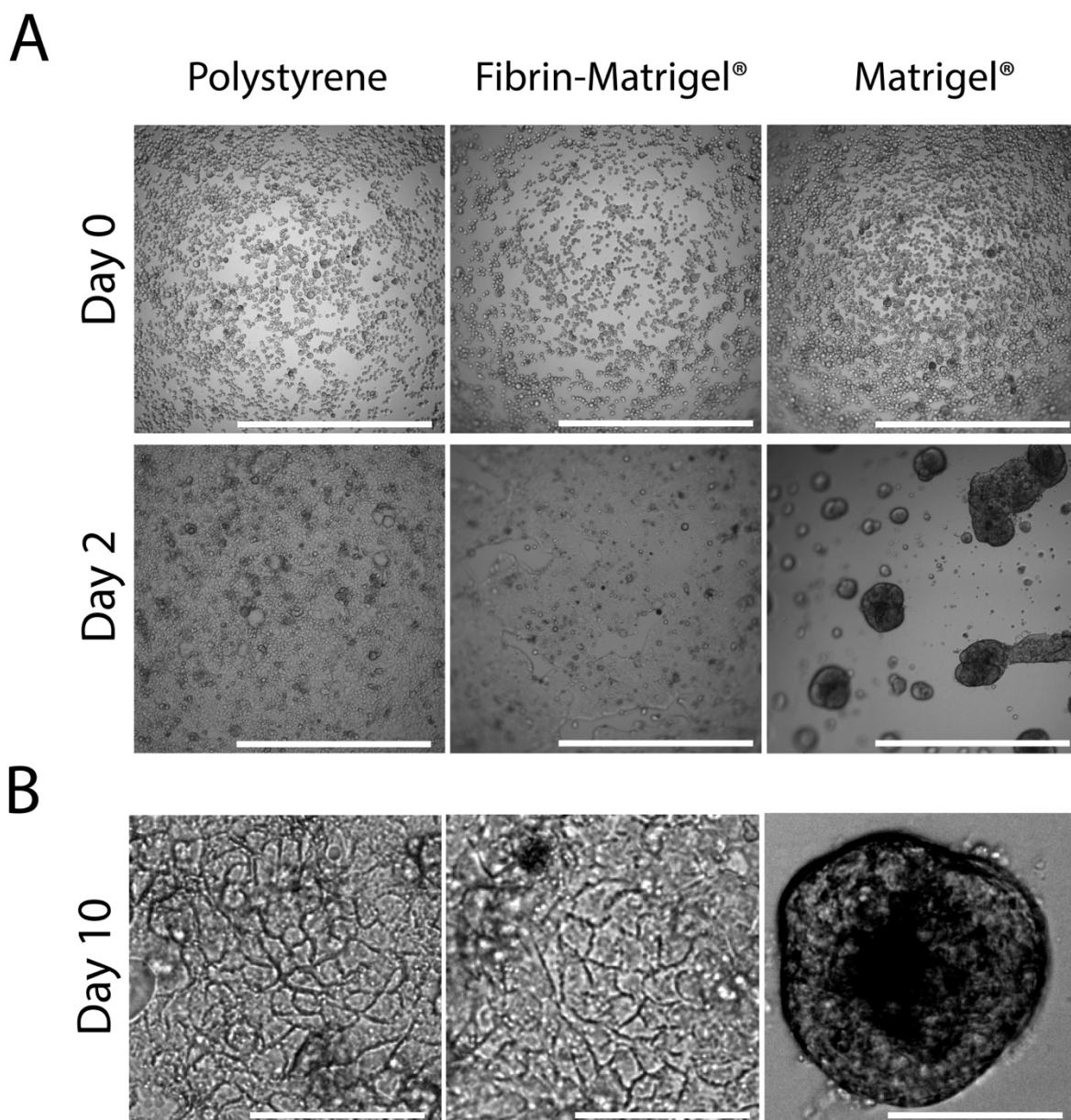


Figure 21. Caco-2 cells form hallmark cobblestone epithelium on fibrin-Matrigel®. In a 384-well plate, Caco-2 cells were subcultured on substrates ranging in stiffness. At the extreme ends, polystyrene (stiff) and Matrigel® (soft) served as positive and negative controls, respectively, for monolayer formation. (A) 22,000 Caco-2 cells were seeded per well to achieve high surface area coverage (Day 0). Matrigel® promoted spontaneous organization of cells into 3D aggregates that resembled cysts, and cells cultured on polystyrene and fibrin-Matrigel® formed monolayers (Day 2). 4X microscopy images show surface area coverage by cells. Scale bar, 1 mm. (B) 10X microscopy images show mature Day 10 cell culture morphologies. Scale bar, 0.1 mm.

Caco-2 Cells Express E-cadherin

Light microscopy is useful for indicating confluence of Caco-2 cells, however; confluence is a precondition of barrier formation and does not indicate that a barrier has formed.¹⁰⁷ Epithelial barriers are created by tight junction proteins that seal the clefts between cells and control passive transport via the paracellular pathway.¹⁹ The expression of tight junction proteins at borders of neighbouring cells is commonly visualized using immunofluorescence and is an accepted indicator of barrier formation.^{107,108} E-cadherin is a calcium-dependent adhesion protein that plays an important role in the assembly of tight junctions and is present in all epithelial barriers.¹⁹ Immunofluorescence was performed to visualize E-cadherin expression in postconfluent Caco-2 cells cultured on top of fibrin-Matrigel® (**Figure 22**).

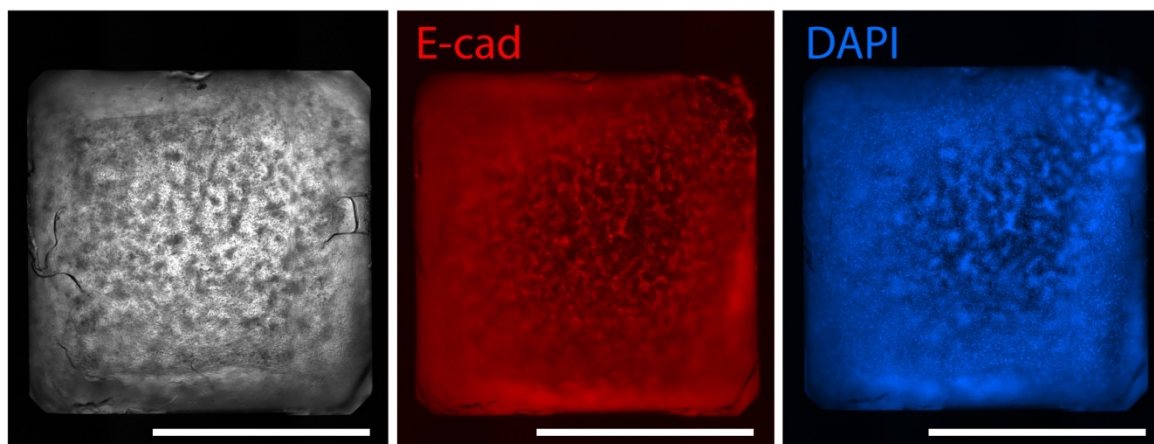


Figure 22. Caco-2 cells stained for junction marker E-cadherin to assess barrier integrity. In IFlowPlate™, Caco-2 cells were cultured for 7 days on fibrin-Matrigel® (with GFP-HUVECs and fibroblasts) and stained for E-cadherin (*red*) and nuclei (*blue*). Images are 4X, stitched montage. Scale bar, 2 mm.

Using conventional fluorescence microscopy, the phenomenon of Caco-2 cell multilayering²² and the optical distortion around the well perimeter due to the meniscus

effect, make it difficult to discern expression of E-cadherin at cell borders and view the whole growth area simultaneously. While advanced imaging techniques that utilize optical sectioning (e.g., confocal microscopy) can be used to obtain higher quality images in non-planar scenarios, these techniques are cumbersome and can complicate high-throughput analysis of epithelial barrier integrity. Moreover, immunofluorescence precludes real-time monitoring of barrier integrity since the process requires tissue fixation, and it cannot provide information about barrier function. For these reasons, label-free quantitative methods for real-time monitoring of barrier function were explored.

Not unlike transwell systems, IFlowPlate™ microfluidic systems provide accessible apical and basolateral compartments that are separated by cell monolayers grown on a porous substrate. In principle, this should allow for routine methods for assessing barrier function and transport properties of epithelial monolayers in transwell systems to be applied to IFlowPlate™ microfluidic systems.

4.1.2 Barrier Function

Paracellular Permeability to Fluorescent-Dextrans

Having established microscopically that Caco-2 cells cultured on fibrin-Matrigel® form confluent monolayers that cover the substrate, the barrier function of the epithelium was assessed. For this, the paracellular flux of hydrophilic membrane impermeable fluorescent compounds across Caco-2 monolayers was visualized and measured. FITC and TRITC conjugated dextran of high and low molecular weight, respectively, was added to the apical compartment of Caco-2 intestine models in IFlowPlate™. Fluorescence

microscopy and detection were used to visualize and quantify eluted fluorescent dextrans received by reservoir wells of microfluidic systems.

The size-exclusion properties of the intestinal barrier are determined by the dimensions of the pores created by tight junction complexes between adjacent epithelial cells.¹⁰⁹ The dimensions of paracellular pores are not fixed; they are dynamically regulated to control the passive flow of water and solutes across the epithelium.¹⁰⁹ Moreover, the size-exclusion profiles of epithelium differ between regions of the gastrointestinal tract.^{19,110} Under steady-state conditions, the diameter of paracellular pores in rat and rabbit small intestine are estimated to be between 10 to 15 Å and may be slightly smaller in human.¹⁰⁹ These dimensions are large enough to accommodate macromolecules with molecular weights less than ~3.5 kDa, but macromolecules with molecular weights that exceed this are excluded from paracellular transport via the pore pathway.¹⁰⁹ In colonic epithelia, including Caco-2 monolayers, the dimensions of paracellular pores are smaller and more discriminating.^{19,110} Herein, qualitative and quantitative methods were used to show that +8 days postconfluent monolayers impede the permeation of 70 kDa FITC and 4.4 kDa TRITC conjugated dextrans.

Fluorescence microscopy images acquired 0 and 22 hours after introducing fluorescent dextrans to the apical compartment of Caco-2 monolayers show that fluorescent dextrans diffuse through the gel under subconfluent monolayers and are received by reservoir wells (**Figure 23**), whereas postconfluent monolayers retain fluorescent dextrans in the apical compartment (**Figure 24**). Quantification of fluorescent dextrans in reservoir wells of microfluidic systems with subconfluent and postconfluent monolayers show that

the transport of fluorescent dextrans across postconfluent monolayers was significantly less (**Figure 25**). Importantly, 70 kDa and 4.4 kDa fluorescent dextrans were largely excluded from transport across postconfluent monolayers. The minimal leakage of fluorescent dextrans across postconfluent epithelium observed after 22 hours could occur via a secondary, low-capacity paracellular pathway that has limited size-selectivity.^{111,112} This pathway has been termed the leak pathway and is thought to be due to larger diameter pores at tricellular junctions or transient, local disruptions to tight junction complexes.^{111,112} These results indicate the development of an intestine epithelial barrier model in IFlowPlate™.

The permeation of tracer compounds, such as fluorescent dextrans, is a powerful tool to assess paracellular permeability. However, tested monolayers are rendered unusable for further experiments, as chemical dyes have been purported to affect transport processes and/or barrier integrity.¹⁸ Moreover, tracers could interact with a compound of interest that is added to the system and confound experimental results.¹¹³ For continuous monitoring of barrier function during cellular growth, differentiation, and before/after barrier perturbation or treatment with a compound of interest, a non-invasive method for assessing barrier function is required.

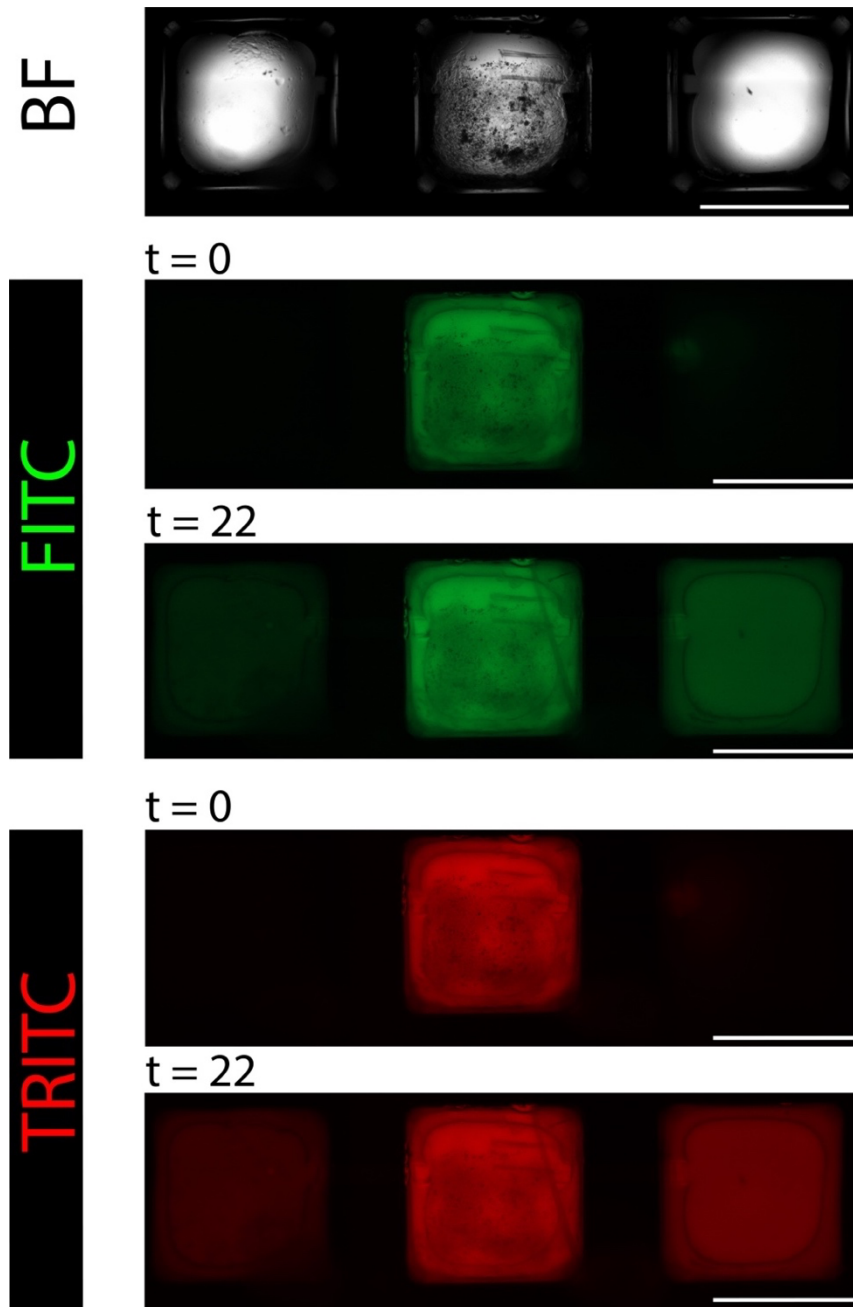


Figure 23. Microscopy images showing the permeability of a representative subconfluent (~80 % confluence) Caco-2 monolayer to high and low molecular weight fluorescent dextrans. A 0.5 mg/mL solution of 70 kDa FITC- and 4.4 kDa TRITC-dextran was added to the apical compartment of subconfluent intestine model systems in IFlowPlate™. Images acquired 0 hours and 22 hours after introduction of fluorescent dextrans show that dextrans diffuse through the gel and are received by reservoir wells. Scale bar, 2.5 mm.

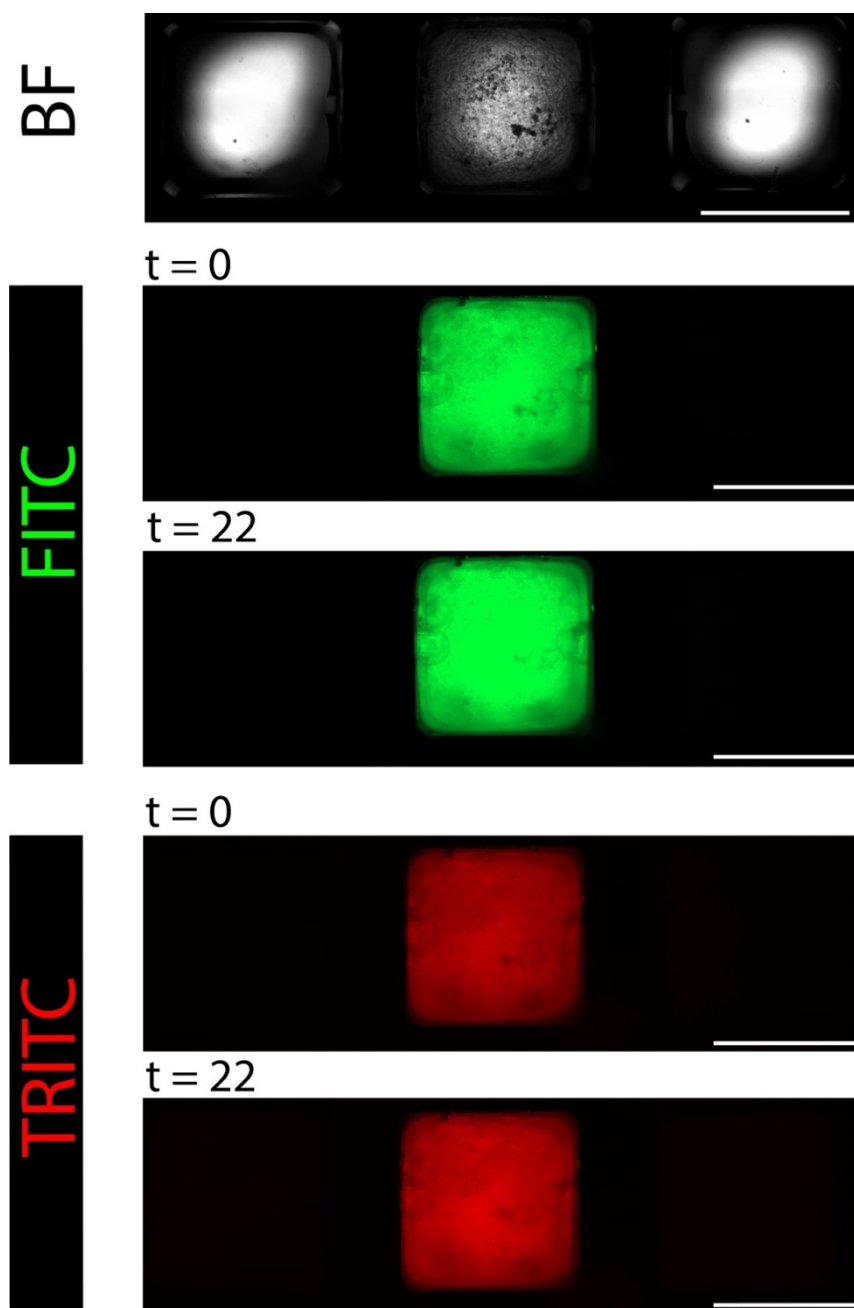


Figure 24. Microscopy images showing the permeability of a representative postconfluent (+8 days from confluence) Caco-2 monolayer to high and low molecular weight fluorescent dextrans. A 0.5 mg/mL solution of 70 kDa FITC- and 4.4 kDa TRITC-dextran was added to the apical compartment of postconfluent intestine model systems in IFlowPlate™. Images acquired 0 hours and 22 hours after introduction of fluorescent dextrans demonstrate the formation of a strong barrier that excludes transport of fluorescent dextrans across the epithelium via the paracellular pathway. Scale bar, 2.5 mm.

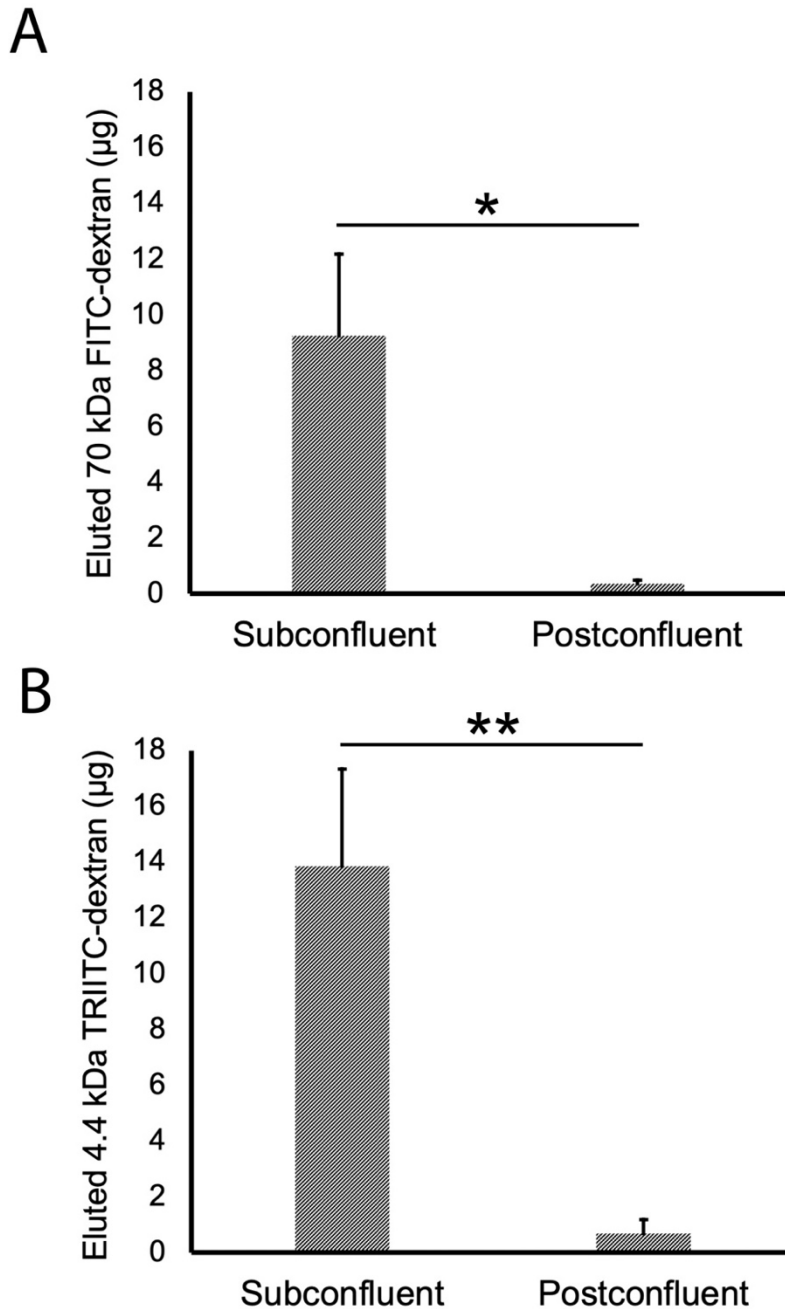


Figure 25. Quantification of amount of eluted fluorescent dextran as an indicator of the barrier function of Caco-2 monolayers in IFlowPlate™. A 0.5 mg/mL solution of 70 kDa FITC- and 4.4 kDa TRITC-dextran was added to the apical compartment of intestine model systems. The amount of fluorescent dextran that permeated subconfluent/postconfluent monolayers and was received by reservoir wells was quantified. Results are presented as means (n = 3). Error bars indicate standard deviation. A Student's t-test was performed to determine statistical significance. A p-value < 0.05 was considered significant. * = p < 0.05; ** = p < 0.005.

Transepithelial Electrical Resistance (TEER)

Transepithelial electrical resistance (TEER) measures the electrical resistance across a cellular monolayer and reflects the passive transport of ions via the paracellular pathway.¹⁸ Unlike permeability assays using chemical dyes, the TEER method is regarded as non-invasive and provides the sensitivity to detect subtle changes in barrier function.¹⁸ However, a caveat of using this method to assess barrier function is that there are many factors that can affect resistance measurements and the risk of obtaining erroneous results that do not reflect barrier quality is high.¹¹⁴ A pilot study was conducted to evaluate the feasibility of using TEER to assess barrier function of Caco-2 monolayers in IFlowPlate™.

At least four consecutive resistance measurements were recorded per condition for three different conditions: (1) no cells, (2) subconfluent (~80% confluence), and (3) postconfluent (+6 days from confluence). The results of this study are presented in **Table 1**. Resistance measurements for each sample were highly unstable and did not reflect differences in barrier quality between conditions. For example, the postconfluent monolayer condition should display a higher average resistance value compared to the subconfluent monolayer condition; however, the average resistance value was lower.

To examine the reproducibility of resistance measurements in IFlowPlate™, resistance measurements were performed on two technical replicates of the acellular model. One of the acellular replicates displayed the highest average resistance value of all three conditions, whereas the other acellular replicate displayed the lowest average resistance value of all three conditions. These results indicate that non-biological factors were affecting resistance measurements.

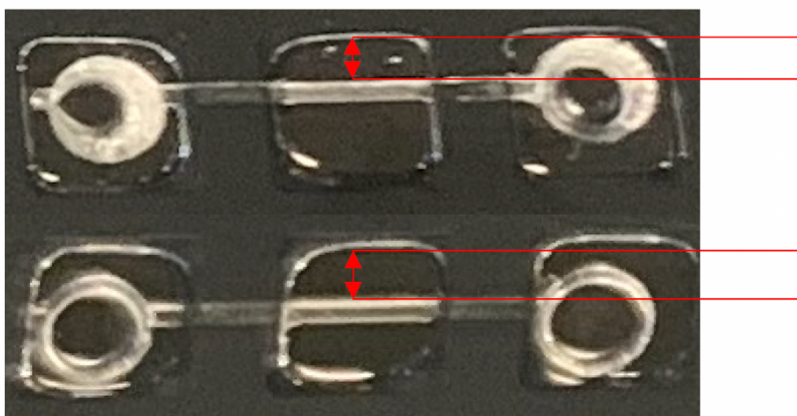
Table 1. Results of pilot study testing the measurement of electrical resistance of Caco-2 monolayers in IFlowPlate™ as a non-invasive method for assessing barrier function. Electrical resistance measurements were made using the EVOM2 (World Precision Instruments Inc.). STX100C96 electrodes were inserted in the middle well above the Caco-2 monolayer (or gel) and outlet well of microfluidic systems. Four consecutive resistance measurements were recorded per condition.

Well	Description	Electrical Resistance Reading
M14	No cells	1. 9252 2. 9080 3. 9274 4. 9286
M17	No cells	1. 13435 2. 13452 3. 13463 4. 13663
E8	Subconfluent (~80% confluence)	1. 10987 2. 11009 3. 11023 4. 11044
F17	Postconfluent (+6 days from confluence)	1. 10280 2. 10312 3. 10355 4. 10370

Inconsistent IFlowPlate™ microfluidic system geometries and the presence of air bubbles or other non-conducting inhomogeneities (e.g., PDMS glue) compromise the reproducibility of resistance measurements performed on technical replicates and obscure differences in resistance measurements that are of biological origin. For relatively inexpensive and technically facile prototyping of IFlowPlate™ within our academic research lab, plates were manually fabricated using photolithography, soft lithography, injection moulding, and PDMS “glue” to bond polystyrene. While these techniques are well-established, many aspects cannot be precisely controlled, and microfluidic systems with consistent geometries cannot be achieved (**Figure 26**). The TEER method has low

tolerance for irregularities especially in microfluidic systems which have high internal electrical resistances compared to the resistance across monolayers.¹¹⁴

A



B

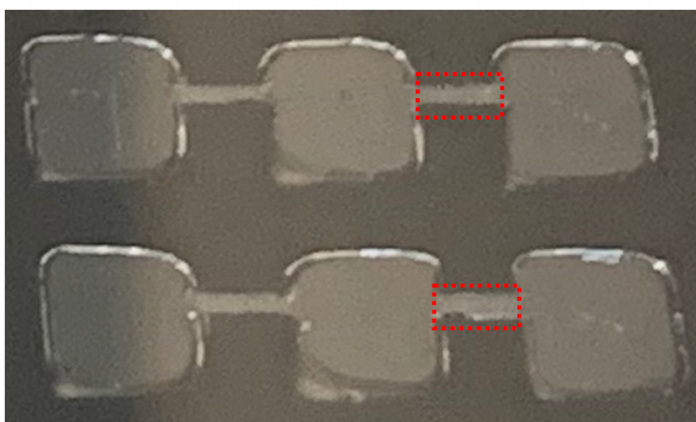


Figure 26. In-house fabricated IFlowPlate™ microfluidic systems exhibit inconsistent geometries. Photographs of the bottom of an IFlowPlate™ fabricated using soft lithography, injection moulding to pattern a polystyrene sheet with PEGDM, and PDMS “glue” to bond the patterned polystyrene to a 384-well bottomless plate. Representative images captured before (A) and after (B) PEGDM was dissolved show variation in positions and dimensions, respectively, of microfluidic channels.

Consistent system performance requires consistency in system geometry and that is best delivered by automated manufacturing. By leveraging the production capabilities of a

contract manufacturer, IFlowPlate™ is now being produced using computer numerical control milling and laser plastic welding. While this is expected to reduce variations in resistance caused by geometrical inconsistencies between microfluidic systems, other sources of variation will have to be addressed before TEER can be reliably employed in IFlowPlate™. For example, differences in the placement (i.e., distance from plastic well walls), immersion depth, and angle of electrodes affects resistance measurements. The adapter on the STX100C96 electrodes was designed for hands-free use with a 96-well plate and guarantees that the spatial orientation of electrodes is consistent between wells. The STX100C96 is poorly compatible with IFlowPlate™ resulting in inconsistent positioning of electrodes between microfluidic systems. Production of a custom electrode lid that can be placed on top of IFlowPlate™ would be ideal for acquiring resistance measurements in a consistent and high-throughput manner. The feasibility of this has been demonstrated by Mimetas – a biotechnology company that has developed OrganoTEER® for their microfluidic 3D cell culture platform OrganoPlate®.¹¹³

Erroneous electrical resistance readings can also be caused by non-conducting inhomogeneities, such as PDMS glue and air bubbles in fluidic channels or gel. In addition to being a non-conducting polymer, PDMS also exhibits nanoscale surface roughness that can be a source of Harvey nuclei which can grow into larger bubbles.¹¹⁵ PDMS-free manufactured plates will eliminate PDMS-related inconsistencies in microfluidic systems. Other sources of undesirable air bubbles in microfluidic systems are related to incompletely filled fluidic channels or wells. The incorporation of standard cell-culture grade polystyrene

or treatment of manufactured plates to improve surface wettability should make device “priming” more effective¹¹⁵ and help to mitigate air bubbles.

The cell coverage of the gel surface is also important to consider, as minor discontinuities in the monolayer (e.g., 0.4% of substrate) can reduce the measured TEER by 80%.¹¹⁶ It was found that Caco-2 cells were typically denser near the centre of the gel surface and increasingly sparse towards the periphery due to the concave meniscus of the hydrogel. Optical distortion at the periphery of the substrate surface caused by the meniscus makes it challenging to confirm that there are no discontinuities in the cellular monolayer. Moreover, the non-uniform distribution of Caco-2 cells on the gel surface is an undesirable phenomenon that can create “islands of confluence” and contribute to asynchronous differentiation among cells in the same well. Eliminating the meniscus effect in IFlowPlate™ is ideal for convenient, high-quality imaging of cells across the entire growth area simultaneously, enhanced reproducibility of experimental results, and high-throughput applications that require Caco-2 cultures within the same IFlowPlate™ to evolve in synchrony. Modification of the styrene surface to improve wettability could reduce the tapping of the plate required to overcome the surface tension of liquid gel and fill well cavities. Moreover, physical disturbance of unpolymerized pre-gel during casting could lead to an exaggerated or heterogenous meniscus effect. Casting gel in fewer wells and allowing for partial to full polymerization before tilting the plate to cast pre-gel in additional wells could be a way to minimize this.

4.2 IFlowPlate™ Vascular Intestine Model

Fabrication of channels to be seeded and lined with endothelial cells, and the self-assembly of endothelial cells encapsulated in 3D ECM environments are two approaches to creating vascular networks in vitro.^{52,55,117,118} Both patterned and naturally-derived vascular networks can be integrated with microfluidics to achieve perfusion.^{55,117-119}

De novo assembly of a perfusable vascular network in a 3D matrix begins with the coalescence of HUVECs to form solid cords.¹²⁰ Tubulogenesis refers to the transition from solid cord to tube, and cell hollowing is a mechanism by which this transition occurs.¹²⁰ Intracellular lumens initiate from large vacuoles that form and align at the centre of cells and fuse with one another.¹²⁰ These intracellular lumens will connect with similar lumens formed in adjacent cells and ultimately generate a hollow tube.¹²⁰ Endothelial assembly models more closely recapitulate vascular formation during development and can better represent the complex topologies and lumen diameters of native capillaries.⁵²

The central role that fibrin plays in haemostasis and wound healing in vivo is what makes it well-suited for use in vitro as a scaffold for the development of microvasculature.^{52,68} Fibrin gel is widely used for endothelial assembly models.^{52,55,59,117-119,121} Using a fibrin-gel sandwich technique, Chalupowicz et al. showed that endothelial cells that formed monolayers on the surface of fibrin gel rapidly rearranged to form a network of capillary-like tubes when overlaid with a fibrin gel.¹²² Experiments showed that the induction of capillary morphogenesis was dependent on the interaction of the apical surface of the endothelial monolayer with the N-terminus amino acids 15 – 42 of β fibrin generated via thrombin cleavage of fibrinogen.¹²² In addition, fibrin reversibly binds angiogenic growth factors that stimulate endothelial cell proliferation⁵² and displays a

porosity and susceptibility to cell-mediated degradation that facilitates cell migration necessary for blood vessel formation.^{68,72}

A fibrin-based gel supplemented with growth factor-reduced Matrigel[®] was used as a structurally supportive and biologically instructive substrate for establishing a vascular intestine model in IFlowPlate[™]. The limitations presented by fibrin and Matrigel[®] when used alone, are overcome when the two are blended to create a fibrin-Matrigel[®] composite gel. Matrigel[®], enriched with laminin, emulates the composition of the intestinal crypt basement membrane⁷⁵ and provides the biological signals required for intestinal organoid growth.⁷⁶ However, Matrigel[®] is a soft hydrogel that does not support the formation of a 2D monolayer when intestinal organoid-derived crypts/cells²⁵ or Caco-2 cells are cultured on its surface (**Figure 21**). Another disadvantage of using Matrigel[®] is the lack of control over its degradation making it an unsuitable scaffold for long-term cell culture. The stiffness and degradation of fibrin is more amenable to tuning by increasing fibrinogen concentration and adding aprotinin, respectively. Moreover, fibrin is a relatively inexpensive and well-defined matrix. Together, these characteristics make fibrin-based gel ideal for developing a vascular intestine model in IFlowPlate[™] which was designed with high-content screening applications in mind.

4.2.1 Self-Assembled Vascular Networks

Drawing on established approaches to creating self-assembled vascular networks in vitro, vascular networks were formed in IFlowPlate[™] by encapsulating endothelial cells and fibroblasts at a ratio of 5:1, respectively, in a 3D fibrin-based matrix. Several studies

have identified mixed or adjacent coculture of endothelial cells and fibroblasts as critical for formation of stable capillary tubes in fibrin matrices.^{53,55,59} Of note, proximity of fibroblasts to endothelial cells has been shown to be important.^{59,123} Findings from diffusion experiments suggest that fibrin matrices can limit the diffusive transport of soluble factors.¹²³ Mixed coculture of endothelial cells and fibroblasts is purported to enhance capillary formation by reducing diffusion distances and increasing transport of fibroblast-derived proangiogenic factors.¹²³ While endothelial cells have the capacity to self-assemble into vascular networks in the absence of flow, it has been shown that interstitial flow greatly enhances tubulogenesis and supports more extensive networking,¹²⁴ and luminal flow is essential for vessel stabilization.¹²⁵ To achieve continuous flow in our system, IFlowPlate™ was placed on a rocker platform that induces passive levelling of liquid.

By Day 6 of culture under the described conditions, GFP-HUVECs dispersed in fibrin-Matrigel® at a concentration of 5 million cells/mL associated with nearby endothelial cells and assembled into a branching network of vessels (**Figure 27**). By manual focusing along the z-axis (vertical dimension) of the gel, it was observed that vascular networks were especially well-visualized near the bottom of the well. It is speculated that the area near the bottom of the well might possess the right oxygen concentration and/or cell density to enhance vascular network formation.

The phenomenon of enhanced vascular network formation at the bottom of wells has been previously reported and presumed to be due to proangiogenic mechanisms induced by hypoxia.¹²⁶ Within each well, a gradient of dissolved oxygen is established whereby cells are exposed to decreasing oxygen levels as the distance from the air-liquid

interface increases. In the body, hypoxia plays a prominent role in the wound healing process.¹²⁷ Wound sites are often hypoxic because of (1) diminished oxygen delivery due to the disruption of vasculature and (2) increased oxygen consumption due to the influx of responding cells (e.g., fibroblasts, macrophages) with high metabolic demands.¹²⁷ Ischemia in damaged tissue stimulates vascular repair in order to restore normoxic conditions.¹²⁷

Prior to encapsulation, suspended cells in liquid gel precursor can settle under the influence of gravity and give rise to a cell density gradient in the hydrogel. The settling of cells due to gravity alone is a slow process and the rapid polymerization of the fibrin-Matrigel[®] should hinder this effect. However, the current IFlowPlate[™] protocol requires the plate to be tapped on the working surface to overcome the surface tension of liquid fibrin-Matrigel[®] and fill well cavities. Tapping could accelerate cell settling and lead to a greater density of endothelial cells and fibroblasts near the bottom of the well.

Low oxygen levels and high cell density could also enhance vascular network formation through synergistic positive feedback loops. For example, lower oxygen levels near the well bottom could stimulate increased fibroblast proliferation, and thus increase cell density.¹²⁷ A higher cell density near the bottom of the well could increase the rate of oxygen consumption, and thus lower oxygen levels.

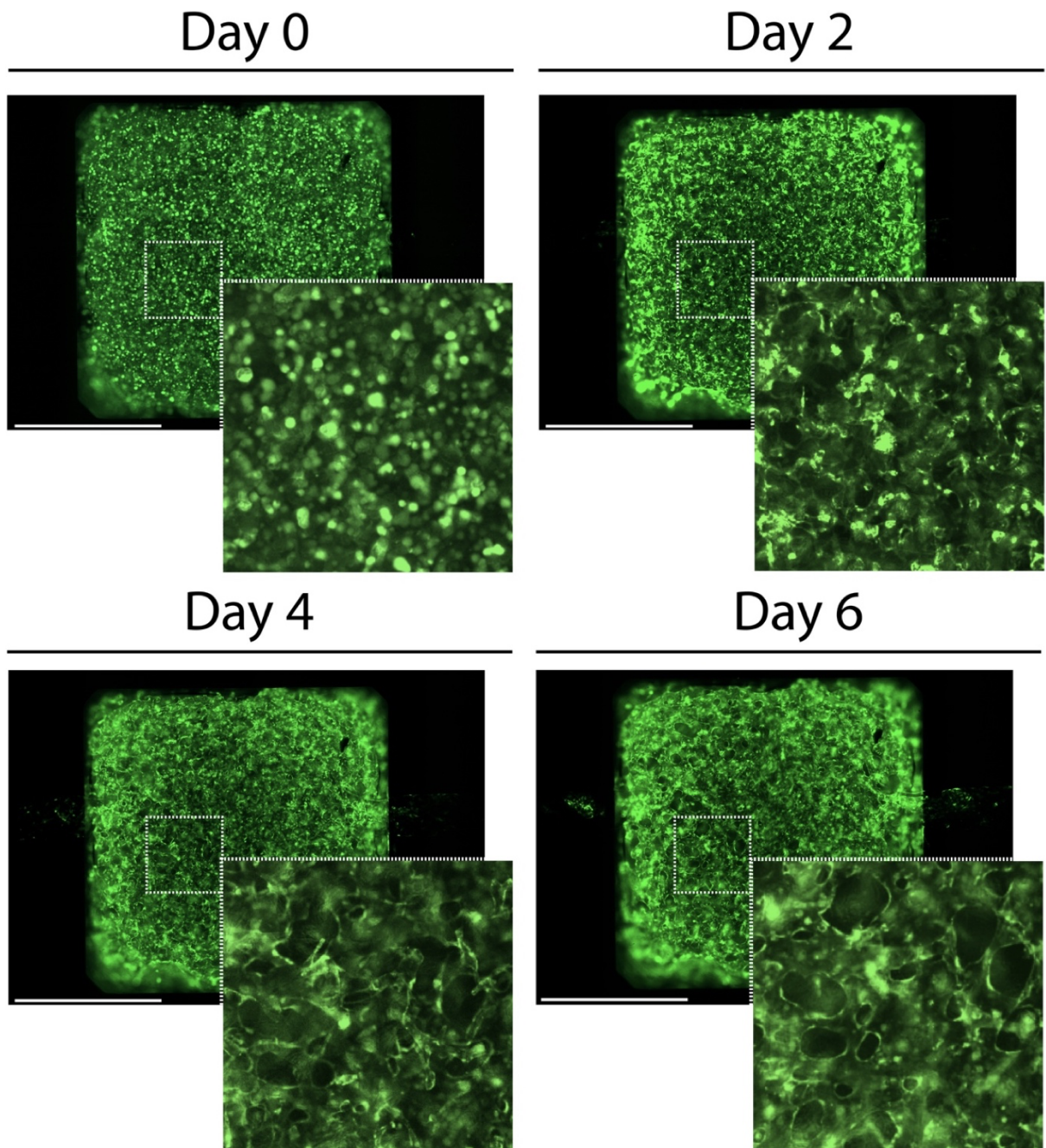


Figure 27. Fibrin gel-encapsulated GFP-HUVECs self-assemble into a vascular network by Day 6 of culture in IFlowPlate™. GFP-HUVECs and fibroblasts at a concentration of 5 million cells/mL and 1 million cells/mL, respectively, were encapsulated in 15 μ l of fibrin-Matrigel®. Perfusion culture was initiated on Day 1 by placing IFlowPlate™ on a rocker platform to induce passive liquid levelling. Cells were cultured in ECGM-2-DMEM (1:1). Images were acquired every two days. Scale bar, 1.5 mm.

To confirm the formation of an interconnected network of patent vessels and assess the paracellular permeability of vessels to macromolecules ≥ 70 kDa, 70 kDa TRITC-dextran was added to the outlet (or inlet) reservoir well of IFlowPlate™ microfluidic systems. 70 kDa is the approximate molecular weight of albumin which is retained in the lumen of microvessels in vivo.¹²⁸ The height of the liquid column in each well of the microfluidic system was manipulated to establish a hydrostatic pressure gradient that would drive the movement of TRITC-dextran through the vascular network and into the distal reservoir well. As visualized using fluorescence microscopy, TRITC-dextran filled the lumen of vessels and was retained (**Figure 28**). These results indicate the formation of patent vessels with barrier function comparable to in vivo microvessels which are impermeable to macromolecules ≥ 70 kDa.

A prerequisite of the paracellular permeability assay is the anastomotic connection of vessels with lateral microfluidic channels to facilitate the movement of TRITC-dextran through the vascular network from the source to the sink. Moreover, the connection should be tight to minimize non-physiological leakage. Robust formation of tight anastomotic connections between living capillary networks and microfluidic channels was a major challenge that hindered the scalability of IFlowPlate™ vascular models. Section 4.2.2 will discuss work to address this.

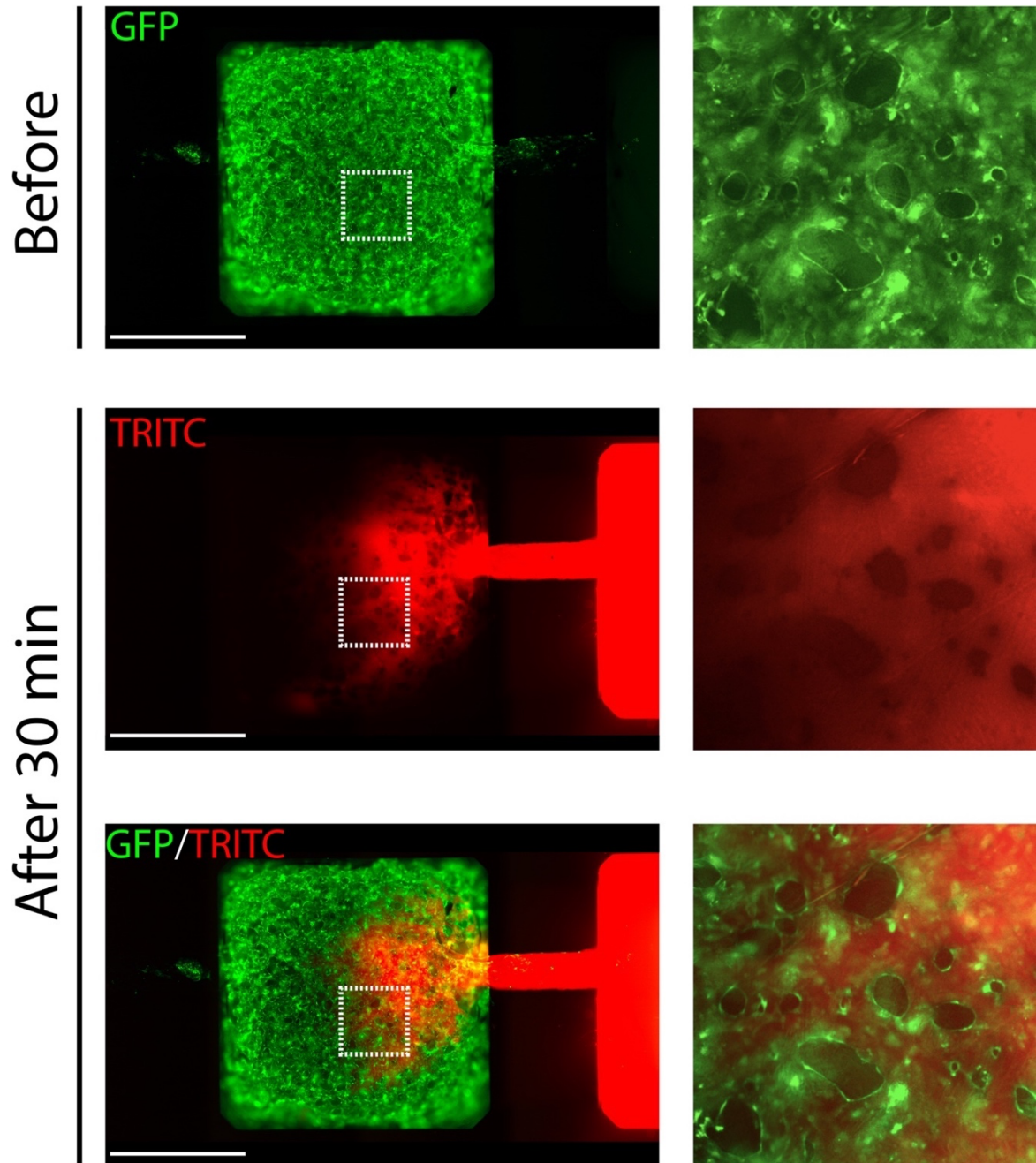


Figure 28. 70 kDa TRITC-dextran is transported and retained in lumens indicating the formation of patent vessels with a functional endothelial barrier. 70 kDa TRITC-dextran was added to the outlet reservoir well of an IFlowPlate™ microfluidic system. TRITC-dextran was transported down an established hydrostatic pressure gradient through an interconnected network of Day 6 self-assembled vessels. Real-time fluorescence microscopy images captured 30 minutes after introduction of TRITC-dextran indicates the impermeability of the endothelium to macromolecules ≥ 70 kDa. Scale bar, 1.5 mm.

4.2.2 Anastomoses of Self-Assembled Vessels with Fluidic Channels

Establishing perfusable vascular networks in IFlowPlate™ requires the fusion of the lumina of growing endothelial tubules embedded in ECM with lateral fluidic channels. Anastomoses of fluidic channels with endothelial tubules of smaller diameter simulates the architecture of a unit of the circulatory system consisting of larger diameter arterioles that branch into capillaries.

The anastomotic connection of vessels in fibrin gel with fluidic channels to establish perfusable vascular models has been reported.^{55,96,117} These microfluidic systems consist of fluidic channels connected to tissue chambers which are loaded with a solution of endothelial cells suspended in fibrin gel. In this environment, endothelial cells spontaneously assemble into vessels that interconnect to form vascular networks. Under the right conditions, vessel lumina fuse with fluidic channels allowing for perfusion of the vascular networks.

The lack of standard practices for establishing anastomotic connections between self-assembled vessels and fluidic channels and the multiplicity of factors that can affect anastomoses in microfluidic devices presents a challenge for the development of high throughput platforms which demand a robust method for establishing perfusable vascular networks. Guided by insights from the literature and experimental observations, this section will discuss work to improve the success rate of anastomoses of self-assembled vessels with fluidic channels in IFlowPlate™.

Sealing Gel

Fibrin gel leakage into fluidic channels precludes the fusion of vessel lumina in tissue chambers with lateral fluidic channels and thus compromises perfusion of vascular networks. One approach to prevent fibrin gel loaded into tissue chambers from leaking into connected fluidic channels is to design the microfluidic device with boundaries (e.g., microposts or connecting pores) whose geometry and dimensions are configured to increase interfacial surface tension and restrict fluid flow into the channel.^{55,96,117}

It was observed that the design of IFlowPlate™ does not prevent fibrin pre-gel solution loaded in the middle well from leaking into connected fluidic channels. **Figure 29A** shows a schematic representation of the consequence of gel leakage into fluidic channels of a microfluidic system in IFlowPlate™. Leaked fibrin gel-entrapped endothelial cells can form attenuated microvessels that do not interconnect in a continuous network that bridges the liquid-gel interface (**Figure 29B**). The introduction of a fluorescent dye solution into the outlet well of an IFlowPlate™ vascular model demonstrated that vessels within gel-filled channels fail to support efficient fluid transport into the vascular network (**Figure 29C**).

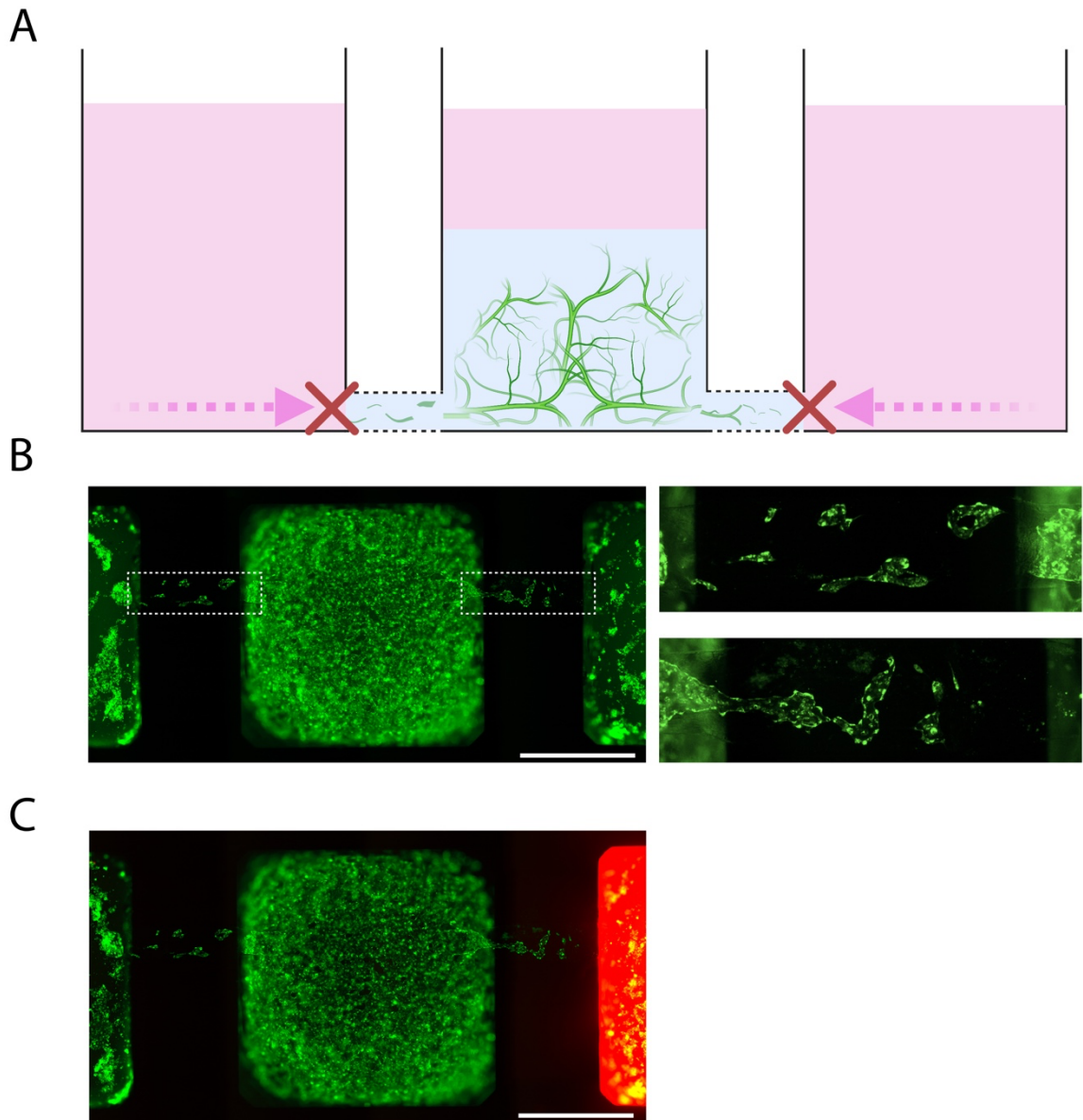


Figure 29. Fibrin pre-gel cast in the middle well leaks into fluidic channels of IFlowPlate™ microfluidic systems and compromises perfusion of vascular networks. (A) Schematic showing the outcome of fibrin pre-gel leakage into fluidic channels of an IFlowPlate™ microfluidic system. Gel obstructs fluid flow and encapsulated GFP-HUVECs assemble into attenuated and incompletely connected microvessels that do not bridge the liquid-gel interface and fail to support efficient transport of fluid into the vascular network. (B) Fluorescence images of a Day 6 vascular network in an IFlowPlate™ microfluidic system. Right images show zoomed-in view of inlet channel (*top image*) and outlet channel (*bottom image*) with endothelial tubules in fibrin gel. (C) Fluorescence image showing that 70 kDa TRITC-dextran solution (*red*) introduced into the outlet well does not perfuse the vascular network after 30 minutes. Scale bar, 1.5 mm.

To prevent the entry of fibrin pre-gel solution into connected fluidic channels, channels were temporarily sealed. Prior to casting the fibrin pre-gel solution in the middle well, channels were loaded with a pre-gel solution that upon gelation would provide a physical barrier to the entry of the fibrin pre-gel solution loaded in the middle well. Following gelation of the fibrin solution in the middle well, the sealing gel would be replaced with cell culture medium.

Fibrin pre-gel solution for sealing channels was prepared by mixing 30 μl of 10 U/mL thrombin in BSA with 150 μl of 10 mg/mL fibrinogen in D-PBS. To load channels, 30 μl of fibrin pre-gel solution was dispensed into the inlet and outlet well. After enzymatic-induced gelation at room temperature, fibrin pre-gel solution was cast in the middle well. Using fibrin gel to temporarily seal fluidic channels was not sufficient to reproducibly achieve perfusable vascular networks. It was speculated that this could be due to (1) incomplete aspiration of sticky sealing gel from channels, and/or (2) the presence of air bubbles caused by incomplete liquid filling of dry, dead-end channels.

To address this, fibrin was substituted for gelatin for use as a temporary sealing gel. Prior to casting the fibrin pre-gel solution in the middle well of an IFlowPlate™ microfluidic system, channels were loaded with 50 μl hot, liquid 10% (wt/v) gelatin. Upon cooling, gelatin undergoes a sol-gel transition and provides a physical barrier to the entry of the fibrin pre-gel, cast in the middle well, into lateral fluidic channels. Following polymerization of the fibrin pre-gel in the middle well, IFlowPlate™ is placed in the 37 °C incubator and gelatin (from bovine skin) undergoes a rapid gel-sol transition (**Figure 13**). The unique thermo-reversible character of gelatin makes it better suited for use as a

temporary sealing gel in IFlowPlate™ because liquid gelatin can be replaced by dilution with culture medium which precludes the challenge of filling dry, dead-end microfluidic channels. Filling dead-end microfluidic channels can lead to trapped air at the liquid-gel interface which compromises anastomosis as it can obstruct fluid flow and kill cells.⁹⁰ The substitution of fibrin for gelatin as a temporary sealing gel did not deliver the expected improvements to the success rate of vessel-fluidic channel anastomosis. This encouraged a better understanding of the factors that influence anastomosis.

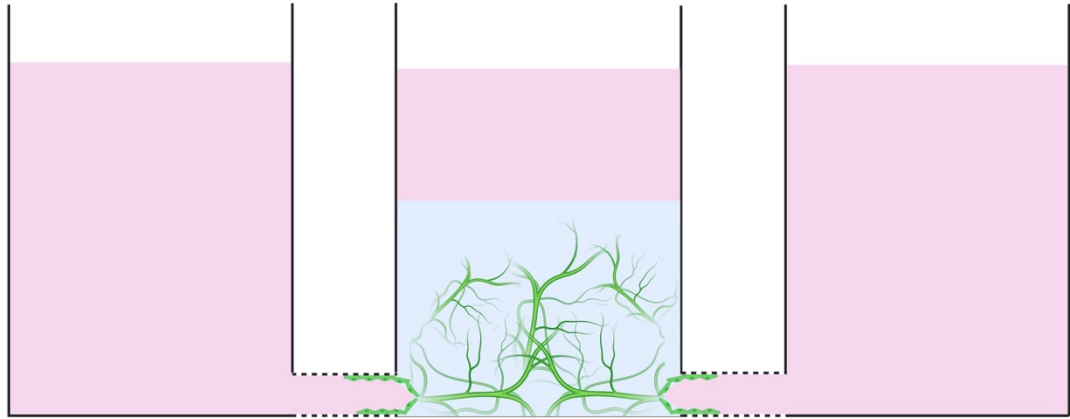
Bidirectional Anastomoses

Anastomoses between living vessels embedded in gel and fluidic channels can be induced bidirectionally.⁹⁶ During vasculogenesis, gel-encapsulated endothelial cells in the tissue chamber can migrate into the fluidic channels, attach to walls, and form a proliferating monolayer which facilitates vessel-fluidic channel anastomoses (**Figure 30A**). Anastomoses can also be facilitated by the invasion of sprouts from endothelialized fluidic channels into the gel of the tissue chamber (**Figure 30B**). In IFlowPlate™, it was found that vascular models in which fluidic channels were loaded with GFP-HUVECs did not show a higher rate or higher quality (i.e., leak-free) of anastomoses compared to vascular models that relied solely on the migration of endothelial cells from the tissue chamber into fluidic channels (**Figure 31**). These seemingly counterintuitive results could be explained by insufficient endothelialization of fluidic channels. The extension of a new vascular branch from fluidic channels requires that the channel is lined by a continuous endothelial monolayer.⁹⁶ The poor cell adhesion properties of PDMS and polystyrene

which comprise 3/4 and 1/4 of the walls of IFlowPlate™ fluidic channels, respectively, is consistent with observations of channels sparsely populated with GFP-HUVECs. Moreover, increasing detachment of GFP-HUVECs from the cell culture surface was observed with increasing culture time independent of whether cells were cultured under perfusion (**Figure 32**) or static conditions (**Figure 33**). These results indicated that perfusion culture conditions created by placing IFlowPlate™ on an interval rocker platform contributed negligibly to the detachment observed.

The failure of endothelial cells to adhere to ECM results in cessation of proliferation and apoptosis.¹²⁹ It was hypothesized that improving endothelial cell adhesion to fluidic channels would facilitate endothelialization and more robust, leak-free anastomoses. It is widely accepted that the choice of substrate material and surface modification plays a critical role in cell adhesion.⁹⁰ The next section will discuss work to improve endothelial cell adhesion by modifying the cell culture surface of IFlowPlate™ microfluidic systems.

A Endothelial cells from gel migrate into channels



B Sprouts from endothelialized channels invade gel

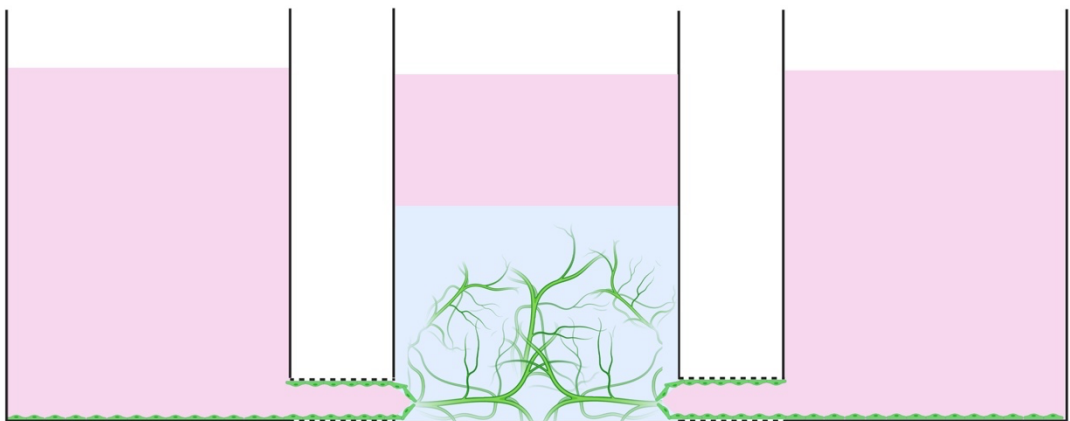


Figure 30. Schematic showing that anastomoses between living vessels embedded in gel and fluidic channels of IFlowPlate™ microfluidic systems can be induced bidirectionally. (A) During vasculogenesis, gel-encapsulated GFP-HUVECs in the tissue chamber can migrate into lateral fluidic channels, attach to walls, and form a proliferating monolayer which facilitates vessel-fluidic channel anastomoses. (B) GFP-HUVECs loaded into fluidic channels can form monolayers that line channel walls. Sprouts from endothelialized channels can invade the gel and facilitate fluidic channel-vessel anastomoses.

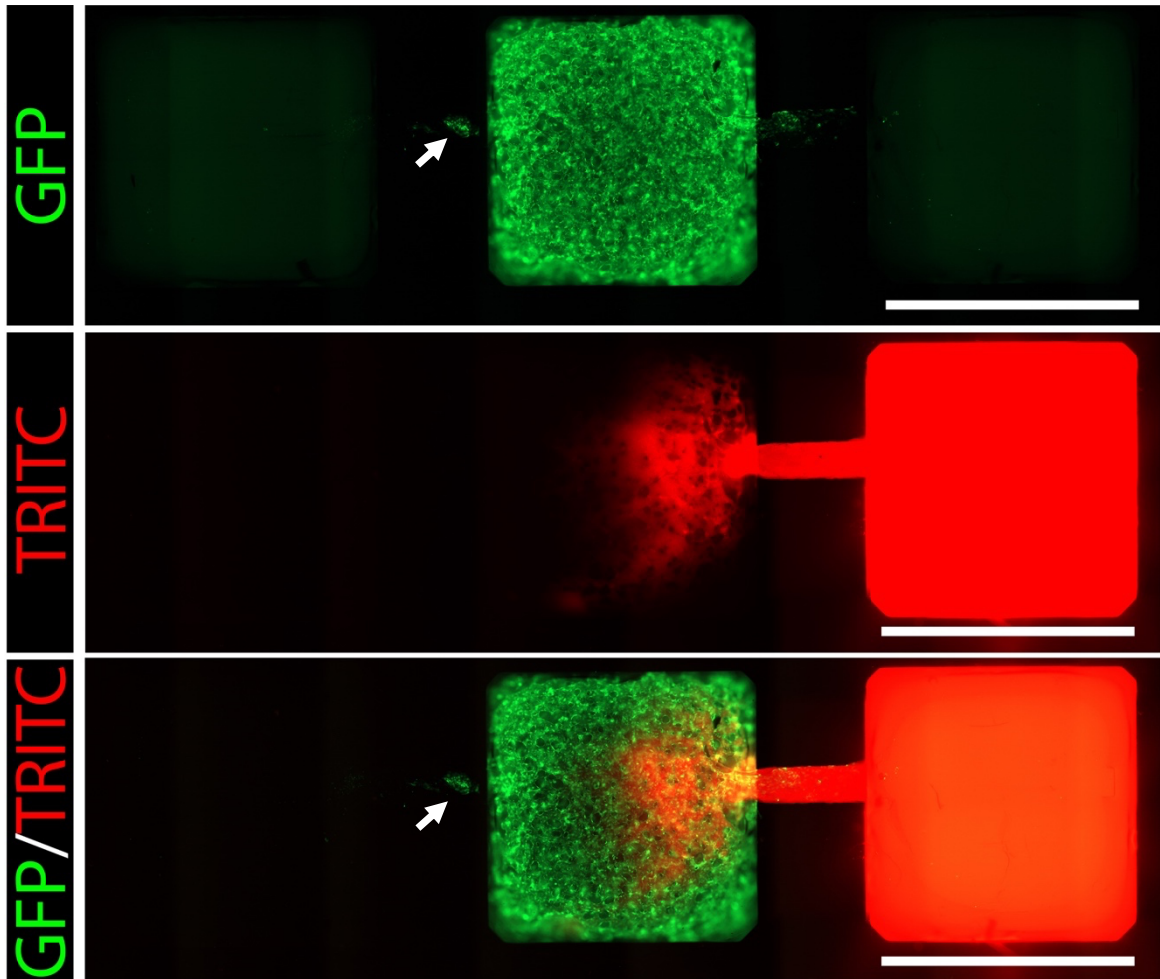


Figure 31. Encapsulated GFP-HUVECs migrate from the gel into fluidic channels and form a “leaky” anastomotic connection with only one of the fluidic channels. 70 kDa TRITC-dextran was added to the outlet reservoir well of a Day 6 IFlowPlate™ vascular model. Fluorescence microscopy images captured 30 minutes after introduction of TRITC-dextran indicates a “leaky” anastomotic connection between the vascular network and outlet fluidic channel. No anastomotic connection is visible between the vascular network and inlet fluidic channel. Cell clustering (*white arrow*) instead of spreading indicates a lack of cell adhesion. Scale bar, 3 mm.

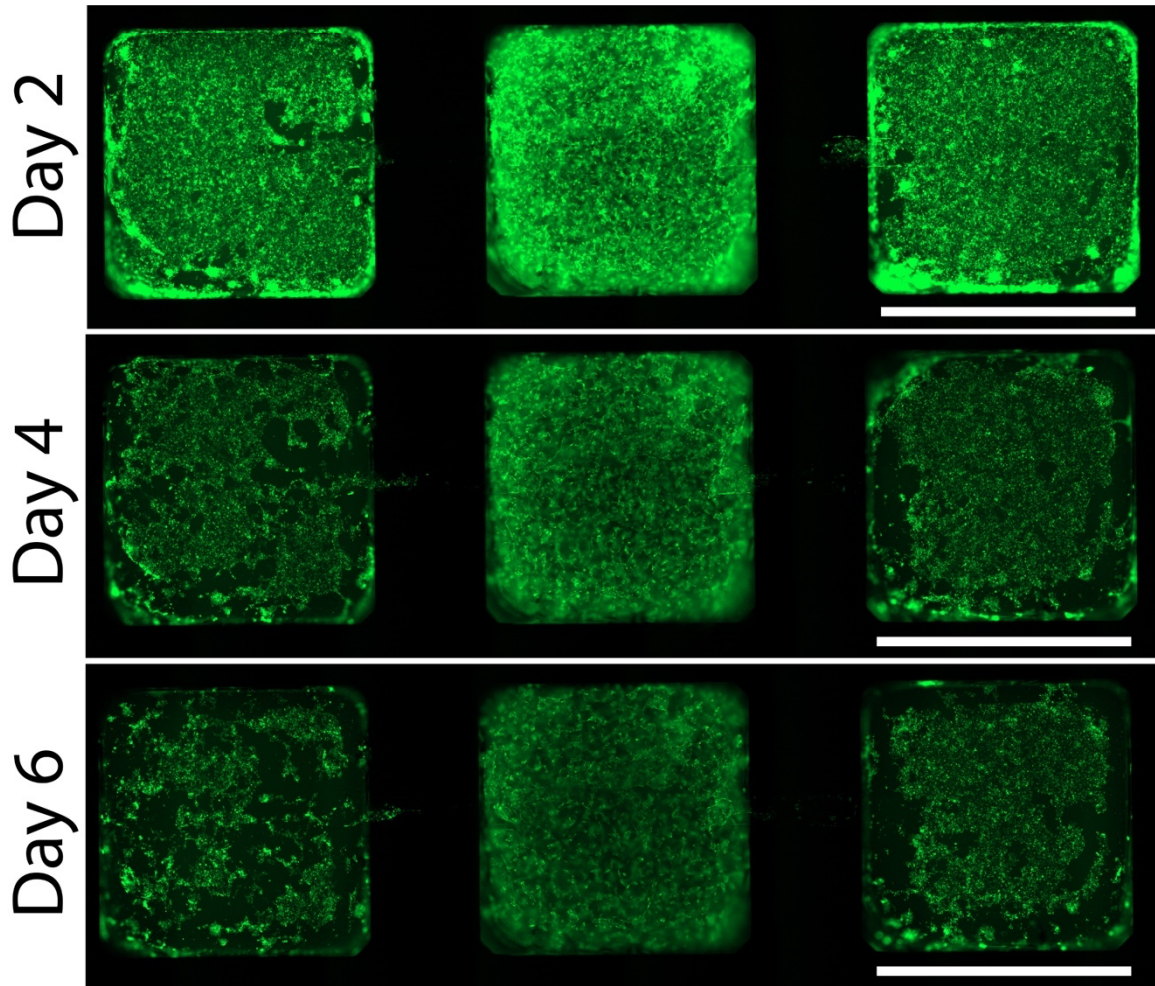


Figure 32. GFP-HUVECs loaded into fluidic channels of IFlowPlate™ microfluidic systems insufficiently endothelialize channels under perfusion culture conditions. Following encapsulation of GFP-HUVECs and fibroblasts in the middle well, 90 μl of GFP-HUVEC suspension at a concentration of 600,000 cells/mL was added to inlet and outlet wells to load connected fluidic channels. Representative fluorescence images captured every two days show sparsely populated fluidic channels and increasing detachment of GFP-HUVECs with increasing culture time. Scale bar, 3 mm.

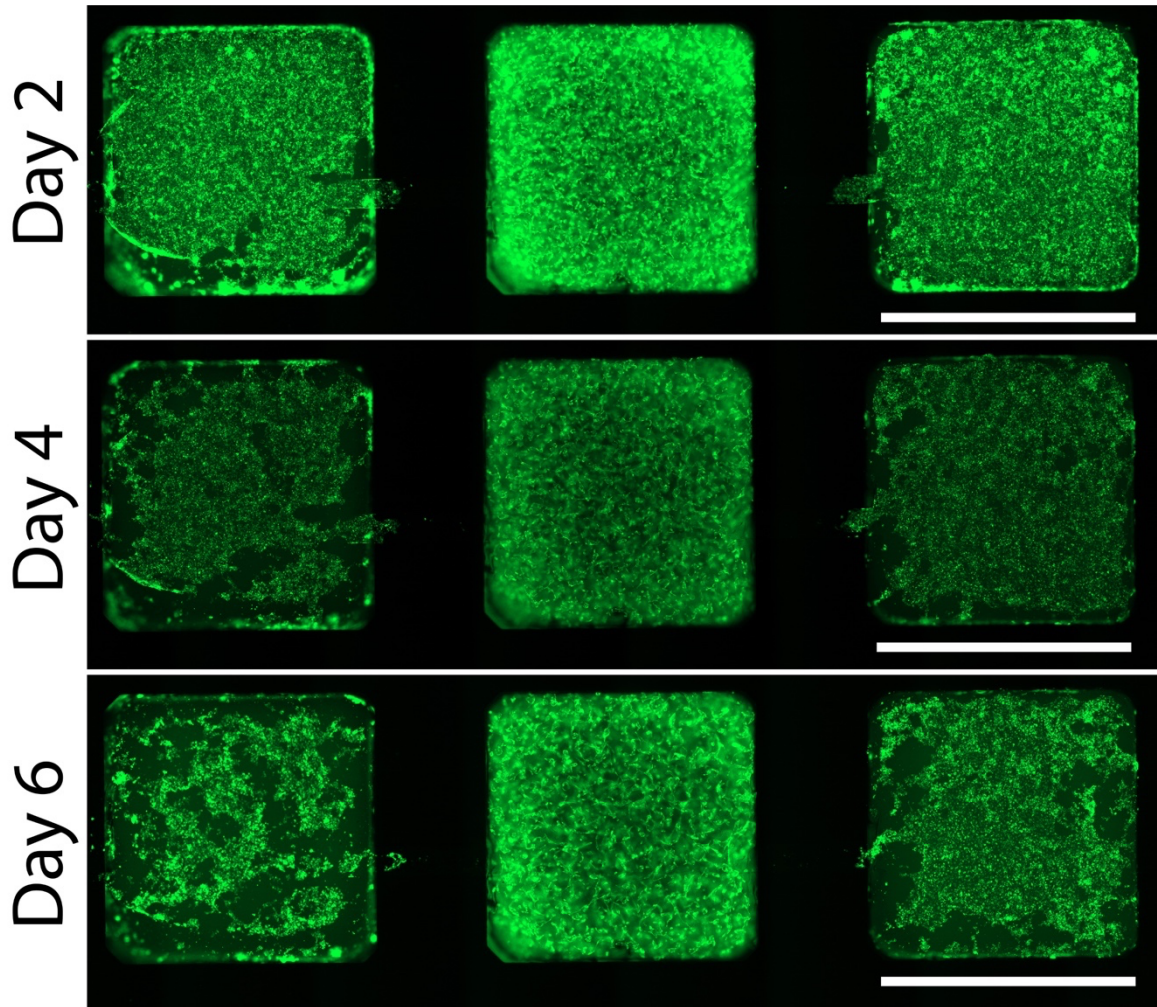


Figure 33. GFP-HUVECs loaded into fluidic channels of IFlowPlate™ microfluidic systems insufficiently endothelialize channels under static culture conditions. Following encapsulation of GFP-HUVECs and fibroblasts in the middle well, 90 μ l of GFP-HUVEC suspension at a concentration of 600,000 cells/mL was added to inlet and outlet wells to load connected fluidic channels. Representative fluorescence images captured every two days show sparsely populated fluidic channels and increasing detachment of GFP-HUVECs with increasing culture time. Scale bar, 3 mm.

Coating IFlowPlate™ Microfluidic Channels with ECM Protein

Consistent with what has been reported in the literature,⁹⁶ seeding microfluidic channels with GFP-HUVECs to achieve a continuous endothelial monolayer that lines the length of channels is not a prerequisite for anastomosis. Indeed, without the addition of GFP-HUVECs added to channels, the migration of gel-encapsulated endothelial cells from the tissue chamber into fluidic channels was sufficient to facilitate anastomosis (**Figure 32**). However, the frequency and quality of anastomotic connections in IFlowPlate™ microfluidic systems was low.

The inherent hydrophobicity of IFlowPlate™ channel surfaces is unfavourable for endothelial cell adhesion and compromises robust formation of leak-free anastomotic connections between living vessels in the tissue chamber and fluidic channels. Coating PDMS-based microfluidic devices with ECM protein has been identified as critical for endothelial cell adhesion and migration.⁹⁶ To improve the quality and robustness of anastomoses in IFlowPlate™ microfluidic systems, three different ECM protein coatings, fibrinogen, collagen-I, and Matrigel®, were tested for their capacity to enhance GFP-HUVEC adhesion. For this experiment, GFP-HUVECs were seeded in ECM-coated channels so that GFP-HUVEC adhesion to PDMS/polystyrene surfaces could be assessed directly and not be contingent on the migration of endothelial cells from the tissue chamber. In a parallel experiment, GFP-HUVECs were not seeded in ECM-coated channels so that directional migration of gel-encapsulated GFP-HUVECs into lateral fluidic channels in response to a chemoattractant gradient could be assessed.

Interestingly, while some groups have reported successful anastomotic connections in microfluidic systems with fibroblast and HUVEC mixed co-cultures,¹¹⁷ others have reported that anastomotic connections rarely formed when fibroblasts and HUVECs were cultured together and success was much greater when fibroblasts were cultured in flanking channels.⁵⁵ Authors speculate that a chemical gradient of fibroblast secreted factors promoted spontaneous anastomotic connections between living vessels and fluidic channels.¹³⁰ Chemotactic stimuli that promote endothelial cell migration are dependent on endothelial cell adhesion to ECM protein.¹²⁹ Indeed, it has been shown that only ECM-coated substrates induced HUVECs to form visible filopodial projections indicating reorganization of the actin cytoskeleton which is a prerequisite for cell migration.¹³¹ Commercially available Boyden chambers are widely used to study the directional migration of endothelial cells across an ECM-coated membrane in response to a chemoattractant gradient.¹³² Studies have shown that FBS is a significantly more powerful chemoattractant than vascular endothelial growth factor (VEGF) and 5% (v/v) FBS has been used as a positive control in endothelial cell migration assays using Boyden chambers.¹³² To establish a chemoattractant gradient in IFlowPlate™ microfluidic systems, 5% (v/v) FBS was added to reservoir wells with or without ECM-coating.

To coat channels with ECM protein, 250 µg/mL of fibrinogen, 100 µg/mL collagen-I, or 3% (v/v) Matrigel® was added to reservoir wells of IFlowPlate™ microfluidic systems in three independent conditions. Following incubation of the plate at 37 °C to allow ECM protein adsorption, 100 µl of GFP-HUVEC suspension was added to reservoir wells. The plate was incubated at 37 °C under static conditions to allow for cell attachment and

fluorescence microscopy images were acquired the next day. **Figure 34** shows the results of the ECM-coating experiment performed to test the capacity for ECM protein to enhance GFP-HUVEC adhesion. There was no appreciable difference between microfluidic systems that received an ECM coating and the control which did not (apart from gelatin sealing gel which is used in the standard preparation of IFlowPlate™).

Figure 35 shows the results of the endothelial cell migration assay in IFlowPlate™. No difference in the migration of GFP-HUVECs from the tissue chamber into ECM-coated fluidic channels was observed in the presence of a strong chemoattractant gradient compared to controls in which no chemoattractant, and/or no ECM protein coating was added.

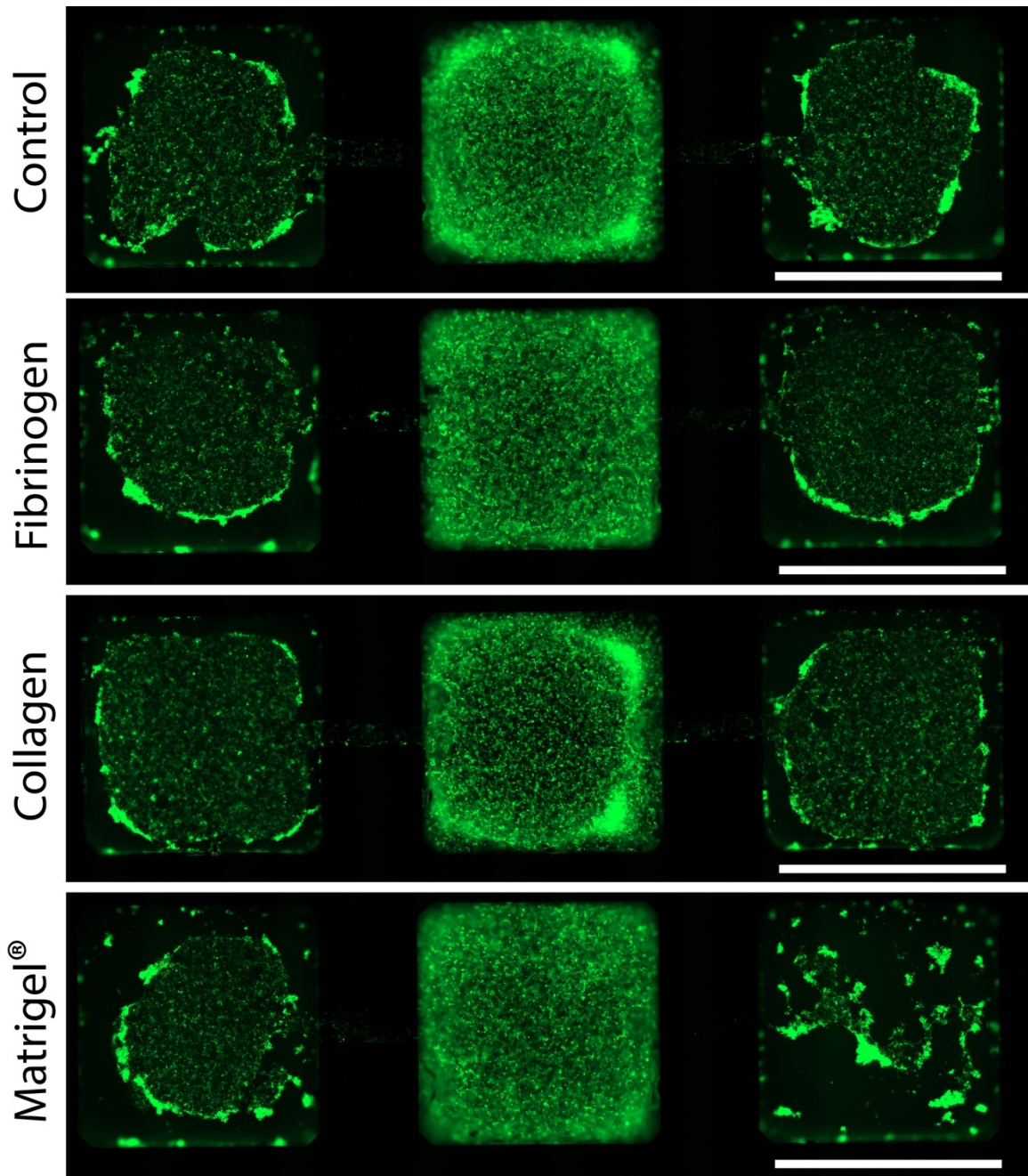


Figure 34. IFlowPlate™ microfluidic systems were coated with ECM protein to modify inherently hydrophobic PDMS and polystyrene surfaces and enhance GFP-HUVEC adhesion. 90 μ l of 250 μ g/mL of fibrinogen, 100 μ g/mL collagen-I, and 3% (v/v) Matrigel® were added to reservoir wells of IFlowPlate™ microfluidic systems (n = 3 per condition). IFlowPlate™ was incubated at 37 °C for 2 hours to allow ECM protein adsorption. 100 μ l of GFP-HUVEC suspension was added to reservoir wells. IFlowPlate™ was incubated at 37 °C under static conditions and fluorescence microscopy images were acquired the next day. Scale bar, 3 mm.

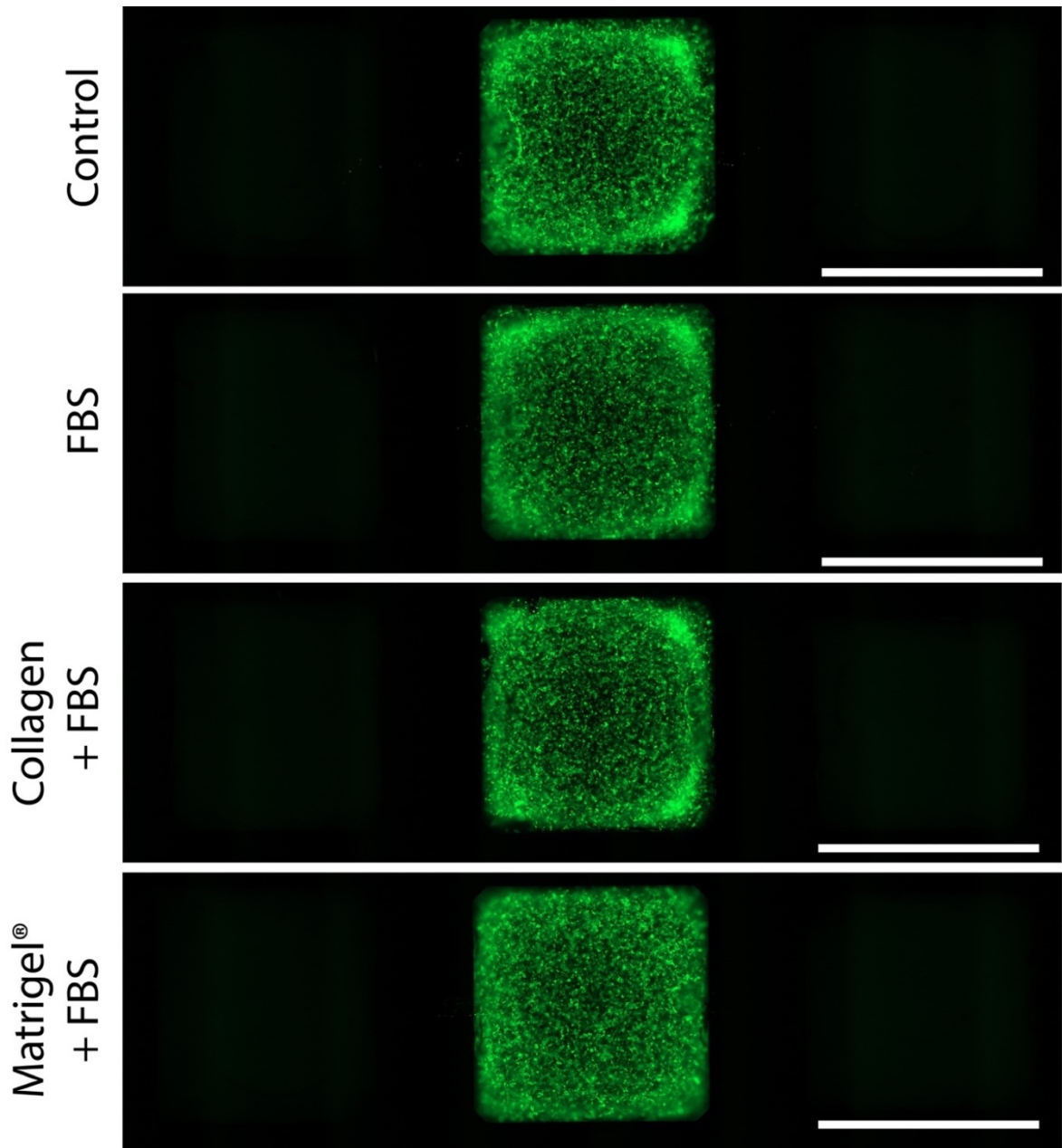


Figure 35. Migration of gel-encapsulated GFP-HUVECs from tissue chamber into ECM-coated lateral fluidic channels in response to a strong chemoattractant gradient. 5% (v/v) FBS was added to reservoir wells of microfluidic systems with or without ECM coating. No ECM-coating and no FBS, FBS-only, and ECM-coating-only (data not shown) conditions served as negative controls (n = 3 per condition). IFlowPlate™ was incubated at 37 °C under static conditions and fluorescence microscopy images were acquired the next day. Scale bar, 3 mm.

The lack of GFP-HUVEC adhesion to surfaces treated with ECM protein could indicate that 1) ECM protein is not adequately coating the hydrophobic PDMS/polystyrene culture surfaces and/or 2) the hydrophobic surfaces induce conformational changes in ECM protein structure which negatively influence the ability of endothelial cells to bind adhesion domains.^{92,133} The hydrophobicity of PDMS leads to rapid non-specific adsorption of proteins and small hydrophobic molecules present in any solution that it comes in contact with.⁹² This is problematic in microfluidic cell culture systems because of inconsistency in the composition of adsorbed proteins, and/or the loss of biologically important proteins, such as ECM proteins, that mediate endothelial cell adhesion via cell integrin receptors.⁹² Proteins compete for adsorption to surfaces and the most abundant protein in cell culture medium, albumin, preferentially adsorbs to hydrophobic surfaces and resists displacement by cell adhesive proteins.^{92,134}

Alternatively, Underwood et al. have shown that for the same density of fibronectin adsorbed to hydrophobic polystyrene or culture-grade polystyrene, the percentage of cell adhesion was much greater on the more hydrophilic culture-grade polystyrene.¹³³ Using physical methods to detect conformational changes in 3D protein structure, it has been found that hydrophobic surfaces cause a general unfolding of the protein that alters the integrity of adhesion domains (e.g., RGD) and results in poorer cell adhesive properties.¹³³

To visualize and quantify the density of ECM protein immobilized on the PDMS/polystyrene surfaces of IFlowPlate™ microfluidic systems, commercially available fluorescently tagged ECM proteins can be purchased. Furthermore, antibodies against cell adhesion domains can be used to infer their accessibility to cell surface receptors.

The reviewed studies suggest that increasing the hydrophilicity of a surface may enhance cell adhesion by (1) reducing non-specific protein adsorption and thus increasing the density of adsorbed ECM protein and (2) reducing undesirable conformational changes in protein structure and thus increasing the biological activity of immobilized cell adhesive proteins.^{92,133,134} At the time of writing, our lab has transitioned to the use of manufactured IFlowPlate™ platforms which are assembled by laser welding and are therefore free of highly hydrophobic PDMS. In future work, consideration should be given to the incorporation of standard cell-culture grade polystyrene plate bottom to make ECM-coating more effective and enhance endothelial cell adhesion.

4.3 Enhancing Physiological Relevance of IFlowPlate™ Intestine Model

4.3.1 IFlowPlate™ Primary Intestine Model

Caco-2 cells were originally isolated from colon tumour samples. They harbour multiple genetic mutations making them inappropriate for evaluating the carcinogenic potential of compounds and studying the transformation of precancerous cells. Caco-2 cells can also form multilayer regions ranging in thickness from two cells to more than twenty cells.²² These protrusions within the monolayer have been likened to polyp-like masses and are a morphological feature of abnormal intestinal epithelium.²²

To better represent normal intestinal physiology and overcome the limitations of using a cancer cell line or 3D organoids, monolayer models derived from primary intestine tissue have been developed.^{20,25-28} These models can serve as a relevant platform for compound screening, studying tissue homeostasis, and precision medicine.⁴⁶ To enhance the physiological relevance of the IFlowPlate™ Caco-2 intestine model, the development of a primary intestine model using colon organoids generated from biopsied intestinal tissue was explored.

As discussed in Section 4.1.1, the stiffness of the cell culture substrate has been identified as a key factor in the determination of primary intestinal epithelial cell culture morphology.^{25,26} Crypts cultured on top of a soft substrate, such as Matrigel®, failed to form a 2D monolayer and instead formed 3D organoids.²⁵ Alternatively, crypts plated on a stiff substrate, such as polystyrene, formed a 2D monolayer.²⁵ Herein, it was demonstrated that Caco-2 cells also display substrate-dependent culture morphologies and their responses to

Matrigel[®] and polystyrene (**Figure 21**) emulate the reported responses of epithelial cells derived from primary intestinal tissue.

In a preliminary experiment performed by a colleague, it was found that the formulated fibrin-Matrigel[®], which supports the culture of Caco-2 cells in a monolayer (**Figure 21**), did not support the culture of colon organoid-derived epithelial cells in a monolayer. In recent years, self-renewing human primary intestinal epithelial cell monolayers have been accomplished by culturing crypts/intestinal stem cells on collagen hydrogels.^{25,28} In an attempt to replicate these results, three collagen hydrogels were formulated: (1) 1 mg/mL collagen-only²⁵, (2) 4 mg/mL collagen with 25% (v/v) Matrigel[®],²⁸ and (3) 1.6 mg/mL collagen with 10 mg/mL fibrin and 20% (v/v) Matrigel[®]. Formulations 1 and 2 have been reported to possess appropriate stiffness to support monolayer formation when epithelial cells derived from primary intestinal tissue are plated on the surface.^{25,28} A third formulation that included fibrin was also developed and tested for its ability to support monolayer formation. Dilution of collagen with Matrigel[®] at increasing percentages by volume, generates hydrogels with increased stiffness.¹³⁵ A blended acellular hydrogel composed of 1.6 mg/mL collagen and 20% (v/v) Matrigel[®] has a reported stiffness of > 6 kPa on Day 3 of incubation at 37 °C.¹³⁵ Based on the stiffness values reported in the literature for acellular blended collagen-fibrin⁸³ and collagen-Matrigel[®]¹³⁵ constructs, this custom formulation was presumed to possess a stiffness value greater than that of 1 mg/mL collagen-only constructs; therefore, it was a promising candidate gel for use in the IFlowPlate[™] primary intestine model.

Multicellular organoid fragments were seeded on the surface of three differently formulated collagen gels and cultured for one week to assess their ability to form monolayers. Additional wells with gel (no cells) enabled tactile probing with a pipette tip to sense the compliance of each gel formulation. Consistent with estimates of stiffness values based on the literature, Formulation 1 was the most compliant and Formulation 3 was the least compliant.

Colon organoid fragments failed to form monolayers on the surface of all three collagen gels – (1) collagen-only, (2) collagen-Matrigel[®], and (3) collagen-fibrin-Matrigel[®] gels (**Figure 36**). Organoid fragments sunk through the very delicate 1 mg/mL collagen-only gel within the first days of culture. Contact with the plastic substrate resulted in patches of monolayers that were observed by Day 6.

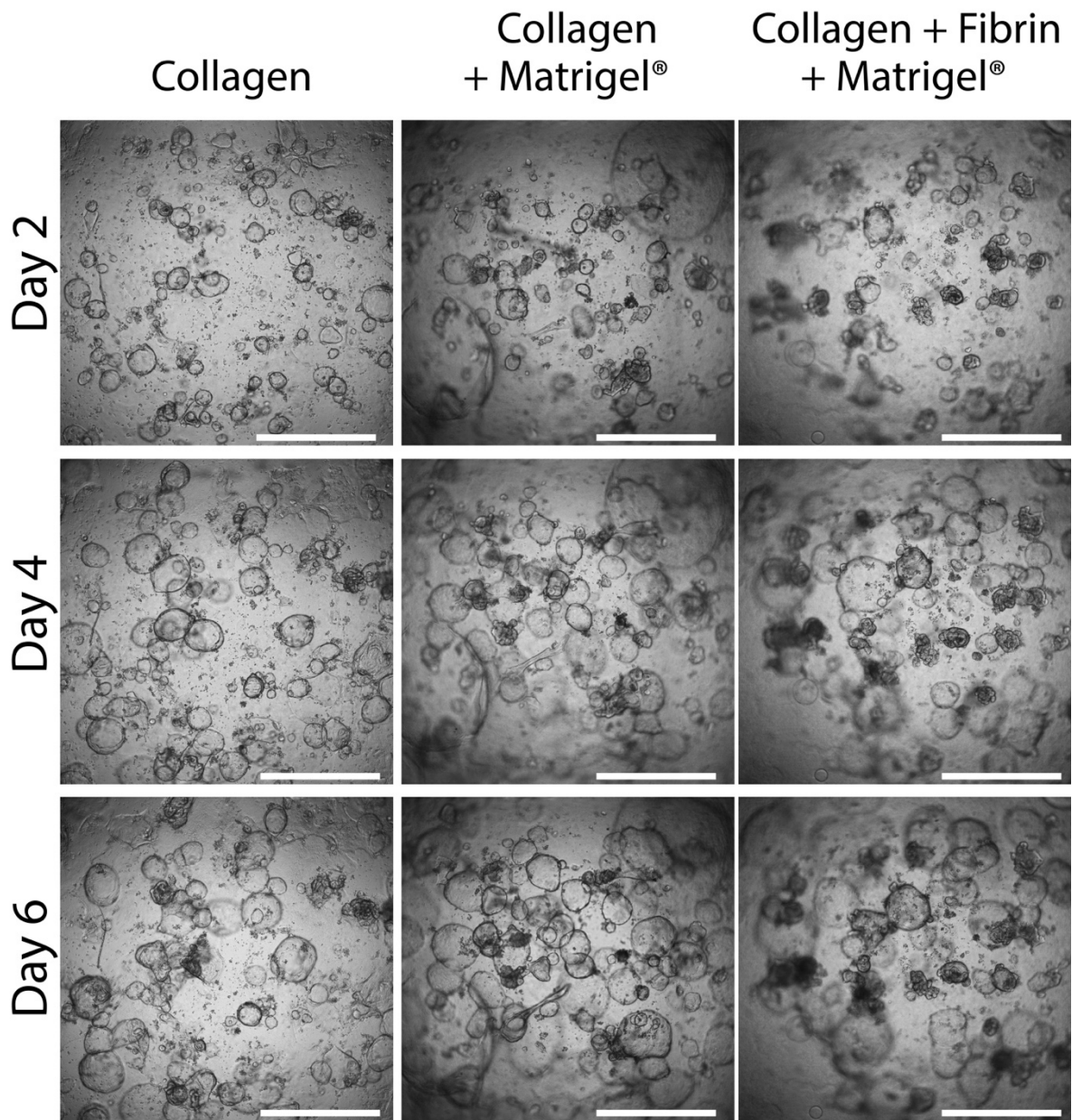


Figure 36. Patient-derived colon organoid fragments seeded on top of collagen hydrogels to assess substrate-dependent monolayer formation. Multicellular fragments generated from mild enzymatic dissociation of colon organoids were seeded on top of (1) collagen-only, (2) collagen-Matrigel[®], and (3) collagen-fibrin-Matrigel[®] hydrogels in a 384-well plate (n = 3, representative images are shown). Scale bar, 1 mm.

A recent Nature Protocols publication⁸⁴ details the methods Wang et al. used to form a self-renewing primary colon monolayer on 1 mg/mL collagen gel.²⁵ This recent publication provides some insight into the failure to replicate the findings reported in their initial publication. Firstly, they advised that the 1 mg/mL collagen hydrogel is “very fragile” and that room temperature incubation for 15 days in PBS could be critical for successful cell attachment and spreading.⁸⁴ They speculate that mature gels have different mechanical properties (i.e., stiffness) and biochemical properties, as any contaminants originating from the batch of collagen diffuse out of the gel.⁸⁴ This extended incubation step as described, is not compatible with the protocol for the IFlowPlate™ vascular intestine model, wherein live cells are encapsulated in the gel.

Another possible explanation for the fragility of the collagen-only gel could be the resolubilization of collagen due to increased acidity of the culture medium that occurs as cells consume nutrients and release metabolites.⁸⁴ The accumulation of metabolites in culture medium increases concomitantly with the number of cells. This makes 1 mg/mL collagen-only gels whose integrity critically depends on pH not ideal for IFlowPlate™ tri-culture models comprised of GFP-HUVECs, fibroblasts, and intestine cells.

Rather than a direct replication of the previously published work, the experiment performed was a conceptual replication designed to test the underlying hypothesis that substrate stiffness determines intestinal cell culture morphology.^{25,26,28} The failure of organoid fragments to form monolayers on Formulations 2 and 3 (as well as the original fibrin-Matrigel® formulation) could indicate that stiffness is just one of multiple parameters that determine primary intestinal epithelial cell culture morphology, and that other

parameters (e.g., cell origin, seeding protocol) that influence the experimental outcome were inadvertently manipulated because they have not yet been identified as relevant. This is plausible given that the culture of organoid-derived intestinal epithelial cells in monolayers is a relatively recent advance and there is a paucity of research in this area. The failure to replicate previously published results highlights the need for systematic inquiry and experimentation to discover what other factors might be relevant to the conversion of 3D organoids to 2D monolayers. A comparison of the experimental methods used in each of the studies provides clues that could be used to generate hypotheses for testing.

It is a normal occurrence for 3D organoid models derived from the same tissue type to exhibit different morphologies; thus, indicating that morphology primarily reflects characteristics of the donor, not necessarily the type of tissue.¹³⁶ In each study, the primary intestine monolayers established were generated from biopsied tissue from donors of distinct age, gender, and health status.^{25,26,28} Given their unique origins, intestinal epithelial cells from different donors could have unique cellular properties and therefore, unique responses to the same culture conditions (e.g., substrate stiffness). The cells used in this study originated from a macroscopically unaffected area of the colon in a 69-year-old female patient with colorectal adenocarcinoma. Since cancer is a progressive disease, the collection of tissue from a morphologically unremarkable region does not exclude the possibility that the tissue possesses epigenetic, transcriptional, or genetic alterations that are associated with field cancerization.¹³⁷ Indeed, targeted DNA sequencing performed on endoscopically collected paired samples from colorectal neoplasms and adjacent macroscopically unaffected tissue demonstrated that the latter can harbour cancer-

associated mutations.¹³⁷ A caveat of using cells isolated from macroscopically unaffected tissue in patients with cancer, is that these cells could be precancerous and/or possess mutations that modulate cell behaviour in ways that confound experimental results. For example, it has been shown that mutations in components of cellular mechanosignalling pathways can alter the sensitivity of cells to substrate stiffness.¹³⁸ Cells with a mutation in the bone morphogenetic protein (BMP) type 1 receptor inappropriately sense substrate stiffness and respond to soft substrates with a spread morphology that emulates the morphology of wild-type cells on stiff substrates.¹³⁸ To help rule out that the origin of the cells used in this study has biased the results, cells could be genetically screened for mutations and biological replicates (i.e., tissue from at least three donors with distinct clinical variables) should be included in the experimental design.

The isolation procedure and density of crypts or cells seeded on the substrate surface are other parameters that might be relevant to establishing primary intestinal epithelial monolayers. The long-term culture of primary intestinal tissue as 3D organoids or 2D monolayers depends on self-renewing intestinal stem cells.⁴² It is estimated that between four and six intestinal stem cells reside in each crypt.⁴² Crypts can be cultured in Matrigel[®] and undergo continuous budding events to generate an organoid with many crypt domains.⁴² Alternatively, a single intestinal stem cell cultured in Matrigel[®] can grow into an organoid structure that is indistinguishable from organoids generated by cultured crypts.⁴²

Primary intestinal epithelial monolayers have been established by plating (1) crypts/multicellular fragments²⁵⁻²⁷ or single cells^{28,29} on ECM-coated membranes and

natural hydrogel substrates. Moon et al. reported the first example of growing dissociated 3D organoids as a monolayer.²⁹ It was found that reproducible formation of 2D monolayers on the surface of a 0.33 cm² transwell insert required a large number ($\sim 5 \times 10^5$) of cells.²⁹ Two-fold serial dilution of a suspension of $\sim 5 \times 10^5$ cells demonstrated that at a dilution of 1:16, monolayer formation could not be reproducibly achieved.²⁹ These results suggest that cell seeding density plays a role in monolayer formation.

To obtain the large number of viable cells required for monolayer culture on a single transwell insert, colonic spheroids were first expanded in 3D Matrigel[®] cultures for three days.²⁹ Three-day-old colonic spheroids from three wells of a 24-well plate (400 to 500 spheroids/well) were recovered, mechanically dissociated, and passed through a 40 μ m cell strainer before being resuspended in culture media and seeded on a single gelatin-coated transwell insert.²⁹ A large number of cells might be required to compensate for intestinal stem cells lost during the procedure to isolate single cells.⁴² This could explain why other studies have failed to reproducibly form confluent monolayers ($\sim 40\%$ success rate) when seeding single cells on top of a membrane, but found greater success ($\sim 90\%$ success rate) when seeding multicellular fragments generated from mildly dissociated organoids.²⁷

As an alternative approach, Altay et al. report plating crypts at a density of 1000 – 1500 crypts/cm² to establish a monolayer on a transwell insert.²⁶ Similarly, Wang et al. established a monolayer by plating crypts on top of a collagen hydrogel in a 6-well plate at a density of 1000 crypts/cm².²⁵ In a Nature Protocols publication, the authors give troubleshooting advice to increase the crypt seeding density in the event that cells do not establish a growing monolayer over the collagen gel.⁸⁴ Together, these findings suggest

that optimizing the isolation procedure and/or seeding density might be important for establishing a primary intestine monolayer in IFlowPlate™.

4.3.2 SynoPlate™ Intestine Model

IFlowPlate™ is a tissue agnostic platform that can be used to develop 2D monolayer or 3D spheroid/organoid models^{51,97} of a variety of organs. In IFlowPlate™, vascularization of organ tissue occurs by vasculogenesis. Gel-encapsulated endothelial cells self-assemble into a perfusable vasculature that emulates the complex topologies and lumen diameters of native capillaries.

SynoPlate™ is most notably distinguished from IFlowPlate™ by the integration of tissue-specific scaffolds that guide the assembly of parenchymal cells and endothelial cells. The specialized functions of the intestine are supported by the 3D topographical features that span multiple length scales including the macroscale (e.g., coiled tube and circular folds), microscale (e.g., villi and crypts), and nanoscale (e.g., ECM proteins).¹³⁹ Encapsulation of moulded alginate in a fibrin-based gel and subsequent dissolution and flushing is used to produce an intestine-specific scaffold that provides the multiscale topographical cues of the native intestine.

The intestine scaffold joins dedicated inlet and outlet reservoirs allowing intestinal epithelial cells to be exposed to luminal fluid flow and shear stress. The significance of incorporating mechanical stimuli, such as shear stress, that are present in the intestine environment was demonstrated by Kim et al. using their Gut-on-a-Chip microfluidic device.⁴⁰ Caco-2 cells cultured in the presence of fluid flow exhibited accelerated

differentiation as indicated by well-developed tight junctions and barrier function after only 3 days of culture compared to 3 weeks for cells cultured in static transwell systems.⁴⁰ Furthermore, Caco-2 cells that experienced fluid flow were morphologically similar to cells within native tissue.⁴⁰ Compared to Caco-2 cells cultured under static conditions which were flattened and resembled non-physiological squamous epithelium, Caco-2 cells that experienced fluid flow were columnar in shape and almost 6-fold taller in size.⁴⁰ Moreover, Caco-2 cells cultured under perfusion conditions formed three-dimensional crypt and villus-like structures and differentiated into Paneth and goblet cells.¹⁴⁰ In these studies, steady and unidirectional fluid flow was achieved using syringe⁴⁰ or peristaltic¹⁴⁰ pumps. In SynoPlate™, passive liquid levelling induced by an interval rocker platform exposes cells to oscillatory and bidirectional fluid flow. The biological significance of flow direction is unclear, and future work will investigate whether the reported phenotypic changes in Caco-2 cells exposed to unidirectional flow can be replicated in SynoPlate™. Of note, Trietsch et al. showed that the experimental time required to obtain a differentiated Caco-2 epithelium could be reduced from 21 days in static culture to only ~4 days in the presence of bidirectional flow.¹⁴¹ This finding is consistent with what has been reported for Caco-2 cells cultured in the presence of unidirectional flow.^{40,140}

Two-level single-mould patterning was used in the fabrication of the SynoPlate™ intestine model. To develop a PDMS template that could be used to pattern polystyrene with multilevel features, a multilevel silicon master was fabricated using two-step photolithography. By manipulating the thickness of the spin-coated photoresist and

applying different photomasks, silicon masters with geometries of different heights can be achieved in two sequential photolithography steps.

The 11.6 cm x 7.5 cm x 0.081 cm polystyrene sheet that serves as the bottom of SynoPlate™ was patterned with a 3% (w/v) solution of sodium alginate using a combination of injection moulding and vacuum filling (**Figure 37A, left**). To generate a hydrogel, cross-linking of sodium alginate polymers with calcium ions was induced by submerging the device in a 5.5% (w/v) calcium chloride bath. After overnight incubation, the device was cleaned with water to remove excess calcium-alginate gel. **Figure 37A, right** shows a typical Day 0 hydrated calcium-alginate feature. To dry the calcium-alginate feature, the device was placed inside the fume hood under a stream of compressed air. After 48 hours of drying, calcium-alginate features were microscopically examined. **Figure 37B** shows a typical Day 2 dehydrated calcium-alginate feature. Dehydrated calcium-alginate features exhibited volumetric shrinkage and most features were not intact with breakage observed most frequently at channel-vascular junctions. Further scrutiny of the drying process over 48 hours revealed that calcium-alginate gel at channel-vascular junctions was being stretched and elongated. Presumably, breakage occurred when a critical stretch value had been exceeded resulting in material failure. Given the frequency of breaks at channel-vascular junctions where there is a level change (**Figure 37C, left**), it was presumed that the gel at this location was subjected to particularly high tension that it was unable to withstand. Consideration of this problem from both a material and a design perspective led to the formulation of two hypotheses. It was hypothesized that changes to the composition and microstructure of calcium-alginate gel would improve its mechanical strength and

make it more resistant to breakage. Literature to support this hypothesis is discussed below. Secondly, it was hypothesized that revision of the feature design from multilevel to single-level would eliminate the extra tension created by the level change at channel-vascular junctions and reduce breakage.

Mechanical tests performed on vascular conduits bioprinted with different concentrations of alginate showed that conduits prepared with a higher alginate concentration exhibited significantly higher tensile strength compared to 3% (w/v) alginate conduits which were described as “fragile”.¹⁴² Consistent with these findings, Jeong et al. showed that increasing the concentration of alginate increases the rupture strength of calcium-alginate.¹⁴³ The increased mechanical strength associated with increased concentration of polymer is attributed to increased crosslinking density.¹⁴⁴

Using the original multilevel PDMS templates, two SynoPlate™ platforms were fabricated in parallel using 3% (w/v) sodium alginate or 5% (w/v) sodium alginate. By Day 1, 20% of dehydrated calcium-alginate features prepared with 3% (w/v) sodium-alginate were intact, and 30% of dehydrated calcium-alginate features prepared with 5% (w/v) sodium-alginate were intact.

Following the redesign of the SynoPlate™ intestine model, a single-level silicon master was fabricated by one-step photolithography and replica moulding was used to fabricate single-level epoxy and PDMS moulds. Using the single-level PDMS template, polystyrene was patterned with single-level sodium-alginate features and ionic gelation was induced by submerging the device in a CaCl₂ bath. Microscopic observation of dehydrated features after 48 hours of drying revealed that more than 50% of calcium-alginate features

were completely intact (**Figure 37C, right**). These results suggest that the two-level design played a large role in creating extra tension during drying that resulted in breaks. It is expected that the combination of higher alginate concentration and single-level features would yield an even higher success rate and future work should test this.

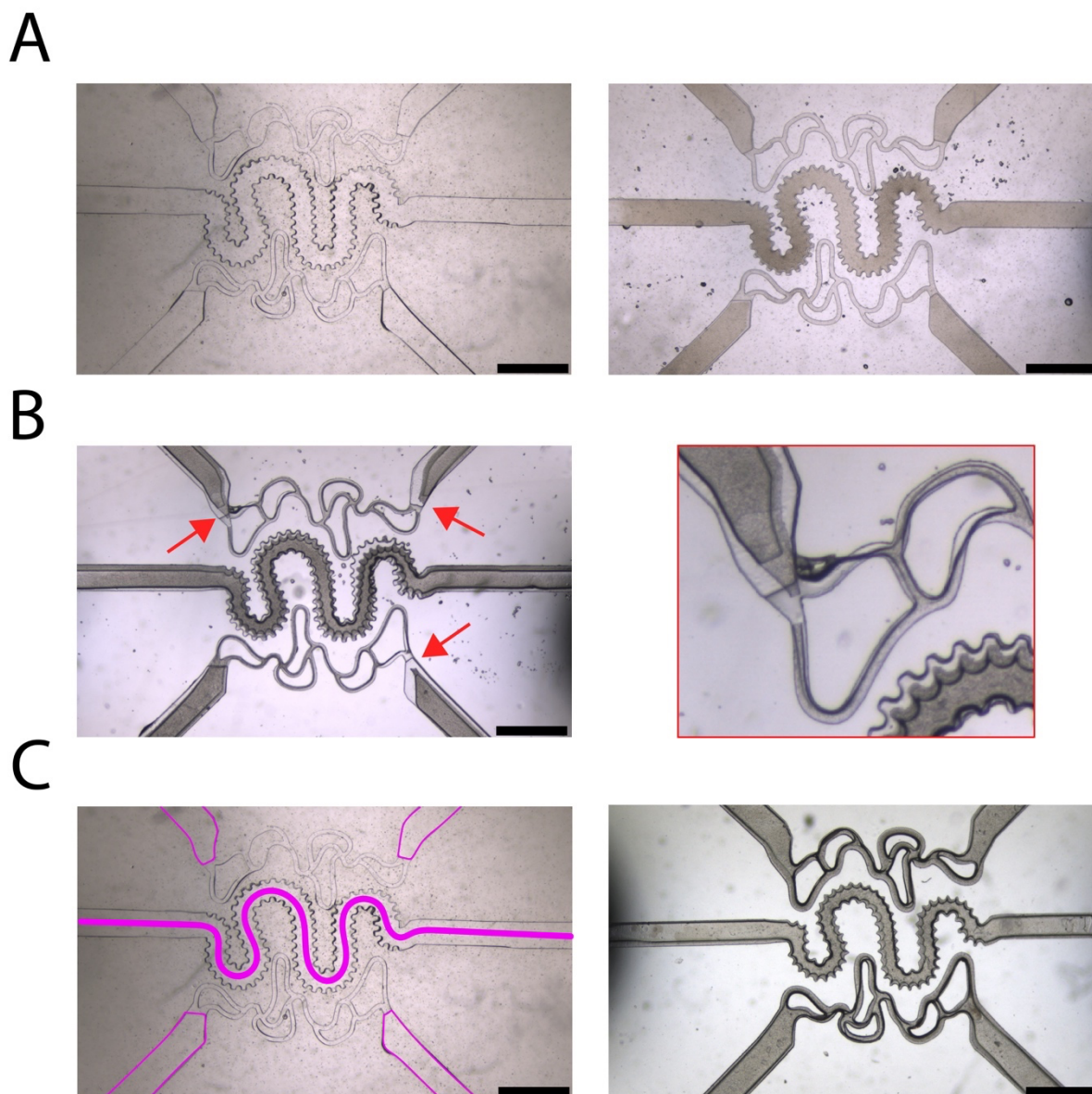


Figure 37. Microscopy images of styrene patterned with alginate via injection moulding using a two-level or single-level PDMS template. (A) Left image shows a 3% (w/v) sodium alginate two-level feature. Right image shows a typical Day 0 hydrated calcium-alginate two-level feature. (B) Left image shows a typical Day 2 dehydrated calcium-alginate two-level feature. Dehydrated calcium-alginate gel exhibits volumetric shrinkage and breakage at vascular-channel junctions (*red arrows*). Right image shows zoomed-in view of upper left vascular-channel junction. (C) Left image shows a two-level PDMS template. Magenta highlights structures (channels and intestine tube) that are on the same level. Unhighlighted vascular networks are a step down. Right image shows a Day 2 dehydrated single-level calcium-alginate feature. Scale bar, 0.586 mm.

Chapter 5: Conclusion

5.1. Summary

This work described the development a scalable human intestine model with an accessible lumen and perfusable branched vasculature within a custom-fabricated 384-well plate, termed IFlowPlate™. Using well-established soft lithography techniques pioneered by the semiconductor industry and adopted for organ-on-a-chip fabrication, PDMS templates with an array of 128 channel-like grooves were fabricated. Punched templates were used to pattern polystyrene sheets with PEGDM via injection moulding. PDMS was used as an inert and biocompatible adhesive to bond patterned polystyrene sheets to 384-well bottomless plates. To generate a platform with 128 microfluidic units each comprised of 3 wells connected by channels, PEGDM was sacrificed and flushed from the device. The open-top, 384-well plate format of IFlowPlate™ is compatible with standard laboratory equipment (e.g., plate reader) and practices (e.g., changing media, histology). To make judicious use of resources and to make it easier to diagnose and address problems, the intestinal epithelium and vascular components of the model were developed independently.

Firstly, it was shown that Caco-2 cells cultured in T75 flasks under standard conditions formed tightly packed monolayers with domes – a contact-dependent differentiation phenotype that indicates vectorial transport and barrier function. Although biologically significant, the phenomenon of dome formation is a non-physiological consequence of culturing cells on an impermeable plastic substrate. The next step was to culture Caco-2 cells on an ECM-based hydrogel and verify that they could form a confluent monolayer with barrier function.

A fibrin-based gel supplemented with Matrigel[®] was used as an ECM-based substrate in IFlowPlate[™] intestine models because fibrin supports vasculogenesis, and Matrigel[®] is enriched with laminin which provides the required signals for intestinal organoid growth. Substrate stiffness has been identified as a key determinant of organoid morphology, with intestinal organoid cells forming 2D monolayers on stiff substrates and 3D organoids on soft substrates. Within a standard 384-well plate, Caco-2 cells were cultured on three different substrates representing a range of stiffnesses. It was shown that Caco-2 cells displayed substrate-dependent morphology. On the fibrin-Matrigel[®] of intermediate stiffness, Caco-2 cells formed the hallmark cobblestone pattern of intestinal epithelium. This contrasted the 3D multicellular cyst-like aggregates that formed on the soft Matrigel[®].

To assess barrier formation of postconfluent Caco-2 monolayers cultured on fibrin-Matrigel[®], cells were stained for junction marker E-cadherin. Moreover, the multilayering of Caco-2 cells and the optical distortion at the well periphery due to the concave meniscus of the hydrogel made it difficult to discern E-cadherin expression at cell borders and view the whole growth area simultaneously. Moreover, while immunofluorescence can be a valuable tool for assessing barrier formation, it cannot provide information about barrier function. For these reasons, the fluorescent dextran permeability assay and TEER were explored as label-free quantitative approaches to monitoring barrier function.

Traditional transwell and organ-on-a-chip systems utilize a stacked configuration in which an upper (apical) and lower (basal) compartment is separated by a horizontal membrane upon which epithelium is cultured. This configuration precludes the ability to

assess macromolecular diffusion across the epithelial barrier in situ and in real-time, and instead relies on sample collection from the basal compartment. Herein, it was shown that the fluorescent dextran permeability assays could be conducted in situ and in real-time in IFlowPlate™ in a high-throughput manner using automated fluorescence microscopy/detection. The three-well configuration of IFlowPlate™ microfluidic systems allows for macromolecules that permeate the epithelium to be received by lateral reservoir wells where they can be visualized/detected. To assess the size-exclusion properties of postconfluent Caco-2 cell monolayers in IFlowPlate™, FITC and TRITC conjugated dextrans of high (70 kDa) and low (4.4 kDa) molecular weight, respectively, were added to the apical compartment. Qualitative and quantitative data showed that 70 kDa and 4.4 kDa fluorescent dextrans were largely excluded from transport across postconfluent monolayers indicating strong barrier function. Using a Student's t-test, it was determined that the observed difference in the quantity of eluted dextran between the postconfluent monolayer group and the subconfluent monolayer (negative control) group was statistically significant. Incubation of cells with chemical dyes for extended periods renders them unusable for further experimentation.

TEER is a non-invasive, sensitive, and widely used method for assessing barrier function in transwell systems. A pilot study conducted to test the feasibility of using TEER to assess the barrier function of Caco-2 monolayers in IFlowPlate™ found that resistance measurements were highly unstable and did not reflect differences in barrier quality between (1) no cells, (2) subconfluent, and (3) postconfluent groups. Non-biological factors, such as system geometries, the presence of non-conducting inhomogeneities (e.g.,

PDMS, air bubbles), and electrode positioning can greatly affect resistance measurements and could not be well-controlled. More consistent system geometries and the elimination of PDMS can be achieved by the manufacture of plates using computer numerical control milling and laser welding. To acquire resistance measurements in a consistent and high-throughput manner, a custom electrode lid that fits on top of IFlowPlate™ would be ideal.

To establish a de novo vascular network in IFlowPlate™, GFP-HUVECs and fibroblasts were encapsulated in fibrin-Matrigel® at a ratio of 5:1. By Day 6 of culture on an interval perfusion rocker, GFP-HUVECs self-assembled into a branched network of patent vessels that retained 70 kDa TRITC-dextran within the luminal space indicating endothelial barrier function. The scalability of IFlowPlate™ vascular models was hindered by the lack of robust anastomoses of vessels with lateral fluidic channels. Observations of decreasing GFP-HUVEC coverage on culture surfaces with increasing culture time suggested the weak adhesion of cells.

In an attempt to modify the inherently hydrophobic PDMS and polystyrene channel surfaces and make them more favourable for cell adhesion, fibrinogen, collagen-I, or Matrigel® was added to reservoir wells. Visualization of GFP-HUVEC coverage using fluorescence microscopy showed no appreciable difference between standard culture conditions and conditions with ECM protein. Endothelial cell adhesion to ECM protein is a precondition of haptotactic and chemotactic migration. In a parallel experiment, 5% (v/v) FBS was added to reservoir wells to establish a strong chemotactic gradient and stimulate migration of gel-encapsulated GFP-HUVECs into fluidic channels. No differences were observed between any of the test conditions and the control. These results could be

explained by (1) low density, unstable ECM coating of PDMS/polystyrene surfaces, and/or (2) undesirable conformational changes in ECM protein structure that alters the integrity of cell adhesion domains. The density of ECM protein adsorbed to surfaces can be visualized and quantified using commercially available fluorescently tagged ECM protein. Similarly, antibodies against cell adhesion domains can be used to infer their accessibility to cell surface receptors.

In Section 4.3, I discussed work to enhance the physiological relevance of the IFlowPlate™ intestine model by (1) replacing Caco-2 cells with biopsy-derived intestinal cells and (2) integrating scaffolds to enable luminal flow and guide the assembly of cells into the complex architecture of the native intestine. To convert 3D intestinal organoids into 2D monolayers with an accessible luminal surface, three different collagen hydrogels were formulated: (1) 1 mg/mL collagen-only, (2) 4 mg/mL collagen with 25% (v/v) Matrigel®, and 1.6 mg/mL collagen with 10 mg/mL fibrin and 20% (v/v) Matrigel®. These gels were formulated according to reports that they possessed appropriate stiffness to support monolayer formation. Colon organoid fragments seeded on the surface of all three gel formulations failed to form monolayers. The following explanations were discussed: (1) collagen-only gel was too fragile, (2) the patient-derived organoid cells possess abnormalities that alter the sensitivity of cells to substrate stiffness, and (3) the isolation procedure and/or seeding density needs to be optimized.

Lastly, work to improve the fabrication procedure for the sister platform SynoPlate™ was presented. Unlike IFlowPlate™ which is tissue agnostic, SynoPlate™ incorporates tissue-specific scaffolds which provide multiscale topographical features (i.e.,

tubular structure and crypts) and enable luminal flow. Fabrication of SynoPlate™ relies on the encapsulation of moulded alginate in a hydrogel and subsequent dissolution and flushing to generate cavities of complex architectures in the gel that will guide the self-assembly of cells. The fidelity of tissue architectures critically depends on the moulded alginate being intact. It was found that dehydrated calcium-alginate features were not intact. This was addressed from both a material and a design perspective. Redesigning the features to be single-level led to a much greater improvement compared to the increase in sodium alginate concentration.

Organ-on-a-chip systems are modular abstractions of their exceedingly complex in vivo counterparts, and by modulating which components are included and their properties, they can be used to address a diversity of biological questions. The preferred model is the one that is only as complex as necessary to answer a biological question of interest. This implies a trade-off between enhanced physiological relevance and reduced ambiguity in the interpretation of findings. Herein, the development of an increasingly biomimetic intestine model was pursued as an iterative process. However, it is worth stating that a new iteration (e.g., vascularized intestine model) does not make the one that preceded it (e.g., avascular intestine model) obsolete. An earlier iteration can have utility depending on the question of interest. For example, the majority of drugs administered by the oral route are delivered to the systemic circulation by way of passive diffusion across a series of barriers.^{19,110} The single layer of intestinal epithelial cells has been identified as the most significant barrier to drug absorption, and therefore, the structure of greatest interest when modelling drug absorption.¹¹⁰

5.2 Prospective Application of IFlowPlate™ Intestine Model

For a research thesis driven by a biological question, well-established tissue models and methods are used to test a hypothesis, and the significance of the work is contextualized in terms of a gap that is filled in scientific knowledge. This thesis presented the prototyping of the IFlowPlate™ intestine model which will require improvement and further validation before it can be considered credible and usefully applied to address gaps in scientific knowledge. However, to illustrate the potential of this work, a prospective application of the IFlowPlate™ intestine model is proposed.

The many desirable attributes of plastic has made it one of the most pervasive materials on the planet.¹⁴⁵ The significant environmental burden of microplastics (MPs) has stimulated growing concern about routes of human exposure and health risks. In recent years, evidence has emerged that MPs contaminate tap water, seafood, and a variety of processed food and beverages, with airborne MPs settling on food/drink possibly representing one of the greatest pathways of human MP exposure.^{146,147} Of the organs of the gastrointestinal tract, the colon is a major target of putative toxic effects of MPs and their associated chemicals. This is due to the storage of waste products in the colon prior to elimination. The long residence time of food waste in the colon offers greater opportunities for the interaction of MPs with the epithelium.¹⁴⁸

It is speculated that toxicity of MPs could arise from the chemical additives incorporated in plastics during manufacturing, and their capacity to adsorb and concentrate hydrophobic contaminants, such as polychlorinated biphenyls (PCBs) and heavy metals, making MPs both a potential source and vector of harmful chemicals with known adverse

health effects.^{147,148} For example, population studies suggest a causal link between exposure to PCBs and increased risk of colorectal cancer, with a proposed mechanism of PCB-induced mutations in k-ras, and p53 – thought to be critical in driving the transformation of healthy colonic epithelia.^{148,149}

In one of the few studies on MP ingestion in land animals, it was shown that 5 μm polystyrene microplastic exposure in mice results in significant decrease in mucus secretion.¹⁵⁰ Mucins are proteins that comprise the mucosa that is presumed to protect the underlying epithelium from exposure to potentially injurious dietary constituents, chemicals, and bacteria. Mice deficient in the most abundantly secreted mucin, Muc2, display an elevated ratio of proliferative to apoptotic cells, aberrant crypt morphology, and eventually develop tumours.¹⁵¹ Reduced mucin expression has also been reported in human colon cancer specimens.¹⁵¹ It is hypothesized this might be a potential mechanism through which MPs could induce colon cancer in humans.

The IFlowPlate™ intestine model with a colon organoid-derived epithelial monolayer and perfusable vasculature is well-suited for investigating the potential for acute/chronic exposure to MPs to (1) disrupt intestinal homeostasis and (2) cross the epithelial barrier and enter the circulation. The entry of MPs into the circulation could create the opportunity for ingested pollutants to interact with cells/tissue remote from the colon and induce toxicity at secondary sites.¹⁵⁰ Analogous to how the dextran permeability assay was performed in this work to assess epithelial barrier function (Section 3.5.3), MPs of different polymer types and shapes can be labelled with dyes,¹⁵² added to the apical compartment, and their fate tracked in situ using fluorescence microscopy.

Using organ-on-a-chip systems to acquire human-relevant data on the hazardous potential of engineered materials that humans ingest could have important implications for public and environmental health. Enhanced scientific understanding of risk-factors for intestinal pathophysiology can inform preventative healthcare strategies and bolster movements aimed at protecting the natural world and living sustainably (e.g., the ban of single-use plastics and replacement with re-usable alternatives). The application of organ-on-a-chip systems to disease modelling and drug development has been the focus of the field thus far. To my knowledge, this proposed application of the IFlowPlate™ intestine model would represent the first example of a study of the adverse health effects of MP ingestion on untransformed human intestinal tissue.

List of References

- 1 Cromer, W. E., Mathis, J. M., Granger, D. N., Chaitanya, G. V. & Alexander, J. S. Role of the endothelium in inflammatory bowel diseases. *World J Gastroenterol* **17**, 578-593, doi:10.3748/wjg.v17.i5.578 (2011).
- 2 Wang, R. *et al.* B7-H3 promotes colorectal cancer angiogenesis through activating the NF-kappaB pathway to induce VEGFA expression. *Cell Death Dis* **11**, 55, doi:10.1038/s41419-020-2252-3 (2020).
- 3 Boudreau, N. & Myers, C. Breast cancer-induced angiogenesis: multiple mechanisms and the role of the microenvironment. *Breast Cancer Res* **5**, 140-146, doi:10.1186/bcr589 (2003).
- 4 Voutouri, C. *et al.* Experimental and computational analyses reveal dynamics of tumor vessel cooption and optimal treatment strategies. *Proc Natl Acad Sci U S A* **116**, 2662-2671, doi:10.1073/pnas.1818322116 (2019).
- 5 Semela, D. & Dufour, J. F. Angiogenesis and hepatocellular carcinoma. *J Hepatol* **41**, 864-880, doi:10.1016/j.jhep.2004.09.006 (2004).
- 6 Folberg, R. & Maniotis, A. J. Vasculogenic mimicry. *APMIS* **112**, 508-525, doi:10.1111/j.1600-0463.2004.apm11207-0810.x (2004).
- 7 Michor, F., Nowak, M. A. & Iwasa, Y. Evolution of resistance to cancer therapy. *Curr Pharm Des* **12**, 261-271, doi:10.2174/138161206775201956 (2006).
- 8 D'Arcangelo, E., Wu, N. C., Cadavid, J. L. & McGuigan, A. P. The life cycle of cancer-associated fibroblasts within the tumour stroma and its importance in disease outcome. *Br J Cancer*, doi:10.1038/s41416-019-0705-1 (2020).
- 9 Venning, F. A., Wullkopf, L. & Erler, J. T. Targeting ECM Disrupts Cancer Progression. *Front Oncol* **5**, 224, doi:10.3389/fonc.2015.00224 (2015).
- 10 Dutton, J. S., Hinman, S. S., Kim, R., Wang, Y. & Allbritton, N. L. Primary Cell-Derived Intestinal Models: Recapitulating Physiology. *Trends Biotechnol* **37**, 744-760, doi:10.1016/j.tibtech.2018.12.001 (2019).
- 11 Turner, L. A. & M, J. D. Nanotopography - potential relevance in the stem cell niche. *Biomater Sci* **2**, 1574-1594, doi:10.1039/c4bm00155a (2014).
- 12 Ferraretto, A. *et al.* New methodological approach to induce a differentiation phenotype in Caco-2 cells prior to post-confluence stage. *Anticancer Res* **27**, 3919-3925 (2007).
- 13 Sambuy, Y. *et al.* The Caco-2 cell line as a model of the intestinal barrier: Influence of culture-related factors on Caco-2 cell functional characteristics. *Cell Biology and Toxicology* **21** (2005).
- 14 Tan, H. Y. *et al.* A multi-chamber microfluidic intestinal barrier model using Caco-2 cells for drug transport studies. *PLoS One* **13**, e0197101, doi:10.1371/journal.pone.0197101 (2018).

- 15 Awortwe, C., Fasinu, P. S. & Rosenkranz, B. Application of Caco-2 cell line in herb-drug interaction studies: current approaches and challenges. *J Pharm Pharm Sci* **17**, 1-19, doi:10.18433/j30k63 (2014).
- 16 Gao, Y. *et al.* Modulation of Intestinal Epithelial Permeability in Differentiated Caco-2 Cells Exposed to Aflatoxin M1 and Ochratoxin A Individually or Collectively. *Toxins (Basel)* **10**, doi:10.3390/toxins10010013 (2017).
- 17 Wang, L., Murthy, S. K., Barabino, G. A. & Carrier, R. L. Synergic effects of crypt-like topography and ECM proteins on intestinal cell behavior in collagen based membranes. *Biomaterials* **31**, 7586-7598, doi:10.1016/j.biomaterials.2010.06.036 (2010).
- 18 Srinivasan, B. *et al.* TEER measurement techniques for in vitro barrier model systems. *J Lab Autom* **20**, 107-126, doi:10.1177/2211068214561025 (2015).
- 19 Deli, M. A. Potential use of tight junction modulators to reversibly open membranous barriers and improve drug delivery. *Biochim Biophys Acta* **1788**, 892-910, doi:10.1016/j.bbamem.2008.09.016 (2009).
- 20 Kasendra, M. *et al.* Duodenum Intestine-Chip for preclinical drug assessment in a human relevant model. *eLife* **9**, doi:10.7554/eLife.50135 (2020).
- 21 Xie, F., Ding, X. & Zhang, Q. Y. An update on the role of intestinal cytochrome P450 enzymes in drug disposition. *Acta Pharm Sin B* **6**, 374-383, doi:10.1016/j.apsb.2016.07.012 (2016).
- 22 Briske-Anderson, M. J., Finley, J. W. & Newman, S. M. The influence of culture time and passage number on the morphological and physiological development of Caco-2 cells. *Proceedings of the Society for Experimental Biology and Medicine* **214** (1996).
- 23 Sato, T. *et al.* Long-term expansion of epithelial organoids from human colon, adenoma, adenocarcinoma, and Barrett's epithelium. *Gastroenterology* **141**, 1762-1772, doi:10.1053/j.gastro.2011.07.050 (2011).
- 24 Rahmani, S., Breyner, N. M., Su, H. M., Verdu, E. F. & Didar, T. F. Intestinal organoids: A new paradigm for engineering intestinal epithelium in vitro. *Biomaterials* **194**, 195-214, doi:10.1016/j.biomaterials.2018.12.006 (2019).
- 25 Wang, Y. *et al.* Self-renewing Monolayer of Primary Colonic or Rectal Epithelial Cells. *Cell Mol Gastroenterol Hepatol* **4**, 165-182 e167, doi:10.1016/j.jcmgh.2017.02.011 (2017).
- 26 Altay, G. *et al.* Self-organized intestinal epithelial monolayers in crypt and villus-like domains show effective barrier function. *Sci Rep* **9**, 10140, doi:10.1038/s41598-019-46497-x (2019).
- 27 Kasendra, M. *et al.* Development of a primary human Small Intestine-on-a-Chip using biopsy-derived organoids. *Sci Rep* **8**, 2871, doi:10.1038/s41598-018-21201-7 (2018).
- 28 Nikolaev, M. *et al.* Homeostatic mini-intestines through scaffold-guided organoid morphogenesis. *Nature*, doi:10.1038/s41586-020-2724-8 (2020).

- 29 Moon, C., VanDussen, K. L., Miyoshi, H. & Stappenbeck, T. S. Development of a primary mouse intestinal epithelial cell monolayer culture system to evaluate factors that modulate IgA transcytosis. *Mucosal Immunol* **7**, 818-828, doi:10.1038/mi.2013.98 (2014).
- 30 Ingber, D. E. Cellular mechanotransduction: putting all the pieces together again. *FASEB J* **20**, 811-827, doi:10.1096/fj.05-5424rev (2006).
- 31 Shyer, A. E., Huycke, T. R., Lee, C., Mahadevan, L. & Tabin, C. J. Bending gradients: how the intestinal stem cell gets its home. *Cell* **161**, 569-580, doi:10.1016/j.cell.2015.03.041 (2015).
- 32 Guiu, J. *et al.* Tracing the origin of adult intestinal stem cells. *Nature* **570**, 107-111, doi:10.1038/s41586-019-1212-5 (2019).
- 33 Nelson, C. M., Vanduijn, M. M., Inman, J. L., Fletcher, D. A. & Bissell, M. J. Tissue geometry determines sites of mammary branching morphogenesis in organotypic cultures. *Science* **314**, 298-300, doi:10.1126/science.1131000 (2006).
- 34 Yi, B. *et al.* Three-dimensional in vitro gut model on a villi-shaped collagen scaffold. *BioChip Journal* **11**, 219-231, doi:10.1007/s13206-017-1307-8 (2017).
- 35 Jansson-Knodell, C. L., Hujoel, I. A., Rubio-Tapia, A. & Murray, J. A. Not All That Flattens Villi Is Celiac Disease: A Review of Enteropathies. *Mayo Clin Proc* **93**, 509-517, doi:10.1016/j.mayocp.2017.10.025 (2018).
- 36 Jalili-Firoozinezhad, S. *et al.* A complex human gut microbiome cultured in an anaerobic intestine-on-a-chip. *Nat Biomed Eng*, doi:10.1038/s41551-019-0397-0 (2019).
- 37 Jalili-Firoozinezhad, S. *et al.* Modeling radiation injury-induced cell death and countermeasure drug responses in a human Gut-on-a-Chip. *Cell Death Dis* **9**, 223, doi:10.1038/s41419-018-0304-8 (2018).
- 38 Sung, J. H., Yu, J., Luo, D., Shuler, M. L. & March, J. C. Microscale 3-D hydrogel scaffold for biomimetic gastrointestinal (GI) tract model. *Lab Chip* **11**, 389-392, doi:10.1039/c0lc00273a (2011).
- 39 Creff, J. *et al.* Fabrication of 3D scaffolds reproducing intestinal epithelium topography by high-resolution 3D stereolithography. *Biomaterials* **221**, 119404, doi:10.1016/j.biomaterials.2019.119404 (2019).
- 40 Kim, H. J., Huh, D., Hamilton, G. & Ingber, D. E. Human gut-on-a-chip inhabited by microbial flora that experiences intestinal peristalsis-like motions and flow. *Lab Chip* **12**, 2165-2174, doi:10.1039/c2lc40074j (2012).
- 41 Kim, H. J. & Ingber, D. E. Gut-on-a-Chip microenvironment induces human intestinal cells to undergo villus differentiation. *Integr Biol (Camb)* **5**, 1130-1140, doi:10.1039/c3ib40126j (2013).
- 42 Kaarj, K. & Yoon, J. Y. Methods of Delivering Mechanical Stimuli to Organ-on-a-Chip. *Micromachines (Basel)* **10**, doi:10.3390/mi10100700 (2019).

- 43 Ting, L. H., Fegghi, S., Han, S. J., Rodriguez, M. L. & Sniadecki, N. J. Effect of Silanization Film Thickness in Soft Lithography of Nanoscale Features. *Journal of Nanotechnology in Engineering and Medicine* **2**, doi:10.1115/1.4005665 (2011).
- 44 Boxshall, K. *et al.* Simple surface treatments to modify protein adsorption and cell attachment properties within a poly(dimethylsiloxane) micro-bioreactor. *Surface and Interface Analysis* **38**, 198-201, doi:10.1002/sia.2274 (2006).
- 45 Zhang, H. & Chiao, M. Anti-fouling Coatings of Poly(dimethylsiloxane) Devices for Biological and Biomedical Applications. *J Med Biol Eng* **35**, 143-155, doi:10.1007/s40846-015-0029-4 (2015).
- 46 Lin, Y. *et al.* Vacuum filling of complex microchannels with liquid metal. *Lab Chip* **17**, 3043-3050, doi:10.1039/c7lc00426e (2017).
- 47 Lee, J. N., Jiang, X., Ryan, D. & Whitesides, G. M. Compatibility of mammalian cells on surfaces of poly(dimethylsiloxane). *Langmuir* **20**, 11684-11691, doi:10.1021/la048562+ (2004).
- 48 Qin, Y. The gel swelling properties of alginate fibers and their applications in wound management. *Polymers for Advanced Technologies* **19**, 6-14, doi:10.1002/pat.960 (2008).
- 49 Li, L., Fang, Y., Vreeker, R. & Appelqvist, I. Reexamining the egg-box model in calcium-alginate gels with x-ray diffraction. *Biomacromolecules* **8**, 464-468 (2007).
- 50 Vreeker, R., Li, L., Fang, Y., Appelqvist, I. & Mendes, E. Drying and Rehydration of Calcium Alginate Gels. *Food Biophysics* **3**, 361-369, doi:10.1007/s11483-008-9087-2 (2008).
- 51 Lin, D. S. Y., Rajasekar, S., Marway, M. K. & Zhang, B. From Model System to Therapy: Scalable Production of Perfusable Vascularized Liver Spheroids in “Open-Top” 384-Well Plate. *ACS Biomaterials Science & Engineering*, doi:10.1021/acsbiomaterials.0c00236 (2020).
- 52 Morin, K. T. & Tranquillo, R. T. In vitro models of angiogenesis and vasculogenesis in fibrin gel. *Exp Cell Res* **319**, 2409-2417, doi:10.1016/j.yexcr.2013.06.006 (2013).
- 53 Chen, X. *et al.* Prevascularization of a fibrin-based tissue construct accelerates the formation of functional anastomosis with host vasculature. *Tissue Eng Part A* **15**, 1363-1371, doi:10.1089/ten.tea.2008.0314 (2009).
- 54 Kosyakova, N. *et al.* Differential functional roles of fibroblasts and pericytes in the formation of tissue-engineered microvascular networks in vitro. *npj Regenerative Medicine* **5**, doi:10.1038/s41536-019-0086-3 (2020).
- 55 Kim, S., Lee, H., Chung, M. & Jeon, N. L. Engineering of functional, perfusable 3D microvascular networks on a chip. *Lab Chip* **13**, 1489-1500, doi:10.1039/c3lc41320a (2013).

- 56 Offeddu, G. S. *et al.* An on-chip model of protein paracellular and transcellular permeability in the microcirculation. *Biomaterials* **212**, 115-125, doi:10.1016/j.biomaterials.2019.05.022 (2019).
- 57 Peterson, M. D. & Mooseker, M. S. Characterization of the enterocyte-like brush border cytoskeleton of the C2BBE clones of the human intestinal cell line, Caco-2. *J Cell Sci* **102 (Pt 3)**, 581-600 (1992).
- 58 Jumarie, C. & Malo, C. Caco-2 cells cultured in serum-free medium as a model for the study of enterocytic differentiation in vitro. *Journal of Cellular Physiology* (1991).
- 59 Yeon, J. H., Ryu, H. R., Chung, M., Hu, Q. P. & Jeon, N. L. In vitro formation and characterization of a perfusable three-dimensional tubular capillary network in microfluidic devices. *Lab Chip* **12**, 2815-2822, doi:10.1039/c2lc40131b (2012).
- 60 Mahraoui, L. *et al.* Presence and differential expression of SGLT1, GLUT1, GLUT2, GLUT3 and GLUT5 hexose-transporter mRNAs in Caco-2 cell clones in relation to cell growth and glucose consumption. *Biochem J* **298 Pt 3**, 629-633, doi:10.1042/bj2980629 (1994).
- 61 Nguyen, K. T. & West, J. L. Photopolymerizable hydrogels for tissue engineering applications. *Biomaterials* **23**, 4307-4314, doi:10.1016/s0142-9612(02)00175-8 (2002).
- 62 Gomez-Florit, M. *et al.* Natural-Based Hydrogels for Tissue Engineering Applications. *Molecules* **25**, doi:10.3390/molecules25245858 (2020).
- 63 El-Sherbiny, I. M. & Yacoub, M. H. Hydrogel scaffolds for tissue engineering: Progress and challenges. *Glob Cardiol Sci Pract* **2013**, 316-342, doi:10.5339/gcsp.2013.38 (2013).
- 64 LeBleu, V. S., Macdonald, B. & Kalluri, R. Structure and function of basement membranes. *Exp Biol Med (Maywood)* **232**, 1121-1129, doi:10.3181/0703-MR-72 (2007).
- 65 Zhao, H. *et al.* Fabrication and physical and biological properties of fibrin gel derived from human plasma. *Biomed Mater* **3**, 015001, doi:10.1088/1748-6041/3/1/015001 (2008).
- 66 Duong, H., Wu, B. & Tawil, B. Modulation of 3D fibrin matrix stiffness by intrinsic fibrinogen-thrombin compositions and by extrinsic cellular activity. *Tissue Eng Part A* **15**, 1865-1876, doi:10.1089/ten.tea.2008.0319 (2009).
- 67 Broguiere, N. *et al.* Morphogenesis guided by 3D patterning of growth factors in biological matrices. doi:10.1101/828947 (2019).
- 68 Janmey, P. A., Winer, J. P. & Weisel, J. W. Fibrin gels and their clinical and bioengineering applications. *J R Soc Interface* **6**, 1-10, doi:10.1098/rsif.2008.0327 (2009).
- 69 Ye, Q. *et al.* Fibrin gel as a three dimensional matrix in cardiovascular tissue engineering. *European Journal of Cardio-Thoracic Surgery* **17**, 587-591, doi:10.1016/s1010-7940(00)00373-0 (2000).

- 70 Weisel, J. W. & Litvinov, R. I. Fibrin Formation, Structure and Properties. *Subcell Biochem* **82**, 405-456, doi:10.1007/978-3-319-49674-0_13 (2017).
- 71 Smith, J. D., Chen, A., Ernst, L. A., Waggoner, A. S. & Campbell, P. G. Immobilization of aprotinin to fibrinogen as a novel method for controlling degradation of fibrin gels. *Bioconjugate Chemistry* **18**, 695-701, doi:10.1021/bc060265o (2007).
- 72 Yong Lee, K. & Mooney, D. J. Hydrogels for Tissue Engineering. *Chemical Reviews* **101** (2001).
- 73 LeBleu, V. S., MacDonald, B. & Kalluri, R. Structure and function of basement membranes. *Exp Biol Med (Maywood)* **232**, 1121-1129 (2014).
- 74 Kleinman, H. K. & Martin, G. R. Matrigel: basement membrane matrix with biological activity. *Semin Cancer Biol* **15**, 378-386, doi:10.1016/j.semcancer.2005.05.004 (2005).
- 75 Sato, T. *et al.* Single Lgr5 stem cells build crypt-villus structures in vitro without a mesenchymal niche. *Nature* **459**, 262-265, doi:10.1038/nature07935 (2009).
- 76 Broguiere, N. *et al.* Growth of Epithelial Organoids in a Defined Hydrogel. *Adv Mater* **30**, e1801621, doi:10.1002/adma.201801621 (2018).
- 77 Hughes, C. S., Postovit, L. M. & Lajoie, G. A. Matrigel: a complex protein mixture required for optimal growth of cell culture. *Proteomics* **10**, 1886-1890, doi:10.1002/pmic.200900758 (2010).
- 78 Vukicevic, S. *et al.* Identification of multiple active growth factors in basement membrane Matrigel suggests caution in interpretation of cellular activity related to extracellular matrix components. *Exp Cell Res* **202**, 1-8, doi:10.1016/0014-4827(92)90397-q (1992).
- 79 Antoine, E. E., Vlachos, P. P. & Rylander, M. N. Review of collagen I hydrogels for bioengineered tissue microenvironments: characterization of mechanics, structure, and transport. *Tissue Eng Part B Rev* **20**, 683-696, doi:10.1089/ten.TEB.2014.0086 (2014).
- 80 Parenteau-Bareil, R., Gauvin, R. & Berthod, F. Collagen-Based Biomaterials for Tissue Engineering Applications. *Materials* **3**, 1863-1887, doi:10.3390/ma3031863 (2010).
- 81 Sung, K. E. *et al.* Control of 3-dimensional collagen matrix polymerization for reproducible human mammary fibroblast cell culture in microfluidic devices. *Biomaterials* **30**, 4833-4841, doi:10.1016/j.biomaterials.2009.05.043 (2009).
- 82 Xie, J., Bao, M., Bruekers, S. M. C. & Huck, W. T. S. Collagen Gels with Different Fibrillar Microarchitectures Elicit Different Cellular Responses. *ACS Appl Mater Interfaces* **9**, 19630-19637, doi:10.1021/acsami.7b03883 (2017).
- 83 Kaiser, N. J., Kant, R. J., Minor, A. J. & Coulombe, K. L. K. Optimizing Blended Collagen-Fibrin Hydrogels for Cardiac Tissue Engineering with Human iPSC-derived Cardiomyocytes. *ACS Biomater Sci Eng* **5**, 887-899, doi:10.1021/acsbomaterials.8b01112 (2019).

- 84 Hinman, S. S., Wang, Y., Kim, R. & Allbritton, N. L. In vitro generation of self-renewing human intestinal epithelia over planar and shaped collagen hydrogels. *Nat Protoc*, doi:10.1038/s41596-020-00419-8 (2020).
- 85 Kim, Y.-J. & Uyama, H. Biocompatible Hydrogel Formation of Gelatin from Cold Water Fish via Enzymatic Networking. *Polymer Journal* **39**, 1040-1046, doi:10.1295/polymj.PJ2007007 (2007).
- 86 Cosgrove, T. & Hone, J. H. E. A small-angle neutron scattering study of the structure of gelatin at the surface of polystyrene latex particles. *Langmuir* **14**, 5376-5382 (1998).
- 87 Su, K. & Wang, C. Recent advances in the use of gelatin in biomedical research. *Biotechnol Lett* **37**, 2139-2145, doi:10.1007/s10529-015-1907-0 (2015).
- 88 Wang, X. *et al.* Gelatin-Based Hydrogels for Organ 3D Bioprinting. *Polymers (Basel)* **9**, doi:10.3390/polym9090401 (2017).
- 89 Chen, K. & Vyazovkin, S. Temperature dependence of sol-gel conversion kinetics in gelatin-water system. *Macromol Biosci* **9**, 383-392, doi:10.1002/mabi.200800214 (2009).
- 90 Kim, L., Toh, Y. C., Voldman, J. & Yu, H. A practical guide to microfluidic perfusion culture of adherent mammalian cells. *Lab Chip* **7**, 681-694, doi:10.1039/b704602b (2007).
- 91 Ding, Q.-M., Ko, T. C. & Evers, B. M. Caco-2 intestinal cell differentiation is associated with G1 arrest and suppression of CDK2 and CDK4. *American Journal of Physiology* (1998).
- 92 Wu, M.-H. Simple poly(dimethylsiloxane) surface modification to control cell adhesion. *Surface and Interface Analysis* **41**, 11-16, doi:10.1002/sia.2964 (2009).
- 93 Akther, F., Yakob, S. B., Nguyen, N. T. & Ta, H. T. Surface Modification Techniques for Endothelial Cell Seeding in PDMS Microfluidic Devices. *Biosensors (Basel)* **10**, doi:10.3390/bios10110182 (2020).
- 94 Siddique, A., Pause, I., Narayan, S., Kruse, L. & Stark, R. W. Endothelialization of PDMS-based microfluidic devices under high shear stress conditions. *Colloids Surf B Biointerfaces* **197**, 111394, doi:10.1016/j.colsurfb.2020.111394 (2021).
- 95 Dejana, E., Lampugnani, M. G., Giorgi, M. & Gaboli, M. Fibrinogen induces endothelial cell adhesion and spreading via the release of endogenous matrix protein and the recruitment of more than one integrin receptor. *Blood* **75**, 1509 - 1517 (1990).
- 96 Wang, X. *et al.* Engineering anastomosis between living capillary networks and endothelial cell-lined microfluidic channels. *Lab Chip* **16**, 282-290, doi:10.1039/c5lc01050k (2016).
- 97 Rajasekar, S. *et al.* IFlowPlate-A Customized 384-Well Plate for the Culture of Perfusable Vascularized Colon Organoids. *Adv Mater* **32**, e2002974, doi:10.1002/adma.202002974 (2020).

- 98 Han, S. H. *et al.* Long-term culture-induced phenotypic difference and efficient cryopreservation of small intestinal organoids by treatment timing of Rho kinase inhibitor. *World J Gastroenterol* **23**, 964-975, doi:10.3748/wjg.v23.i6.964 (2017).
- 99 Chantret, I., Barbat, A., Dussaulx, E., Brattain, M. G. & A., Z. Epithelial polarity, villin expression, and enterocytic differentiation of cultured human colon carcinoma cells: a survey of twenty cell lines. *Cancer RES* **48**, 1936-1942 (1988).
- 100 Mayhew, T. M., Myklebust, R., Whybrow, A. & Jenkins, R. Epithelial integrity, cell death and cell loss in mammalian small intestine. *Histol Histopathol* **14**, 257-267, doi:10.14670/HH-14.257 (1999).
- 101 Schreider, C., Peignon, G., Thenet, S., Chambaz, J. & Pincon-Raymond, M. Integrin-mediated functional polarization of Caco-2 cells through E-cadherin-actin complexes. *Journal of Cell Science*, 543-552 (2001).
- 102 Lever, J. E. Inducers of mammalian cell differentiation stimulate dome formation in a differentiated kidney epithelial cell line (MDCK). *Proc Natl Acad Sci U S A* **76**, 1323-1327, doi:10.1073/pnas.76.3.1323 (1979).
- 103 Shlyonsky, V., Goolaerts, A., Van Beneden, R. & Sariban-Sohraby, S. Differentiation of epithelial Na⁺ channel function. An in vitro model. *J Biol Chem* **280**, 24181-24187, doi:10.1074/jbc.M413823200 (2005).
- 104 Gomez, S. *et al.* Independent regulation of adherens and tight junctions by tyrosine phosphorylation in Caco-2 cells. *Biochim Biophys Acta* **1452**, 121-132, doi:10.1016/s0167-4889(99)00124-x (1999).
- 105 Jaffe, A. B., Kaji, N., Durgan, J. & Hall, A. Cdc42 controls spindle orientation to position the apical surface during epithelial morphogenesis. *J Cell Biol* **183**, 625-633, doi:10.1083/jcb.200807121 (2008).
- 106 Salomon, J. *et al.* Contractile forces at tricellular contacts modulate epithelial organization and monolayer integrity. *Nat Commun* **8**, 13998, doi:10.1038/ncomms13998 (2017).
- 107 Francia, V., Aliyandi, A. & Salvati, A. Effect of the development of a cell barrier on nanoparticle uptake in endothelial cells. *Nanoscale* **10**, 16645-16656, doi:10.1039/c8nr03171a (2018).
- 108 Santbergen, M. J. C., van der Zande, M., Gerssen, A., Bouwmeester, H. & Nielen, M. W. F. Dynamic in vitro intestinal barrier model coupled to chip-based liquid chromatography mass spectrometry for oral bioavailability studies. *Anal Bioanal Chem* **412**, 1111-1122, doi:10.1007/s00216-019-02336-6 (2020).
- 109 Nellans, H. N. Paracellular intestinal transport: modulation of absorption. *Advanced Drug Delivery Reviews* **7**, 339-364 (1991).
- 110 Artursson, P. & Karlsson, J. Correlation between oral drug absorption in humans and apparent drug permeability coefficients in human intestinal epithelial (Caco-2) cells. *Biochemical and Biophysical Research Communications* **175** (1991).

- 111 Odenwald, M. A. & Turner, J. R. The intestinal epithelial barrier: a therapeutic target? *Nat Rev Gastroenterol Hepatol* **14**, 9-21, doi:10.1038/nrgastro.2016.169 (2017).
- 112 Menard, S., Cerf-Bensussan, N. & Heyman, M. Multiple facets of intestinal permeability and epithelial handling of dietary antigens. *Mucosal Immunol* **3**, 247-259, doi:10.1038/mi.2010.5 (2010).
- 113 Gijzen, L. *et al.* Culture and analysis of kidney tubuloids and perfused tubuloid cells-on-a-chip. *Nat Protoc* **16**, 2023-2050, doi:10.1038/s41596-020-00479-w (2021).
- 114 van der Helm, M. W. *et al.* Direct quantification of transendothelial electrical resistance in organs-on-chips. *Biosens Bioelectron* **85**, 924-929, doi:10.1016/j.bios.2016.06.014 (2016).
- 115 Pereiro, I., Fomitcheva Khartchenko, A., Petrini, L. & Kaigala, G. V. Nip the bubble in the bud: a guide to avoid gas nucleation in microfluidics. *Lab Chip* **19**, 2296-2314, doi:10.1039/c9lc00211a (2019).
- 116 Odijk, M. *et al.* Measuring direct current trans-epithelial electrical resistance in organ-on-a-chip microsystems. *Lab Chip* **15**, 745-752, doi:10.1039/c4lc01219d (2015).
- 117 Moya, M. L., Hsu, Y. H., Lee, A. P., Hughes, C. C. & George, S. C. In vitro perfused human capillary networks. *Tissue Eng Part C Methods* **19**, 730-737, doi:10.1089/ten.TEC.2012.0430 (2013).
- 118 Zheng, Y. *et al.* In vitro microvessels for the study of angiogenesis and thrombosis. *Proc Natl Acad Sci U S A* **109**, 9342-9347, doi:10.1073/pnas.1201240109 (2012).
- 119 Nashimoto, Y. *et al.* Integrating perfusable vascular networks with a three-dimensional tissue in a microfluidic device. *Integr Biol* **9**, 506-518, doi:10.1039/c7ib00024c (2017).
- 120 Xu, K. & Cleaver, O. Tubulogenesis during blood vessel formation. *Semin Cell Dev Biol* **22**, 993-1004, doi:10.1016/j.semcdb.2011.05.001 (2011).
- 121 Helm, C. L., Zisch, A. & Swartz, M. A. Engineered blood and lymphatic capillaries in 3-D VEGF-fibrin-collagen matrices with interstitial flow. *Biotechnol Bioeng* **96**, 167-176, doi:10.1002/bit.21185 (2007).
- 122 Chalupowicz, D. G., Chowdhury, Z. A., Bach, T. L., Barsigian, C. & Martinez, J. Fibrin II induces endothelial cell capillary tube formation. *J Cell Biol* **130**, 207-215, doi:10.1083/jcb.130.1.207 (1995).
- 123 Ghajar, C. M. *et al.* The effect of matrix density on the regulation of 3-D capillary morphogenesis. *Biophys J* **94**, 1930-1941, doi:10.1529/biophysj.107.120774 (2008).
- 124 Ng, C. P., Helm, C. L. & Swartz, M. A. Interstitial flow differentially stimulates blood and lymphatic endothelial cell morphogenesis in vitro. *Microvasc Res* **68**, 258-264, doi:10.1016/j.mvr.2004.08.002 (2004).

- 125 van Duinen, V. *et al.* Perfused 3D angiogenic sprouting in a high-throughput in vitro platform. *Angiogenesis* **22**, 157-165, doi:10.1007/s10456-018-9647-0 (2019).
- 126 Wörsdörfer, P. *et al.* Generation of complex human organoid models including vascular networks by incorporation of mesodermal progenitor cells. *Scientific Reports* **9**, doi:10.1038/s41598-019-52204-7 (2019).
- 127 Hong, W. X. *et al.* The Role of Hypoxia-Inducible Factor in Wound Healing. *Adv Wound Care (New Rochelle)* **3**, 390-399, doi:10.1089/wound.2013.0520 (2014).
- 128 van Duinen, V. *et al.* 96 perfusable blood vessels to study vascular permeability in vitro. *Sci Rep* **7**, 18071, doi:10.1038/s41598-017-14716-y (2017).
- 129 Davis, G. E. & Senger, D. R. Endothelial extracellular matrix: biosynthesis, remodeling, and functions during vascular morphogenesis and neovessel stabilization. *Circ Res* **97**, 1093-1107, doi:10.1161/01.RES.0000191547.64391.e3 (2005).
- 130 Zhang, B. *et al.* Biodegradable scaffold with built-in vasculature for organ-on-a-chip engineering and direct surgical anastomosis. *Nat Mater* **15**, 669-678, doi:10.1038/nmat4570 (2016).
- 131 Sgarioto, M. *et al.* Collagen type I together with fibronectin provide a better support for endothelialization. *C R Biol* **335**, 520-528, doi:10.1016/j.crv.2012.07.003 (2012).
- 132 Mastuyugin, V., McWhinnie, E., Labow, M. & Buxton, F. A quantitative high-throughput endothelial cell migration assay. *J Biomol Screen* **9**, 712-718, doi:10.1177/1087057104269495 (2004).
- 133 Underwood, P. A., Steele, J. G. & Dalton, B. A. Effects of polystyrene surface chemistry on the biological activity of solid phase fibronectin, analysed with monoclonal antibodies. *Journal of Cell Science* **104** (1993).
- 134 Arima, Y. & Iwata, H. Effect of wettability and surface functional groups on protein adsorption and cell adhesion using well-defined mixed self-assembled monolayers. *Biomaterials* **28**, 3074-3082, doi:10.1016/j.biomaterials.2007.03.013 (2007).
- 135 Dewitt, D. D., Kaszuba, S. N., Thompson, D. M. & Stegemann, J. P. Collagen I-matrigel scaffolds for enhanced Schwann cell survival and control of three-dimensional cell morphology. *Tissue Eng Part A* **15**, 2785-2793, doi:10.1089/ten.TEA.2008.0406 (2009).
- 136 Clinton, J. & McWilliams-Koepfen, P. Initiation, Expansion, and Cryopreservation of Human Primary Tissue-Derived Normal and Diseased Organoids in Embedded Three-Dimensional Culture. *Curr Protoc Cell Biol* **82**, e66, doi:10.1002/cpcb.66 (2019).
- 137 Zhan, T. *et al.* Cancer-Associated Mutations in Normal Colorectal Mucosa Adjacent to Sporadic Neoplasia. *Clin Transl Gastroenterol* **11**, e00212, doi:10.14309/ctg.0000000000000212 (2020).

- 138 Haupt, A. & Minc, N. How cells sense their own shape - mechanisms to probe cell geometry and their implications in cellular organization and function. *J Cell Sci* **131**, doi:10.1242/jcs.214015 (2018).
- 139 Koppes, A. N. *et al.* Complex, multi-scale small intestinal topography replicated in cellular growth substrates fabricated via chemical vapor deposition of Parylene C. *Biofabrication* **8**, 035011, doi:10.1088/1758-5090/8/3/035011 (2016).
- 140 Maurer, M. *et al.* A three-dimensional immunocompetent intestine-on-chip model as in vitro platform for functional and microbial interaction studies. *Biomaterials* **220**, 119396, doi:10.1016/j.biomaterials.2019.119396 (2019).
- 141 Trietsch, S. J. *et al.* Membrane-free culture and real-time barrier integrity assessment of perfused intestinal epithelium tubes. *Nat Commun* **8**, 262, doi:10.1038/s41467-017-00259-3 (2017).
- 142 Zhang, Y. *et al.* In Vitro Study of Directly Bioprinted Perfusable Vasculature Conduits. *Biomater Sci* **3**, 134-143, doi:10.1039/C4BM00234B (2015).
- 143 Jeong, C., Kim, S., Lee, C., Cho, S. & Kim, S. B. Changes in the Physical Properties of Calcium Alginate Gel Beads Under a Wide Range of Gelation Temperature Conditions. *Foods* **9**, doi:10.3390/foods9020180 (2020).
- 144 Kuo, C. K. & Ma, P. X. Ionically crosslinked alginate hydrogels as scaffolds for tissue engineering: Part 1. Structure gelation rate and mechanical properties. *Biomaterials* **22**, 511-521 (2001).
- 145 Azoulay, D. *et al.* Plastic & Health: The hidden costs of a plastic planet. (2019).
- 146 Rist, S., Carney Almroth, B., Hartmann, N. B. & Karlsson, T. M. A critical perspective on early communications concerning human health aspects of microplastics. *Sci Total Environ* **626**, 720-726, doi:10.1016/j.scitotenv.2018.01.092 (2018).
- 147 Wright, S. L. & Kelly, F. J. Plastic and Human Health: A Micro Issue? *Environ Sci Technol* **51**, 6634-6647, doi:10.1021/acs.est.7b00423 (2017).
- 148 Howsam, M. *et al.* Organochlorine exposure and colorectal cancer risk. *Environ Health Perspect* **112**, 1460-1466, doi:10.1289/ehp.7143 (2004).
- 149 Conlin, A., Smith, G., Carey, F. A., Wolf, C. R. & Steele, R. J. The prognostic significance of K-ras, p53, and APC mutations in colorectal carcinoma. *Gut* **54**, 1283-1286, doi:10.1136/gut.2005.066514 (2005).
- 150 Jin, Y., Lu, L., Tu, W., Luo, T. & Fu, Z. Impacts of polystyrene microplastic on the gut barrier, microbiota and metabolism of mice. *Sci Total Environ* **649**, 308-317, doi:10.1016/j.scitotenv.2018.08.353 (2019).
- 151 Velcich, A. *et al.* Colorectal cancer in mice genetically deficient in the Mucin Muc2 gene. *Science* **295** (2002).
- 152 Karakolis, E. G., Nguyen, B., You, J. B., Rochman, C. M. & Sinton, D. Fluorescent Dyes for Visualizing Microplastic Particles and Fibers in Laboratory-Based Studies. *Environmental Science & Technology Letters* **6**, 334-340, doi:10.1021/acs.estlett.9b00241 (2019).